BARISAL UNIVERSITY JOURNAL PART 1

VOLUME 6, ISSUE 1 & 2
JUNE & DECEMBER 2019
ISSN 2411-247X

BARISHAL UNIVERSITY JOURNAL PART 1

ISSN 2411-247X

Volume 6, Issue 1&2, June & December 2019

EDITORIAL BOARD

Published by
Barishal University Journal Part 1
Vol. 6, Issue 1&2, June & December 2019 on Behalf of the Editorial Board

Editorial and Business Address
Dean
Faculty of Science & Engineering and Faculty of Bio-Sciences
University of Barishal
Barishal 8200, Bangladesh
Tel : +88 0431 2177431, 0431 62244, 02 9143546
Fax : +88 0431 61827
Web : www.bu.ac.bd

Price : Taka 500.00
US $ 10.00

Printed by
Skylark Printers
278/A, Elephant Road
Katabon Dhal, Dhaka 1205
Tel: 9669092, 01975282395
E-mail: skylarkdh12@gmail.com

BARISHAL UNIVERSITY JOURNAL PART 1

ISSN 2411-247X

Volume 6 **Issue 1** **June 2019**

CONTENTS

Full Article

Barishal University Journal Part 1, 6(1): 1-12 (2019) ISSN 2411-247X

VISCOUS DISSIPATION EFFECT ON MHD NATURAL CONVECTION FLOW PAST AN INCLINED STRETCHING SURFACE IN PRESENCE OF HEAT GENERATION AND MAGNETIC FIELD

Hena Rani Biswas[*1], Md. Maruf Hasan[2] and Samima Akhter[1]

[1]*Department of Mathematics, University of Barishal, Barishal-8200, Bangladesh*
[2]*Department of Mathematics, Comilla University, Cumilla-3506, Bangladesh*

Abstract

A study on viscous dissipation effect on MHD natural convection flow past an inclined stretching surface in presence of heat generation and magnetic field has been studied. The resulting transformed governing equations are solved numerically by using Nachtsheim-Swigert shooting iteration technique along with sixth order Runge-Kutta iteration scheme. The obtained results are checked against earlier published work and are found to be in good agreement. The influence of important physical parameters on the velocity, temperature and concentration profiles as well as the local skin friction co-efficient, Nusselt and Sherwood numbers is studied. The obtained results are shown graphically and the physical characteristics of the present problem are discussed.

Keywords: Viscous Dissipation, Magnetic Field, Skin friction, Eckert number.

Introduction

The study of laminar boundary layer flow with heat and mass transfer through porous media has been studied due to its importance in scientific and engineering applications such as aerodynamics extrusion of plastic sheets and fibers, paper production, crystal growing and glass blowing. Such applications involve cooling of a molten liquid by drawing it into a cooling system. So the study of heat transfer has become important industrially for determining the quality of the final product. Laminar natural convection flow and heat transfer of fluid with and without heat source in channels with constant wall temperature have been extensively studied by Ostrach (1952). The dynamics of the boundary layer flow over a moving continuous surface originated from the pioneer work

[*] *Corresponding Author's Email: biswas.hena@yahoo.com*

of B.C. Sakiadis (1961) who developed a numerical solution for the boundary layer flow field of a stretching surface. Hossain et al. (1996) studied the free convection flow from an isothermal plate inclined at a small angle to the horizontal. Chen (2004) performed an analysis to study the natural convection flow over a permeable surface with variable wall temperature and concentration. Anderson et al. (1994) studied the diffusion of a chemically reactive species from a linearly stretching sheet. Anjali Devi and Kandasamy (2000) explained the effect of a chemical reaction on the flow in presence of heat transfer and magnetic field. Raptis and Perdikis (2006) considered the viscous flow over a non-linear stretching sheet in presence of chemical reaction and magnetic field. Samad and Mohebujjaman (2009) exposed the effect of a chemical reaction on the flow over a linearly stretching vertical sheet in presence of magnetic field and heat generation. Ferdows and Masahiro (2011) studied the thermophoresis and chemical reaction effects on MHD natural convective heat and mass transfer flow in a rotating fluid.

In a viscous fluid flow the viscosity of the fluid takes kinetic energy from the motion of fluid and transforms it into internal energy of the fluid that heats up the fluid. This process is partially irreversible and is referred as viscous dissipation (Kishan and Kavitha, 2014). The presence of viscous dissipation increases the fluid temperature. So we cannot ignore the viscous dissipation term. The effect of viscous dissipation on MHD flow has many applications. Natural convection flow is often encountered in cooling of nuclear reactors. So it is realistic to include this viscous dissipation effect to explore the impact of the magnetic field on the thermal transport in the boundary layer. The goal of the study is to examine the viscous dissipation effect on MHD natural convection flow past an inclined stretching surface in presence of heat generation and magnetic field. The dimensionless equations are solved numerically and the effects of various physical parameters on velocity, temperature and concentration are shown graphically.

Mathematical Formulation

A steady two-dimensional MHD flow of a viscous incompressible and electrically conducting fluid past a porous plate inclined with an angle α to the vertical embedded in a porous medium under the influence of a uniform magnetic field is considered. The flow is assumed to be in the x-direction, which is chosen along the plate in the upward direction and y-axis normal to it. A strong magnetic field of strength B_0 is applied in the y-direction. Here the effect of the induced magnetic field is neglected in comparison to the applied magnetic field. Two equal and opposite forces are introduced along the x-axis so that the sheet is stretched keeping the origin.

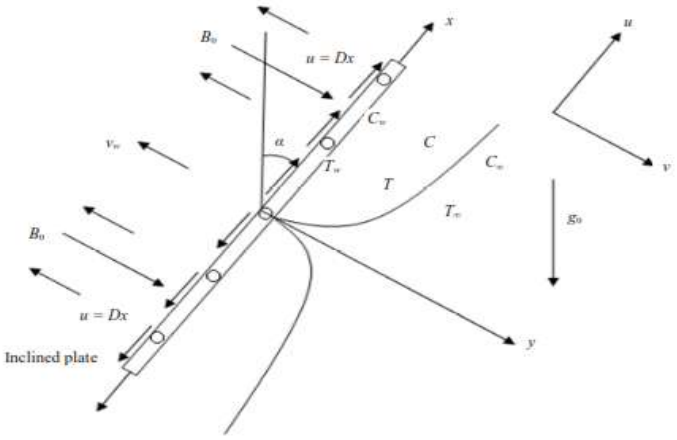

Fig. 1: Geometry of the model

The fluid is considered to be gray, absorbing emitting radiation but non-scattering medium and Rosseland approximation is used to describe the radiation heat flux in the energy equation. The plate temperature and concentration are initially raised to T_w and C_w respectively which are thereafter maintained constant. The ambient temperature of the flow is T_∞ and the concentration of the uniform flow is C_∞.

Under the usual boundary layer and Boussinesq approximation and using the Darcy-Forchhemier model, the governing equations representing the proposed flow field are

$$\frac{\partial u}{\partial x}+\frac{\partial v}{\partial y}=0 \tag{1}$$

$$u\frac{\partial u}{\partial x}+v\frac{\partial u}{\partial y}=\vartheta\frac{\partial^2 u}{\partial y^2}+g\beta(T-T_\infty)cos\alpha+\ g\beta^*(C-C_\infty)cos\alpha-\frac{\sigma B_0^2}{\rho}u-\frac{\vartheta}{k'}u \tag{2}$$

$$u\frac{\partial T}{\partial x}+v\frac{\partial T}{\partial y}=\frac{\kappa}{\rho c_p}\frac{\partial^2 T}{\partial y^2}+\frac{\vartheta}{c_p}\left(\frac{\partial u}{\partial y}\right)^2+\frac{Q_0}{\rho c_p}(T-T_\infty) \tag{3}$$

$$\frac{\partial C}{\partial t}+v\frac{\partial C}{\partial y}=D\frac{\partial^2 C}{\partial y^2} \tag{4}$$

where u and v are the velocity components along x and y-directions respectively, ϑ is the kinematic viscosity, ρ is the density of the fluid, g is the acceleration due to gravity, β is the coefficient of volume expansion, β^* is the volumetric coefficient of expansion with concentration, α is the inclination of the plate, σ is the electric conductivity, B_0 is the uniform magnetic field strength (magnetic induction), k' is the Darcy permeability, c_p is the specific heat at constant pressure, T and T_∞ are the fluid temperature within the

boundary layer and in the free-stream respectively, while C and C_∞ are the corresponding concentrations. Also Q_0 is the heat generation, D is the coefficient of mass diffusivity.

The boundary conditions are:

$$\left.\begin{array}{l} u = 0, v = 0, T = T_w, C = C_w \ \ at\ y = 0 \\ u = 0, \quad T = T_\infty, C = C_\infty \quad as \ \ y \to \infty \end{array}\right\} \tag{5}$$

where T_w is the uniform sheet temperature and C_w is the concentration of the fluid at the sheet.

Similarity Solutions

In order to obtain a similarity solution of the problem we introduce the following non-dimensional variables

$$\eta = y\sqrt{\frac{U_\infty}{\nu x}}, \qquad \psi = \sqrt{U_\infty \nu x}\, f(\eta), \qquad \theta(\eta) = \frac{T - T_\infty}{T_w - T_\infty}, \qquad \phi(\eta) = \frac{C - C_\infty}{C_w - C_\infty} \tag{6}$$

where ψ is the stream function, η is the dimensionless distance normal to the sheet, f is the dimensionless stream function, θ is the dimensionless fluid temperature and ϕ is the dimensionless concentration.

Since $u = \frac{\partial \psi}{\partial y}$ and $= -\frac{\partial \psi}{\partial x}$, we have the velocity components from (6) given by $u = U_\infty f'(\eta)$ and $v = \frac{1}{2}\sqrt{\frac{U_\infty \nu}{x}}\ (\eta f' - f)$, where prime denotes the derivatives with respect to η.

Now introducing all the above similarity variables in equations (2), (3) and (4) and we have the following dimensionless ordinary non-linear differential equations

$$f''' + \frac{1}{2} f f'' + Gr\theta\, cos\alpha + Gm\phi\, cos\alpha - (\mathrm{M} + K) f' = 0 \tag{7}$$

$$\theta'' + \frac{1}{2}\mathrm{Pr}\, f\, \theta' + \mathrm{Pr}\, Q\, \theta + \mathrm{Pr}\, Ec f''^2 = 0 \tag{8}$$

$$\phi'' + \frac{1}{2} Sc f \phi' = 0 \tag{9}$$

where $Gr = \frac{g\beta(T_w - T_\infty)x}{U_\infty^2}$ is the local Grashof number, $Gm = \frac{g\beta^*(C_w - C_\infty)}{U_\infty^2}$ is the modified Grashof number, $K = \frac{\vartheta x}{k' U_\infty}$ is the permeability parameter, $M = \frac{\sigma B_0^2 x}{\rho U_\infty}$ is the magnetic

field parameter, $Pr = \frac{\rho \vartheta c_p}{K}$ is the Prandtl number, $Q = \frac{Q_0 x}{\rho c_{pU_\infty}}$ is the heat generation parameter, $Ec = \frac{u_\infty^2}{c_p(T_w - T_\infty)}$ is the Eckert number, $Sc = \frac{\vartheta}{D}$ is the Schmidt number .

The reduced boundary conditions take the form

$$\left.\begin{aligned} f = 0,\ f' = 0,\ \theta = 1,\ \phi = 1 \quad at \quad \eta = 0 \\ f' = 0,\ \theta = 0,\ \phi = 0 \quad as \quad \eta \to \infty \end{aligned}\right\} \tag{10}$$

Skin friction, rate of heat and mass transfer

The parameters of engineering interest for the present problem are skin friction coefficient, local Nusselt number and Sherwood number. The dimensionless skin friction coefficient, local Nusselt number and Sherwood number are given by

$$C_f = 2(Re_x)^{-1/2} f''(0) \tag{11}$$

$$N_u = -(Re_x)^{1/2} \theta'(0) \tag{12}$$

$$Sh = -(Re_x)^{1/2} \phi'(0) \tag{13}$$

where $Re_x = \frac{U_\infty x}{\vartheta}$ is the Reynolds number.

Thus the values proportional to the skin-friction coefficient, Nusselt number and Sherwood number are $f''(0)$, $-\theta'(0)$ and $-\phi'(0)$ respectively.

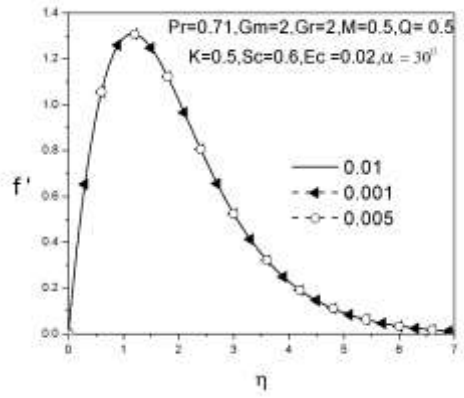

Fig. 2. Velocity profiles for different step size $\Delta\eta$

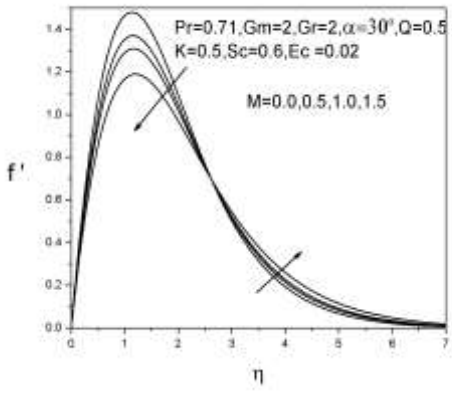

Fig. 5. Effect of M on velocity profiles

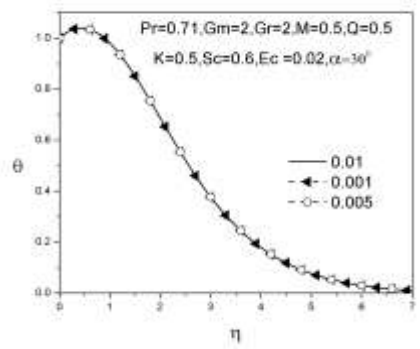

Fig. 3. Temperature profiles for different step size $\Delta\eta$

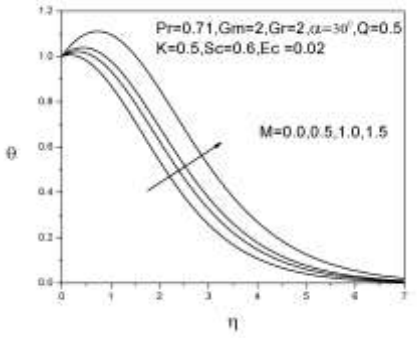

Fig. 6. Effect of M on temperature profiles

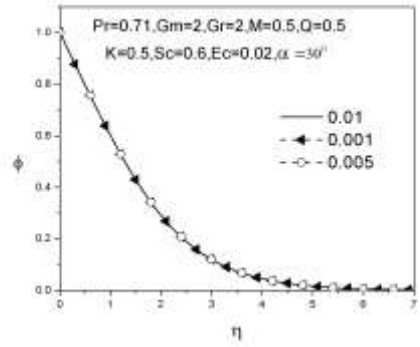

Fig. 4. Concentration profiles for different step size $\Delta\eta$

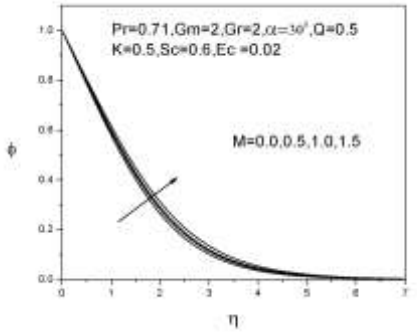

Fig. 7. Effect of M on concentration profiles

Numerical Solution

The numerical solution of the coupled non-linear differential equations (7)-(9) with boundary conditions (10) have been obtained by using Nachtsheim-Swigert (1965) shooting iteration technique (guessing the missing value) together with the sixth order Runge-Kutta initial value solver. We have chosen a step size $\Delta\eta = 0.01$ to satisfy the convergence criterion of 10^{-6} in all cases. In order to verify the effects of the step size $\Delta\eta$, we have run the code for our model with three different step sizes as $\Delta\eta = 0.01$, $\Delta\eta = 0.005$ and $\Delta\eta = 0.001$, and in each case we have found excellent agreement among them. Fig. 2- Fig. 4 show the velocity, temperature and concentration profiles for different step sizes respectively considering $= 2$, $Gm = 2$, $\alpha = 30^0$, $M = 0.5$, $K = 0.5$, $Q = 0.5$, $Pr = 0.71$, $Sc = 0.6$, $Ec = 0.02$.

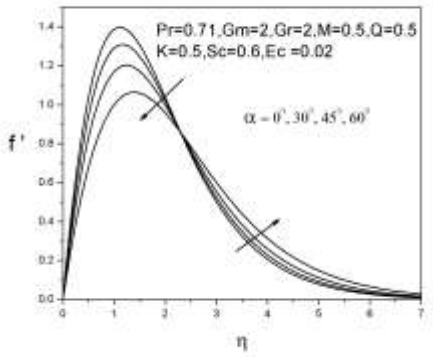

Fig. 8. Effect of α on velocity profiles

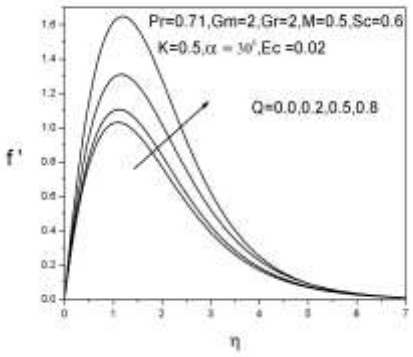

Fig. 11. Effect of Q on velocity profiles

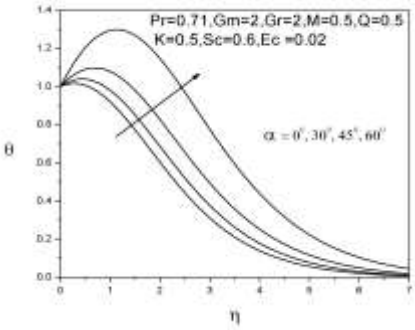

Fig. 9. Effect of α on temperature profiles

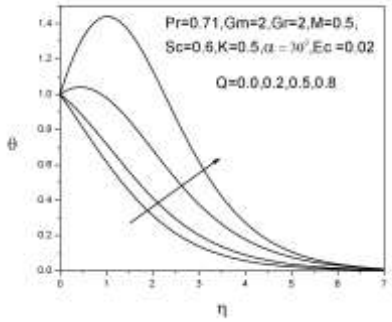

Fig. 12. Effect of Q on temperature profiles

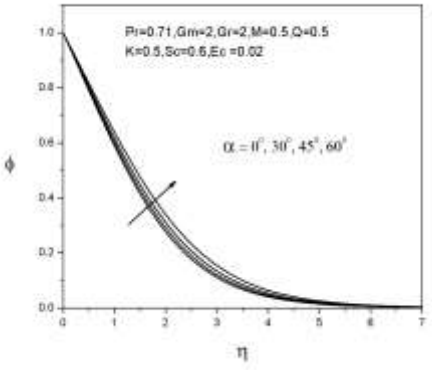

Fig. 10. Effect of α on concentration profiles

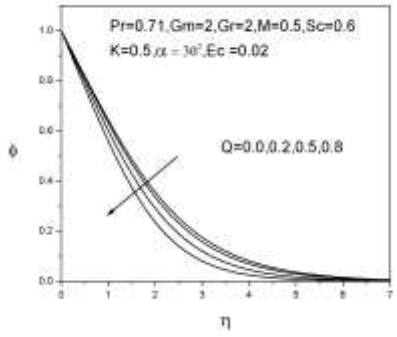

Fig. 13. Effect of Q on concentration profiles

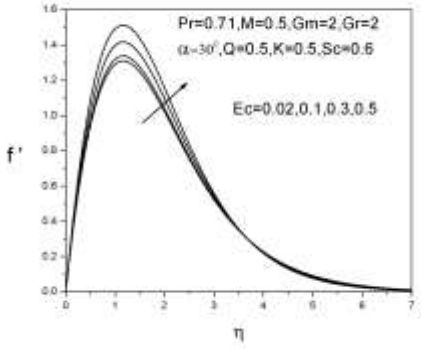

Fig. 14. Effect of Ec on velocity profiles

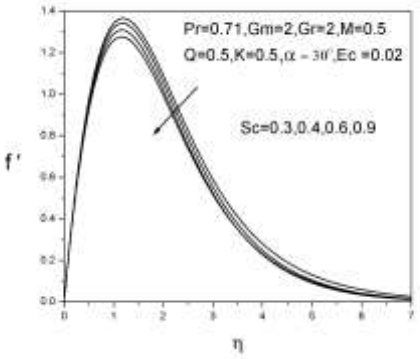

Fig. 17. Effect of Sc on velocity profiles

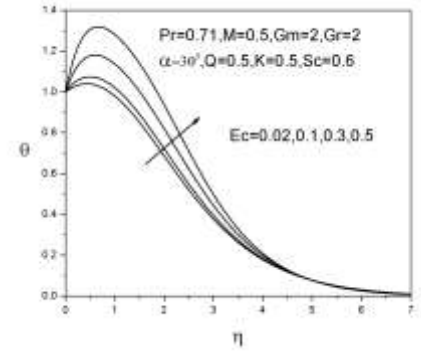

Fig. 15. Effect of Ec on temperature profiles

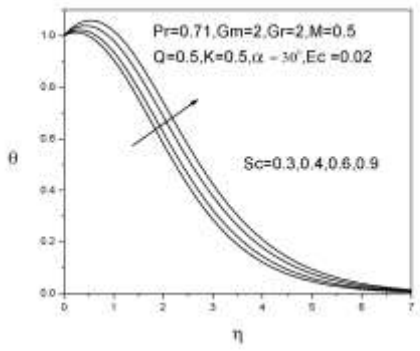

Fig. 18. Effect of Sc on temperature profiles

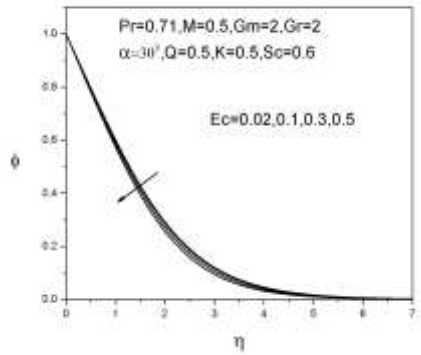

Fig. 16. Effect of Ec on concentration profiles

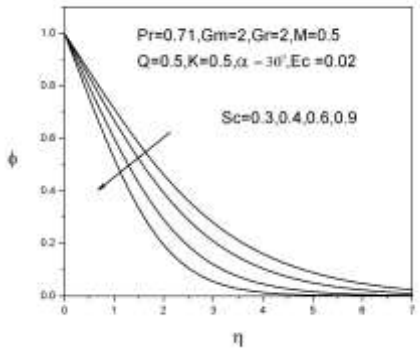

Fig. 19. Effect of Sc on concentration profiles

Results and Discussions

For the purpose of discussing the results of the flow field, the numerical calculations are presented in the form of non-dimensional velocity, temperature and concentration profiles. The parameters are chosen arbitrarily where $Pr = 0.71$ corresponds physically to air at 20^oC and $Sc = 0.6$ corresponds to water vapor at $25^\circ C$ temperature and one atmosphere pressure. The numerical results obtained are discussed in the Fig. 5-Fig. 19.

The influence of magnetic field parameter M on velocity, temperature and concentration profiles is shown in Fig. 5-Fig. 7. Here from Fig. 5, we see that first the velocity decreases rapidly and after $\eta = 2.25$ it starts to increase slowly with the increase of M. This is due to the fact that large M provides resistance to the flow and consequently there is a decrease in the velocity of the fluid. On the other hand, the temperature as well as concentration profiles increase with the increase of M as seen in Fig. 6 and Fig. 7.

The effect of the angle of inclination α on the velocity profiles is shown in Fig. 8. From this figure we see that velocity decreases swiftly with the increase of α upto $\eta = 2.3$. As α increases, the effect of the buoyancy force decreases because of the multiplication factor $cos\alpha$ and the velocity increases. Fig. 9 shows that the temperature profile rises significantly with the increase of α. Finally, from Fig. 10 we observe that the angle of inclination α affects the concentration very slowly near the plate surface.

In Fig. 11-Fig. 13, we have illustrated non-dimensional velocity, temperature and concentration profiles against η for some representative values of the heat source parameter $Q = 0.0, 0.2, 0.5, 0.8$. The positive value of Q represents source i.e. heat generation in the fluid. We know that when heat is generated the buoyancy force increases, which induces the flow rate to increase, giving rise in the velocity profiles as seen in Fig. 11. Again Fig. 12 indicates that the temperature increases rapidly as Q increases. That means when heat generates during the fluid flow there is a significant increase in the thickness of thermal boundary layer. Fig. 13 shows that the concentration profile decreases with the increase of heat source parameter.

The effect of Eckert number Ec on velocity, temperature and concentration profiles are displayed in Fig. 14-Fig. 16. Fig. 14 shows that the velocity profile increases with the increase of Ec. Again Fig. 15 shows quick increasing effect on temperature profiles. It is quite obvious from the definition of Ec that larger value of Ec gives rise to the strong viscous dissipation effect which enhances the temperature and the thermal boundary layer thickness. On the other hand, Ec has negligible decreasing effect on concentration profile seen in Fig. 16.

We have plotted the dimensionless velocity, temperature and concentration profiles showing the effect of Schmidt number Sc in Fig. 17- Fig. 19. Schmidt number Sc is the ratio of momentum diffusivity and mass diffusivity and is used to characterize fluid flows in which there are simultaneous momentum and mass diffusion convection processes. We see that the velocity decreases uniformly with the increase of Schmidt number Sc shown in Fig. 17. Schmidt number Sc has increasing effect on temperature profile viewed in Fig. 18. Again the concentration profile decreases rapidly with the increase of Sc as seen in Fig. 19.

To verify the accuracy of the numerical results, the present study is compared with the previous study of Reddy and Reddy (2011). In table 1, the values of the parameters C_f, Nu and Sh for $Gr = 2, Gm = 2, \alpha = 30^0, Pr = 0.71$ are compared and found to be in excellent agreement.

Table 1. Comparison table

M	K	Q	Sc	Reddy and Reddy (2011)	Present	Reddy and Reddy (2011)	Present	Reddy and Reddy (2011)	Present
				C_f	C_f	Nu	Nu	Sh	Sh
0.5	0.5	0.5	0.6	2.28697	2.28676	0.08245	0.08230	0.43260	0.43249
0.5	0.5	0.5	0.78	2.26675	2.26576	0.07930	0.07923	0.45990	0.45906
1.0	0.5	0.5	0.6	2.07847	2.07787	0.05676	0.05689	0.42036	0.42031
0.5	1.0	0.5	0.6	2.04279	2.04250	0.05232	0.05235	0.41826	0.41832

Conclusion

The main goal of this study was the mathematical and numerical study of the viscous dissipation effect on MHD natural convection flow past an inclined stretching surface in presence of heat generation and magnetic field. The numerical solutions of the governing differential equations were obtained by using shooting method. We observed the behavior of the physical parameters α, M, Q, Sc, Ec and also commented the numerical results from their plots. We can make the following conclusions from the present study:

i) The effect of heat generation is remarkable. An increase in heat generation results in an increase in velocity and temperature.

ii) Schmidt number has important effect on concentration profiles.

iii) The influence of magnetic parameter is to decrease the velocity but it has increasing effect on both temperature and concentration.

iv) The effect of Eckert number on temperature profiles is significant.

Nomenclature

Gr	Grashof number	u	Velocity along x-axis
Gm	Local mass Grashof number	v	Velocity along y-axis
Pr	Prandtl number	α	Angle of inclination
Re	Reynolds number	β	Coefficient of thermal expansion
k'	Permeability of porous medium	β^*	Coefficient of concentration expansion
K	Permeability parameter	g	Acceleration due to gravity
k	Thermal conductivity	ϑ	Kinematic viscosity
D	Mass diffusivity	η	Similarity variable
C	concentration in the flow field	c_p	Specific heat at constant pressure
T	Fluid temperature within boundary layer	σ	Electric conductivity
Q_0	Heat generation constant	ρ	Density of the fluid
Q	Heat generation parameter	θ	Dimensionless temperature
M	Magnetic field parameter	f	Dimensionless stream function
Ec	Eckert number	ϕ	Dimensionless concentration
Sc	Schmidt number		**Subscripts**
B_0	Applied magnetic field	w	Condition at wall
C_f	Skin-friction co-efficient	∞	Condition at infinity
Sh	Sherwood number		**Superscripts**
Nu	Nusselt number	$'$	Differentiation with respect to η

References

Anderson, H. I., Hansen, O. R. and Holmedal, B. 1994. Diffusion of a chemically reactive species from a stretching sheet, International Journal of Heat and Mass transfer. **37(4)**: 659-664.

Anjali Devi, S. P. and Kandasamy, R. 2000. Effects of chemical reaction heat and mass transfer on MHD flow past a semi infinite plate, Journal of Applied Mathematics and Mechanics. **80(10)**: 697-700.

Chen, C. H. 2004. Heat and mass transfer in MHD flow with variable wall temperature and concentration, Acta Mechanica. **172**: 219-235.

Ferdows, M. and Masahiro, O. T. A. 2011. Thermophoresis and Chemical Reaction Effects on MHD Natural Convective Heat and Mass Transfer Flow in a Rotating Fluid Considering Heat and Mass Fluxes, Canadian Journal on Science and Engineering Mathematics. **2(3)**: 114-139.

Hossain, M. A., Pop, I. and Ahamad, M. 1996. MHD free convection flow an isothermal plate, J. Theo. and Appl. Mech. **1**: 194-201.

Kishan, N. and Kavitha, P. 2014. MHD Non-Newtonian Power Law Fluid Flow and Heat Transfer Past a Non-Linear Stretching Surface with Thermal Radiation and Viscous Dissipation, Journal of Applied Science and Engineering. **17(3)**: 267-274.

Nachtsheim, P. R. and Swigert, P. 1965. Satisfaction of the Asymptotic Boundary Conditions in Numerical Solution of the System of Non-linear Equations of Boundary Layer Type. NASA TND 3004.

Ostrach, S. 1952. Laminar natural convection flow and heat transfer of fluid with and without heat source in channels with constant wall temperature. NACA TN 2863.

Raptis, A. and Perdikis, C. 2006. Viscous flow over a non-linearly stretching sheet in the presence of a chemical reaction and magnetic field, International Journal of Non-Linear Mechanics. **41(4)**: 527-529.

Reddy, M. G. and Reddy, N. B. 2011. Mass transfer and heat generation effects on MHD free convection flow past an inclined vertical surface in a porous medium, J. of Appl. Fluid Mech. **4(2)**: 7-11.

Sakiadis, B. C. 1961. Boundary layer behavior on continuous solid surface: I. boundary layer equations for two-dimensional and axisymmetric flow, A. I. Ch. E. **7(1)**: 26-28.

Samad, M. A. and Mohebujjaman, M. 2009. MHD heat and mass transfer free convection flow along a vertical stretching sheet in presence of magnetic field with heat generation, Research Journal of Applied Sciences, Engineering and Technology. **1(3)**: 98-106.

Barishal University Journal Part 1, 6(1): 13-23 (2019) ISSN 2411-247X

SYNTHESIS OF MAIN-CHAIN CHIRAL POLYMERS USING ION- EXCHANGE POLYMERIZATION AND THEIR APPLICATIONS AS POLYMERIC ORGANOCATALYST IN ASYMMETRIC REACTIONS

Md. Masud Parvez[*1] and Shinichi Itsuno[2]

[1]*Department of Chemistry, University of Barishal, Bangladesh*
[2]*Department of Environmental and Life Sciences, Toyohashi University of Technology, Japan*

Abstract

Chiral polymeric organocatalysts bearing cinchonidium moiety in the main-chain have been synthesized using ion-exchange polymerization. The double bond of the cinchonidium dimer was first modified by Heck-Mizoroki reaction and then polymerized with disulfonates by ion-exchange polymerization. The polymers were obtained with higher yield (up to 90%) and higher molecular weight (up to 6300). The polymeric organocatalyst showed excellent catalytic activity when applied in asymmetric benzylation of glycine derivatives.

***Keywords*:** Cinchonidine, Mizoroki-Heck reaction, Main-chain chiral polymers, Glycine derivative, Asymmetric benzylation.

Introduction

In the field of asymmetric organocatalysis, *Cinchona* derived quaternary ammonium salts are one of the most widely used organocatalyst. Due to their several chiral center and functional groups, several modifications of cinchona alkaloid have been done for the appropriate design of organocatalyst. Different groups have reported monomeric (O'Donnell et al. 1989, Lygo et al.1997; Corey et al.1997), dimeric (Jew et al. 2001; Lee et al. 2007, Park et al. 2001 and 2002; Chinchilla et al. 2002) and polymeric organocatalyst (Itsuno et al. 2012; Haraguchi et al. 2011; Chinchilla et al. 2000; Thierry et al. 2001 and 2005; Shi et al. 2008; Arakawa et al. 2008) containing quaternary ammonium salts of cinchona alkaloid. We have recently reported some main-chain chiral polymeric organocatalysts using different polymerization techniques, such as ion exchange polymerization (Itsuno et al. 2010; Parvez et al. 2012; Haraguchi et al. 2012),

[*]*Corresponding author's email: masud.chdu@yahoo.com*

neutralization polymerization (Haraguchi et al. 2012), quaternization polymerization (Haraguchi et al. 2012; Ahamed et al. 2013), etherification polymerization (Itsuno et al. 2010 and 2011). Most of the main-chain chiral polymers showed higher enantioselectivities than those obtained by using the corresponding monomeric catalysts when employed in asymmetric benzylation of glycine derivative.

Mizoroki-Heck coupling is one of the most efficient C-C bond formation reactions. (Heck et al. 1972) and has not widely been used for the modification of double bond of cinchonidine. Only one group has reported the utilization of Heck coupling for the modification of the double bond of cinchonidine (Ma et al. 2007). We found that double of cinchonidium salt **8** can be modified by Mizoroki-Heck reaction and synthesized cinchonidium salt **9** (Parvez et al. 2014) (scheme 1). We have also found that the double bond of the cinchonidium dimer **3A** and **3B** can be modified using Heck coupling reaction and synthesized modified cinchonidium dimer **5A** and **5B** (Parvez et al. 2014) (scheme 2). In this work, we utilized dimer **5A** and **5B** with different types of disulfonates to synthesize main-chain chiral polymers, by the ion exchange polymerization and employed them in asymmetric reaction.

Experimental Section

Materials and General Methods

All reagents were purchased from Sigma-Aldrich, Wako Pure Chemical Industries, Ltd., or Tokyo Chemical Industry Co., Ltd. at the highest available purity and used as is unless noted otherwise. Compound **3A** and **3B** were synthesized (scheme 2) according to the literature procedure reported in ref. 4. Compound **5A** was synthesized (scheme 3) according to the literature procedure (Parvez et al., 2014). Disulfonates **6d** and **6e** were synthesized according to the literature procedure (Parvez et al. 2012). DMF was distilled from calcium hydride before use. Reactions were monitored by thin-layer chromatography (TLC) using Merck precoated silica-gel plates (Merck 5554, 60F254). Column chromatography was performed with a silica-gel column (Wakogel C-200, 100–200 mesh). Melting points were recorded using a Yanaco micro-melting apparatus and are uncorrected. ^{1}H (300 MHz or 400 MHz) and ^{13}C NMR (75 MHz or 100 MHz) spectra were measured on Mercury 300 or JEOL ECS 400 spectrometer. Elemental analyses were performed at the Microanalytical Center of Kyoto University. HPLC analyses were performed with a JASCO HPLC system comprising a three-line degasser DG-980-50, an HPLC pump PV-980, and a CO-965 column oven equipped with a chiral column (CHIRALCEL ODH); hexane/2-propanol was used as an eluent. A UV detector (JASCO UV-975 for JASCO HPLC system) was used for peak detection. Optical rotations were recorded with a JASCO DIP-149 digital polarimeter, using a 10 cm thermostated

microcell. Size exclusion chromatography (SEC) was obtained with Tosoh instrument with HLC 8020 UV (254 nm) or refractive index detection. DMF was used as a carrier solvent at a flow rate of 1.0 mL/min at 40 ^{o}C. Two polystyrene gel columns of bead size 10 µm were used. A calibration curve was made to determine number-average molecular weight (M_n) and molecular weight distribution (M_w/M_n) values with polystyrene standards.

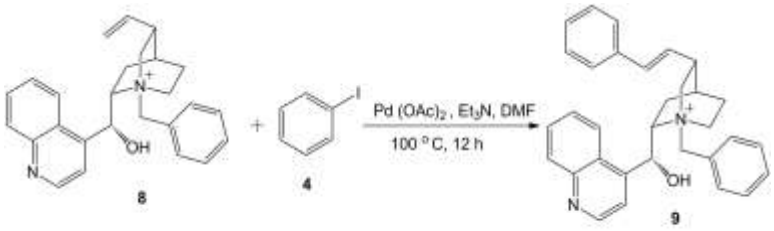

Scheme 1 Mizoroki-Heck phenylation of cinchonidium salt **8**

Synthesis of Dimer and Polymer

First of all, cinchonidium dimer **3A** and **3B** synthesized according to the literature procedure (Scheme 2) (Jew et al., 2001). Main-chain chiral polymeric organocatalyst **7A** and **7B** have been synthesized using ion exchange polymerization (scheme 3) (Itsuno et al., 2010; Parvez et al., 2012; Haraguchi et al., 2012). As the dimeric catalyst **3A** and **3B** contains double bond in cinchonidine moiety, we modified the double bond of cinchonidine dimer by Mizoroki-Heck coupling reaction using iodobenzene **4** and obtained dimer **5A** and **5B** (scheme 3) (Parvez et al. 2014).

Synthesis of 5B

A mixture of cinchonidine dimer **3B** (0.85 g, 1.0 mmol) with iodobenzene **4** (0.45 g, 2.2 mmol) in presence of 3 mol% Pd $(OAc)_2$ and Et_3N (0.14 mL, 1.0 mmol) was stirred in 15 mL dry DMF at 100 ^{o}C for 12 h. After completion of reaction, the reaction mixture was cooled at room temperature. After cooling the reaction mixture to room temperature, the reaction mixture was filtered by filter paper and added drop wise to ether (400 mL) with stirring. The solid precipitated was filtered, washed with water, ether, ethyl acetate and hexane to afford 0.92 g (92 % yield) of the product **5B**. ^{1}H NMR (DMSO- d_6, 400 MHz) δ 8.98 (d, J = 19.2 Hz, 1H), 8.37~8.21 (m, 1H), 7.95~7.73 (m, 4H), 7.32~6.99 (m, 4H), 6.72~6.49 (m, 2H), 5.38~4.84 (m, 3H), 4.45~4.28 (m, 1H), 4.08~3.94 (m, 1H), 3.80~3.65 (m, 1H), 3.11~3.09 (m, 1H), 2.95~2.89 (m, 2H), 2.33~1.68 (m, 3H), 1.55~1.38 (m, 1H),

1.20~1.15 (m, 4H). ^{13}C NMR (d^6-DMSO, 100 MHz) δ 150.09, 147.52, 145.31, 145.03, 138.84, 136.45, 135.34, 135.15, 130.74, 129.91, 129.76, 129.40, 128.37, 127.37, 126.05, 124.34, 124.19, 123.79, 120.09, 67.89, 64.24, 62.43, 59.81, 50.66, 36.58, 26.59, 24.09, 21.18. IR (KBr) ν 3238, 2945, 1654, 1590, 1509, 1491, 1450, 1386, 1233, 1162, 1061, 955, 860. $[\alpha]_D^{25} = +14.80$ (c 0.1, DMSO). mp =206~208.

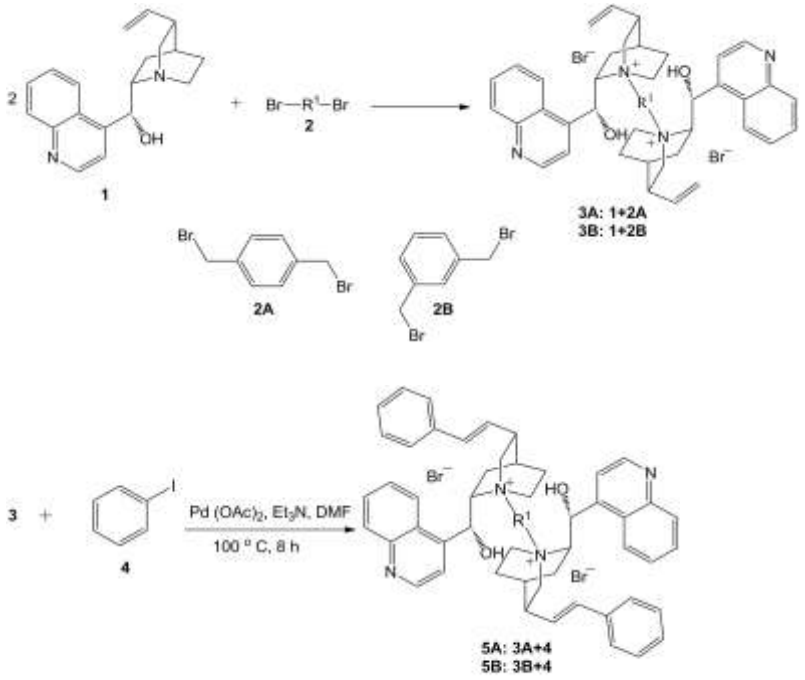

Scheme 2 Synthesis of modified cinchonidium dimer **5**

General Procedure for the Preparation of Main-chain Chiral Ionic Polymer 7A(a~e), 7B (a~e)

A solution of cinchona derived dimeric quaternary ammonium salt **5A/5B** (1 mmol) in 10 mL THF and a solution of disulfonic acid-disodium salt **6** (1 mmol) in 8 mL water were mixed together and stirred vigorously at room temperature for 24 hours. Then the solvent was removed by filtration in a glass filter, washed with water and hexane to obtain the resulting ionic polymer **7A(a~e), 7B (a~e).** The yields of the products were in the range of 78~90%. **Table 1** shows the characterization of the polymers. The number average molecular weight of the polymer varies from 4900 to 6300.

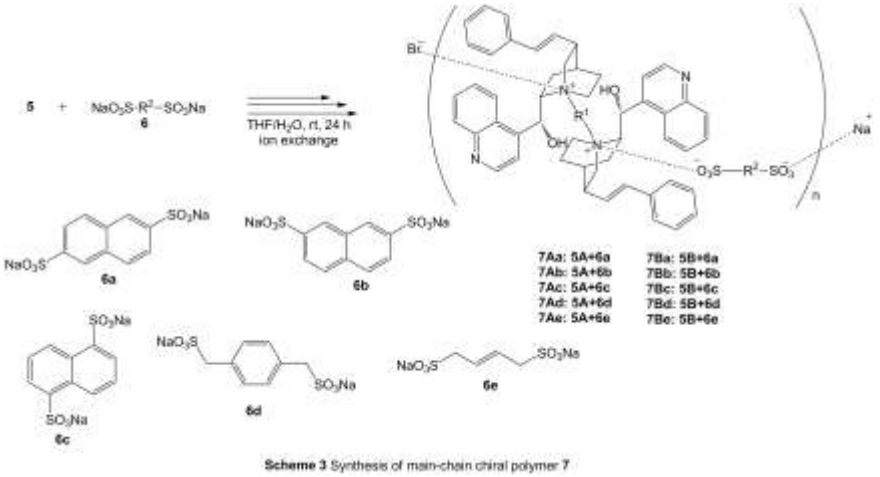

Scheme 3 Synthesis of main-chain chiral polymer 7

Table 1. IR spectral data and molecular weight of the polymers

Polymer	Yield and appearance	IR (KBr) Spectral data/cm^{-1}	M_n (SEC)	M_w/M_n
7Aa	88% yield as violet solid	3219, 2946, 1698, 1653, 1590, 1509, 1490, 1456, 1387, 1318, 1217, 1163, 1061, 1026, 953.	5900	1.17
7Ab	90% yield as violet solid	3398, 2949, 1654, 1591, 1509, 1491, 1458, 1388, 1218, 1184, 1103, 1063, 946.	5100	1.08
7Ac	88% yield as violet solid	3229, 1654, 1590, 1509, 1491, 1457, 1387, 1321, 1216, 1061, 1029, 953	6300	1.17
7Ad	82% yield as violet solid	3225, 2945, 1653, 1590, 1572, 1509, 1491, 1456, 1422, 1387, 1318, 1217, 1164., 1061, 1035, 973.	6200	1.17
7Ae	78% yield as violet solid	3231, 2946, 1654, 1590, 1572, 1509, 1491, 1456, 1422, 1387, 1319, 1216, 1162, 1061, 1030, 954.	6200	1.17
7Ba	86% yield as violet solid	3392, 3054, 1653, 1592, 1508, 1455, 1387, 1267, 1086, 1026, 904.	4900	1.01
7Bb	90% yield as violet solid	3397, 3054, 1592, 1508, 1455, 1317, 1102, 1025, 946.	5400	1.07
7Bc	83% yield as violet solid	3394, 3023, 1700, 1654, 1592, 1508, 1456, 1387, 1209, 1160, 1029, 857.	5000	1.03
7Bd	82% yield as violet solid	3237, 2946, 1653, 1590, 1508, 1456, 1387, 1213, 1129, 1035, 956.	5300	1.02
7Be	80% yield as violet solid	3230, 2947, 1653, 1590, 1508, 1490, 1455, 1387, 1320, 1209, 1122, 1061, 1030, 957.	4900	1.02

General Procedure for Catalytic Enantioselective Benzylation of *N*-diphenylmethylidene Glycine *tert*-butyl Ester 10 Using Chiral Polymeric Catalyst 7Aa

Chiral polymeric catalyst **7Aa** (10 mol %) and *N*-diphenylmethylidene glycine *tert*-butyl ester **10** (0.53 g, 1.78 mmol) were added to a mixed solvent of toluene (7 mL) and chloroform (3 mL). 50 wt% aqueous KOH solution (2.5 mL) was added to the above mixture. Benzyl bromide (0.37 g, 2.14 mmol) was then added drop wise at 0 °C to the mixture. The reaction mixture was stirred vigorously for 8 h. Saturated sodium chloride solution (10 mL) was then added and the organic phase was extracted with ethyl acetate and concentrated in vacuo to give the crude product as colorless oil. Purification of the residual oil by column chromatography on silica gel (ether–hexane = 1:10 as eluent) gave (S)-*tert*-butyl *N*-(diphenylmethylidene) phenylalanine **11**. The enantiomeric excess (91% ee) was determined by HPLC analysis (Daicel Chiralcel OD-H, hexane-2-propanol = 100:1, flow rate = 0.3 mL min^{-1}, retention time: R enantiomer = 27.6 min, S enantiomer = 47.9 min). The absolute configuration was determined by comparison of the HPLC retention time with the authentic sample independently synthesized by the reported procedure (O'Donnell et al., 1989).

Results and Discussion

As the dimeric catalyst **3A** and **3B** synthesized by Jew et al. 2001 had catalytic activity in asymmetric benzylation of glycine derivative, the dimer **5A** and **5B**, polymer **7A** and **7B** synthesized from dimer **3A** and **3B** should show some catalytic activity in asymmetric benzylation of glycine derivative. When the dimeric and polymeric catalysts were applied in asymmetric benzylation of glycine derivative **10** (Scheme 4), quite a high yield and enantioselectivity was obtained.

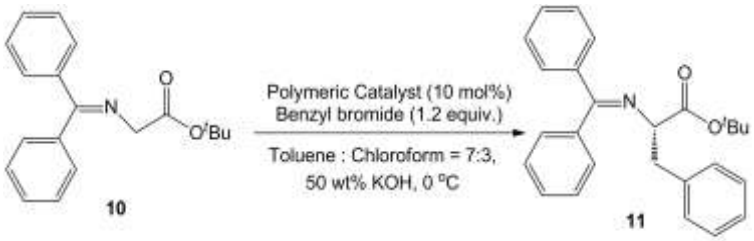

Scheme 4 Asymmetric benzylation of *N*-diphenylmethylene glycine *tert*-butyl ester

Table 2. Asymmetric benzylation of *N*-diphenylmethylene glycine *tert*-butyl ester using monomeric and dimeric catalyst[a]

Entry	Catalyst	Time (h)	Yield[b] (%)	ee[c,d] (%)
1[e]	**8**	5	91	71
2[e]	**9**	5	89	71
3[f]	**3A**	12	91	80
4[e]	**5A**	5	85	88
5[h]	**3B**	4	90	84
6	**5B**	7	79	81

[a]The reaction was carried out with 1.2 eq. of benzyl bromide in the presence 10 mol% catalyst in 50 wt% aqueous KOH-toluene-$CHCl_3$ at 0 ^oC. [b]Determined by ^1H NMR. [c]Determined by HPLC (Chiralcel OD-H). [d]All products have *S* configuration. [e]Parvez et al. 2014. [f]Itsuno et al. 2010. [h]Lee et al. 2007.

Before investigating the catalytic activity of polymeric catalyst, first low molecular weight cinchonidium salts were examined in asymmetric benzylation of *N*-diphenylmethylene glycine *tert*-butyl ester **10** to obtain phenylalanine derivative **11** (scheme 4) and the results are summarized in (Table 2) along with some reported data for the comparison. After modification of the double bond of cinchonidium salt **8** by Mizoroki-Heck coupling reaction compound **9** was obtained (scheme 1) which showed same level of catalytic activity (Table 2, entry 1 and entry 2). Cinchonidine dimer **3A** showed 80% enantioselectivity (entry 3) whereas Mizoroki-Heck modified cinchonidine dimer **5A** showed higher enantioselectivity (88%, entry 4). Among the other modified dimeric catalysts **5B** showed slightly lower catalytic activity (entry 6) compare to the non-modified cinchonidine dimer **3B** (entry 5).

The synthesized main-chain chiral ionic polymers **7A(a-e)** which contain *p*-xylene moiety and different types of disulfonates were applied in asymmetric benzylation of *N*-diphenylmethylene glycine *tert*-butyl ester and the results are summarized in Table 3. Most of the polymeric catalysts showed improved enantioselectivity compare to the dimeric catalysts **3A** and **6A** (Table 2, entry 3 and entry 4). Using polymeric catalyst **7Aa** 90% ee was obtained (Table 3, entry 1). Lowering the temperature to -20 ^oC enantioselectivity increased to 93% (entry 2). Further lowering the temperature to -40 ^oC same level of enantioselectivity was obtained with prolonged reaction time and lowering of yield (entry 3). In the case of **7Ac** similar trend was observed. Lowering the temperature to -20 ^oC enantioselectivity increased from 84% to 92% (entry 5 and entry 6). The polymeric catalyst **7Ad** was reused without the loss of catalytic activity (90% ee,

entry 7 and 8). Polymeric catalyst **7Ae** also showed high level (91% ee) of enantioselectivity.

Table 3. Asymmetric benzylation of *N*-diphenylmethylene glycine *tert*-butyl ester using polymeric catalyst **7A(a~e)**[a]

Entry	Catalyst	Time (h)	Yield[b] (%)	ee[c,d] (%)
1	**7Aa**	8	78	90
2[f]	**7Aa**	14	87	93
3[g]	**7Aa**	48	33	93
4	**7Ab**	6	91	91
5	**7Ac**	6	80	84
6[f]	**7Ac**	12	87	92
7	**7Ad**	4	90	90
8[h]	**7Ad**	6	88	90
9	**7Ae**	5	91	91

[a]The reaction was carried out with 1.2 eq. of benzyl bromide in the presence 10 mol% catalyst in 50 wt% aqueous KOH-toluene-$CHCl_3$ at 0 ^oC. [b]Determined by ^1H NMR. [c]Determined by HPLC (Chiralcel OD-H). [d]All products have S configuration. [f]Carried out at -20 ^oC. [g]Carried out at -40 ^oC. [h]Reused from entry 6.

Main-chain chiral polymeric organocatalyst containing *m*-xylene moiety **7B(a-e)** also showed good catalytic activity (Table 4). Sometimes lowering in enantioselectivity was observed compare to the dimeric catalysts **3B** and **5B** (Table 1, entry 5 and entry 6) when applied in asymmetric benzylation of *N*-diphenylmethylene glycine *tert*-butyl ester. **7Ba** showed higher enantioselectivity (84%, entry 1) compare to other polymeric catalyst from entry 2 to entry 5.

Table 4. Asymmetric benzylation of *N*-diphenylmethylene glycine *tert*-butyl ester using polymeric catalyst 7**B(a~e)**[a]

Entry	Catalyst	Time (h)	Yield[b] (%)	ee[c,d] (%)
1	**7Ba**	12	89	84
2	**7Bb**	5	80	74
3	**7Bc**	4	77	77
4	**7Bd**	12	83	82
5	**7Be**	12	72	80

[a]The reaction was carried out with 1.2 eq. of benzyl bromide in the presence 10 mol% catalyst in 50 wt% aqueous KOH-toluene-$CHCl_3$ at 0 ^oC. [b]Determined by ^1H NMR. [c]Determined by HPLC (Chiralcel OD-H). [d]All products have S configuration.

Conclusion

In this research, we have synthesized some main-chain chiral ionic polymers of cinchonidine, where double bond of cinchonidine was modified by Mizoroki-Heck reaction. These main-chain chiral ionic polymers showed excellent catalytic activity in the asymmetric benzylation of *N*-diphenylmethylene glycine *tert*-butyl ester **10** to give (*S*) phenylalanine derivative **11** with high level of enantioselectivity up to 93%. The insolubility of the polymeric catalyst in the reaction medium ease the separation process of the polymeric catalyst and was reused successfully without losing catalytic activity.

Acknowledgement

This work was done in the Laboratory of Professor Shinichi Itsuno, Department of Environmental and life Sciences, Toyohashi University of Technology, Japan 441-8122.

References

O'Donnell M. J., W. D. Bennett and, S. Wu. 1989.The stereoselective synthesis of alpha-amino acids by phase-transfer catalysis. Journal of American Chemical Society. **111**: 2353-2355.

Lygo B. and P. G Wainwright. 1997. A new class of asymmetric phase-transfer catalysts derived from Cinchona alkaloids -Application in the enantioselective synthesis of α-amino acids. Tetrahedron Letters. **38**:8595- 8598.

Corey E. J., F. Xu and M. C. Noe. 1997. A Rational Approach to Catalytic Enantioselective Enolate Alkylation Using a Structurally Rigidified and Defined Chiral Quaternary Ammonium Salt under Phase Transfer Conditions. Journal of American Chemical Society. **119**:12414-12415.

Jew S.-S., B.-S. Jeong, M.-S.Yoo, H. Huh, and H.-G. Park. 2001. Synthesis and application of dimeric Cinchonaalkaloid phase-transfer catalysts: α, α′-bis[O(9)-allylcinchonidinium]-o,m, or p-xylene dibromide.Chemical Communications.**14**: 1244-1245.

Lee J.-H., M.-S.Yoo, J.-H. Jung, S.-S. Jew, H.-G. Park and B.-S. Jeong, 2007. Polymeric chiral phase-transfer catalysts derived from cinchona alkaloids for enantioselective synthesis of α-amino acids. Tetrahedron. **63**:7906-7915.

Park H.-G., B.-S. Jeong, M.-S. Yoo, M.-K. Park, H. Huh and S.-S. Jew, 2001.Trimeric *Cinchona* alkaloid phase-transfer catalyst: α, α′, α″ -tris [*O*(9)-allylcinchonidinium] mesitylenetribromide. Tetrahedron Letters.**42**: 4645-4648.

Park H.-G., B.-S. Jeong, M.-S. Yoo, J.-H. Lee, M.-K. Park, Y.-J. Lee, M.-J. Kim and S.-S. Jew. 2002. Highly Enantioselective and Practical Cinchona-Derived Phase-Transfer Catalysts for the Synthesis of α-Amino Acids. Angewandte Chemie International Edition. **41**:3036-3038.

Chinchilla R., P. Mazon, and C. Najera. 2002. New dimeric anthracenyl derive *Cinchona quaternary* ammonium salts as phase-transfer catalysts for the asymmetric synthesis of α-amino acids. Tetrahedron: Asymmetry. **13**:927-931.

Itsuno, S., N. Haraguchi. 2012. In Science of Synthesis Asymmetric Organocatalysis 2, Ed. Maruoka, K. Thieme. **2.3.5**: 673-695.

Haraguchi, N., S. Itsuno. 2011. In Polymeric Chiral Catalyst Design and Chiral Polymer Synthesis, Ed. Itsuno, S. Wiley. **2**:17-61.

Chinchilla, R., P. Mazón, C. Nájera. 2000. Asymmetric synthesis of α-amino acids using polymer-supported *Cinchona* alkaloid-derived ammonium salts as chiral phase-transfer catalysts. Tetrahedron: Asymmetry. **11**: 3277-3281.

Thierry, B., J. C. Plaquevent, D. Cahard. 2001. New polymer-supported chiral phase-transfer catalysts in the asymmetric synthesis of α-amino acids: the role of a spacer. Tetrahedron: Asymmetry, **12**: 983-986.

Thierry, B., T. Perrard, C. Audouard, J.-C. Plaquevent, D. Cahard. 2001. Solution- and Solid-Phase Approaches in Asymmetric Phase-Transfer Catalysis by Cinchona Alkaloid Derivatives. Synthesis. **11**: 1742-1746.

Thierry, B., J.- C. Plaquevent, D. Cahard. 2005. Cinchona alkaloid-based polymer-bound phase-transfer catalysts: efficient enantioselective alkylation of benzophenone imine of glycine esters. Molecular Diversity, **9**: 277-290.

Shi, Q., Y. J. Lee, H. Song, M. Cheng, S. S. Jew, H. G. Park, B. S. Jeong. 2008. Electronically Modified Polymer-supported Cinchona Phase-transfer Catalysts for Asymmetric Synthesis of α-Alkyl-α-amino Acid Derivatives. Chem. Lett. **37**: 436-437.

Arakawa, Y., N. Haraguchi, S. Itsuno. 2008. An Immobilization Method of Chiral Quaternary Ammonium Salts onto Polymer Supports. Angew. Chem. Int. Ed. **47**: 8232-8235.

Itsuno, S., D. K. Paul, M. A. Salam, N. Haraguchi. 2010. Main-Chain Ionic Chiral Polymers: Synthesis of Optically Active Quaternary Ammonium Sulfonate Polymers and Their Application in Asymmetric Catalysis. J. Am. Chem. Soc. **132**: 2864-2865.

Parvez, M. M., M. A. Salam, N. Haraguchi, S. Itsuno. 2012. Synthesis of chiral ionic polymers containing quaternary ammonium sulfonate structure and their catalytic activity in asymmetric alkylation. J. Chinese Chem. Soc., **59**: 815-821.

Parvez, M. M., N. Haraguchi, S. Itsuno. 2012. Molecular design of chiral quaternary ammonium polymers for asymmetric catalysis applications. Org. Biomol. Chem., **10**: 2870-2877.

Haraguchi, N., H. Kiyono, Y. Takemura, S. Itsuno. 2012. Design of main-chain polymers of chiral imidazolidinone for asymmetric organocatalysis application. Chem. Commun. **48**: 4011-4013.

Haraguchi, N., P. Ahamed, M. M Parvez, S. Itsuno. 2012. Molecules. Synthesis of Main-Chain Chiral Quaternary Ammonium Polymers for Asymmetric Catalysis Using Quaternization Polymerization. **17:** 7569-7583.

Ahamed, P., M. A. Haque, M. Ishimoto, M. M. Parvez, N. Haraguchi, S. Itsuno. 2013. Synthesis of chiral quaternary ammonium polymers for asymmetric organocatalysis application. Tetrahedron. **69**: 3978-3983.

Itsuno, S., D. K. Paul, M. Ishimoto, N. Haraguchi. 2010. Designing Chiral Quaternary Ammonium Polymers: Novel Type of Polymeric Catalyst for Asymmetric Alkylation Reaction. Chem. Lett., **39**: 86-87.

Itsuno, S., M. M. Parvez, N. Haraguchi. 2011. Polymeric chiral organocatalysts. Polym. Chem. **2**:1942-1949.

Heck R. F. and J. P. Jr. Nolley**.** 1972. Palladium-catalyzed vinylic hydrogen substitution reactions with aryl, benzyl, and styryl halides**.** Journal of Organic Chemistry. **37**: 2320-2322.

Ma, B., J. L. Parkinson, S. L. Castle. 2007. Novel cinchona alkaloid derived ammonium salts as catalysts for the asymmetric synthesis of α-hydroxy α-amino acids via aldol reactions. Tetrahedron Lett. **48**: 2083-2086.

Parvez, M. M., N. Haraguchi, S. Itsuno. 2014**.** Synthesis of cinchona alkaloid-Derived chiral polymers by Mizoroki–Heck polymerization and their application to asymmetric catalysis. Macromolecules. **47**: 1922-1928.

Barishal University Journal Part 1, 6(1): 25-38 (2019) ISSN 2411-247X

NUMERICAL STUDY OF HALL EFFECTS ON A CASSON FLUID FLOW THROUGH PARALLEL PLATES

Abdullah Ahmed Foisal*, Md. Shafiul Alam and Chinmayee Podder

Department of Mathematics, University of Barishal, Barishal-8200, Bangladesh

Abstract

This study deals Hall effects on MHD viscous incompressible fluid through parallel plates. The governing non-linear coupled partial differential equations has been transformed by usual transformations into a non-dimensional system of partial coupled differential equations. The obtained differential equation have been solved numerically by explicit finite difference technique. The stability conditions and convergence criteria of the explicit finite difference schemes are established for finding the restrictions of the values of various parameters. The effects of various governing parameters on the fluid velocity, temperature, local and average shear stress, nusselt number has been investigated and presented graphically.

***Keywords*:** MHD, Casson fluid, Hall current, Explicit Finite Difference technique.

Introduction

The most important non-Newtonian fluid possessing a yield value is the Casson fluid, which has significant applications in polymer processing industries and biomechanics. Casson fluid is a shear thinning liquid which has an infinite viscosity at a zero rate of shear, a yield stress below which no flow occurs and a zero viscosity at an infinite rate of shear such as Nail polish, whipped cream, ketchup, molasses, syrups, paper pulp in water, latex paint, ice, blood, some silicone oils, some silicone coatings. Casson's constitutive equation represents a nonlinear relationship between stress and rate of strain and has been found to be accurately applicable to silicon suspensions, suspensions of bentonite in water and lithographic varnishes used for printing inks. Soundalgekar (1978) has studied the Hall and ion-slip effects in MHD couette flow with heat transfer. Attia (2005) has investigated the unsteady couette flow with heat transfer considering the ion slip. Kanch and Jana (2001) has been described the Hall effects of an unsteady couette flow under boundary layer approximation. Sayed-Ahmed and Attia (1998) analyzed the magneto hydrodynamics flow and heat transfer of a non-Newtonian fluid in an eccentric annulus. Attia (1998) studied the influence of the Hall current on the velocity and temperature fields of an unsteady Hartmann flow of a conducting Newtonian fluid between two

*Corresponding author's E-mail: foisalku_math08@yahoo.com

infinite non-conducting horizontal parallel and porous plates. Attia and Sayed-Ahmed (2010) has studied transient MHD Couette flow of a Casson fluid between parallel plates with heat transfer. Sayed-Ahmed et al., (2011) analyzed time dependent pressure gradient effect on unsteady MHD couette flow and heat transfer of a casson fluid.

The extension of such problem in case of Couette flow of non-Newtonian Casson fluid have been done in the study. The upper plate is moving with a uniform velocity while the lower plate is stationary. An external uniform magnetic field is applied perpendicular to the plates. In this study, the unsteady magneto hydrodynamic flow of an electrically conducting viscous incompressible non-Newtonian Casson fluid bounded by parallel non-conducting porous plates has been studied with Hall current and Viscous dissipation. The governing momentum and energy equations are solved numerically by finite difference technique and Effects of various parameter are showed interesting change in the velocity and temperature distribution.

Mathematical Model of the flow

The fluid is assumed to be laminar, incompressible and obeying a Casson model and flows between two infinite horizontal plates located at the $y = \pm h$ planes and extend from $x = -\infty$ to ∞ and from $z = -\infty$ to ∞. The upper plate is suddenly set into motion and moves with a uniform velocity U_0 while the lower plate is stationary. The upper plate is simultaneously subjected to a step change in temperature from T_1 to T_2. Then, the upper and lower plates are kept at two constant temperatures T_1 and T_2 respectively, with $T_2 > T_1$. The fluid is acted upon by an exponentially decaying pressure gradient in the *x*-direction, and a uniform suction from above and injection from below which are applied at *t* = 0. A uniform magnetic field B_0 is applied in the positive *y*-direction.

The physical model of this study is furnished in the following Fig. 1;

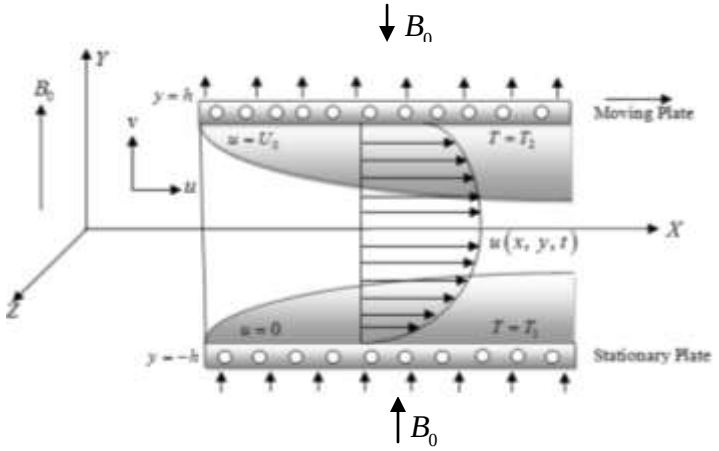

Fig. 1. Geometrical configuration of thermal boundary layer

A uniform magnetic field is assumed undisturbed as the induced magnetic field is neglected by assuming a very small magnetic Reynolds number. The Hall effect is taken into consideration and consequently a *z*-component for the velocity is expected to arise. The fluid motion has been started from rest at $t = 0$, and the no-slip condition at the plates in *z*-direction implies that the fluid velocity has no *z*-component at $y = \pm h$. The initial temperature of the fluid is assumed to be equal to T_1.

The equation of conservation of electric charge, $\nabla.\mathbf{J} = 0$ gives $J_y =$ constant where the current density $\mathbf{J} = (J_{x,} J_{y,} J_z)$, because the direction of propagation is considered only along the *y*-axis and $\mathbf{J}$ does not have any variation along the *y*-axis. Since the plate is electrically non-conducting, the constant is zero i.e. $J_y = 0$ at the plate and everywhere.

Thus accordance with the above assumptions relevant to the problem and Boussinesq's approximation, the basic boundary layer equations are given as follows;

Continuity equation

$$\frac{\partial u}{\partial x} + \frac{\partial v}{\partial y} = 0 \tag{1}$$

Momentum equation in *x*-direction

$$\frac{\partial u}{\partial t} + u\frac{\partial u}{\partial x} + v\frac{\partial u}{\partial y} = -\frac{1}{\rho}\frac{\partial P}{\partial x} + \frac{1}{\rho}\left[\frac{\partial}{\partial y}\left(\mu\frac{\partial u}{\partial y}\right)\right] - \frac{1}{\rho}\left[\frac{\sigma B_0^2}{1+m^2}(u+mw)\right] \tag{2}$$

Momentum equation in *z*-direction

$$\frac{\partial w}{\partial t} + u\frac{\partial w}{\partial x} + v\frac{\partial w}{\partial y} = \frac{1}{\rho}\left[\frac{\partial}{\partial y}\left(\mu\frac{\partial w}{\partial y}\right)\right] - \frac{1}{\rho}\left[\frac{\sigma B_0^2}{1+m^2}(w-mu)\right] \tag{3}$$

Energy equation

$$\frac{\partial T}{\partial t} + u\frac{\partial T}{\partial x} + v\frac{\partial T}{\partial y} = \frac{\kappa}{\rho c_p}\frac{\partial^2 T}{\partial y^2} + \frac{\mu}{\rho c_p}\left[\left(\frac{\partial u}{\partial y}\right)^2 + \left(\frac{\partial w}{\partial y}\right)^2\right] + \frac{1}{\rho c_p \sigma}\frac{\sigma^2 B_0^2}{1+m^2}\left(u^2 + w^2\right) \tag{4}$$

Apparent viscosity

$$\mu = \left[K_c + \left(\frac{\tau_0}{\sqrt{\left(\frac{\partial u}{\partial y}\right)^2 + \left(\frac{\partial w}{\partial y}\right)^2}}\right)^{1/2}\right]^2 \tag{5}$$

with the corresponding initial and boundary conditions are as follows;

$$t \le 0, \quad u = 0, \quad v = 0, \quad w = 0, \quad T = T_1 \quad \text{everywhere} \tag{6}$$

$$t > 0, \quad u = 0, \quad w = 0, \quad T = T_1 \quad \text{for } y = -h$$

$$u = U_0, \quad w = 0, \quad T = T_2 \quad \text{for } y = h \tag{7}$$

where x, y are cartesian coordinate system; u, v are x, y component of flow velocity respectively; υ is the kinematic viscosity; ρ is the density of the fluid; m is the Hall parameter; σ is the electrical conductivity; κ is the thermal conductivity; c_p is the specific heat at the constant pressure; K_c^2 is the Casson's coefficient of viscosity; τ_0 is the yield stress; μ is the apparent viscosity.

Mathematical Formulation

The following non-dimensional variables are introduced to obtain the non-dimensional governing equations as follows;

$$X = \frac{x}{h}, \quad Y = \frac{y}{h}, \quad U = \frac{u}{U_0}, \quad V = \frac{v}{U_0}, \quad W = \frac{w}{U_0}, \quad \tau = \frac{tU_0}{h}, \quad P = \frac{p}{\rho U_0^2},$$

$$\theta = \frac{T - T_1}{T_2 - T_1} \quad \text{and} \quad \bar{\mu} = \frac{\mu}{K_0^2}.$$

The above dimensionless variables become;

$$x = hX, \quad y = hY, \quad u = U_0 U, \quad v = U_0 V, \quad w = U_0 W, \quad t = \frac{\tau h}{U_0}, \quad p = \rho U_0^2 P,$$

$$T = T_1 + (T_2 - T_1)\theta \quad \text{and} \quad \mu = K_0^2 \bar{\mu}.$$

Now the values of the above derivatives are substituted into the equations (1)-(5) and after simplification the following nonlinear coupled partial differential equations interms of dimensionless variables are obtained as follows;

$$\frac{\partial U}{\partial X} + \frac{\partial V}{\partial Y} = 0 \tag{8}$$

$$\frac{\partial U}{\partial \tau} + U\frac{\partial U}{\partial X} + V\frac{\partial U}{\partial Y} = -\frac{dP}{dX} + \frac{1}{R_e}\left[\frac{\partial}{\partial Y}\left(\bar{\mu}\frac{\partial U}{\partial Y}\right) - \frac{H_a^2}{1+m^2}(U + mW)\right] \tag{9}$$

$$\frac{\partial W}{\partial \tau} + U\frac{\partial W}{\partial X} + V\frac{\partial W}{\partial Y} = \frac{1}{R_e}\left[\frac{\partial}{\partial Y}\left(\bar{\mu}\frac{\partial W}{\partial Y}\right) - \frac{H_a^2}{1+m^2}(W - mU)\right] \tag{10}$$

$$\frac{\partial\theta}{\partial\tau}+U\frac{\partial\theta}{\partial X}+V\frac{\partial\theta}{\partial Y}=\frac{1}{P_r}\frac{\partial^2\theta}{\partial y^2}+E_c\,\bar{\mu}\left[\left(\frac{\partial U}{\partial Y}\right)^2+\left(\frac{\partial W}{\partial Y}\right)^2\right]+\frac{H_a^2\,E_c}{1+m^2}\left(U^2+W^2\right) \tag{11}$$

$$\bar{\mu}=\left[1+\left(\frac{\tau_D}{\sqrt{\left(\frac{\partial U}{\partial Y}\right)^2+\left(\frac{\partial W}{\partial Y}\right)^2}}\right)^{1/2}\right]^2 \tag{12}$$

where,

$R_e=\dfrac{\rho U_0 h}{K_c^2}$ (**Reynolds Number**)

$H_a^2=\dfrac{\sigma B_0^2 h^2}{K_c^2}$ (**Hartmann Number Squared**)

$P_r=\dfrac{\rho c_p U_0 h}{\kappa}$ (**Prandtl Number**)

$E_c=\dfrac{U_0 K_0^2}{\rho c_p h\left(T_2-T_1\right)}$ (**Eckert Number**)

$m=\sigma\beta B_0$ (**Hall Parameter**)

$\tau_D=\dfrac{\tau_0 h}{U_0 K_0^2}$ (**Casson Number**)

with the associated initial (6) and boundary (7) conditions become;

$\tau=0,\quad U=0,\quad V=0,\quad W=0,\quad \theta=0$ everywhere (13)

$\tau>0,\quad U=0,\quad W=0,\quad \theta=0$ for $Y=-1$

$U=1,\quad W=0,\quad \theta=1$ for $Y=1$ (14)

Shear Stress and Nusselt Number

From the velocity field, it is studied that the effects of various parameters on the local and average shear stress. The following equations represent the local and average shesr stress in case of moving plate.

Local shear stress, $\tau_L=\mu\left(\dfrac{\partial u}{\partial y}\right)_{y=h}$ and Average shear stress, $\tau_A=\mu\int\left(\dfrac{\partial u}{\partial y}\right)_{y=h}dx$

which are proportional to $\bar{\mu}\left(\frac{\partial U}{\partial Y}\right)_{Y=1}$ and $\bar{\mu}\int_0^{80}\left(\frac{\partial U}{\partial Y}\right)_{Y=1} dX$ respectively.

From the temperature field, the effects of various parameters on the local and average heat transfer coefficients in case of moving plate have been investigated. The following equations represent the local and average heat transfer rate that is well known Nusselt number

Local Nusselt number, $N_{u\,L} = \mu\left(-\frac{\partial T}{\partial y}\right)_{y=h}$ and

Average Nusselt number, $N_{u\,A} = \mu\int\left(-\frac{\partial T}{\partial y}\right)_{y=h} dx$

which are proportional to $\bar{\mu}\left(-\frac{\partial \theta}{\partial Y}\right)_{Y=1}$ and $\bar{\mu}\int_0^{80}\left(-\frac{\partial \theta}{\partial Y}\right)_{Y=1} dX$ respectively.

Numerical Solution

The explicit finite difference method has been used to solve equations (1)-(5) with the help of the conditions given by (6) and (7). To obtain the difference equations the region of the flow is divided into a grid or mesh of lines parallel to *X* and *Y* axes where *X*-axis is taken along the plate and *Y*-axis is normal to the plate.

Here it is considered that the plate of height is $X_{\max}(=80)$ i.e. *X* varies from 0 to 80 and regard $Y_{\max}(=2)$ i.e. *Y* varies from -1 to 1. There are $m=98$ and $n=98$ grid spacing in the *X* and *Y* directions respectively as shown in Fig. 2;

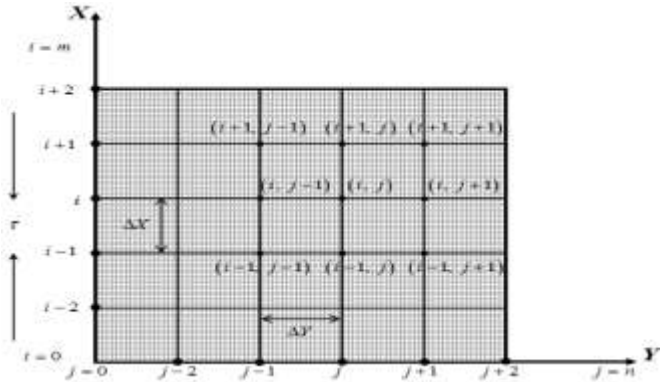

Fig. 2. Finite difference space grid

It is assumed that ΔX, ΔY are constant mesh sizes along *X* and *Y* directions respectively and taken as follows,

$$\Delta X = 0.8163\left(0 \le x \le 80\right)$$
$$\Delta Y = 0.0204\left(-1 \le y \le 1\right)$$

with the smaller time-step, $\Delta\tau = 0.0001$

Let U^{n+1}, W^{n+1} and θ^{n+1} denote the values of U^n, W^n and θ^n at the end of a time-step respectively. The explicit finite difference approximation becomes;

$$\frac{U_{i,j}^n - U_{i-1,j}^n}{\Delta X} - \frac{V_{i,j}^n - V_{i,j-1}^n}{\Delta Y} = 0 \tag{15}$$

$$\frac{U_{i,j}^{n+1} - U_{i,j}^n}{\Delta\tau} + U_{i,j}^n \frac{U_{i,j}^n - U_{i-1,j}^n}{\Delta X} + V_{i,j}^n \frac{U_{i,j+1}^n - U_{i,j}^n}{\Delta Y} = -\frac{dP}{dX} + \frac{1}{R_e}\left[\bar{\mu}_{i,j}^n \left(\frac{U_{i,j+1}^n - 2U_{i,j}^n + U_{i,j-1}^n}{\left(\Delta Y\right)^2}\right)\right]$$
$$+ \frac{1}{R_e}\left[\left(\frac{\bar{\mu}_{i,j+1}^n - \bar{\mu}_{i,j}^n}{\Delta Y}\right)\left(\frac{U_{i,j+1}^n - U_{i,j}^n}{\Delta Y}\right) - \frac{H_a^2}{1+m^2}\left(U_{i,j}^n + mW_{i,j}^n\right)\right] \tag{16}$$

$$\frac{W_{i,j}^{n+1} - W_{i,j}^n}{\Delta\tau} + U_{i,j}^n \frac{W_{i,j}^n - W_{i-1,j}^n}{\Delta X} + V_{i,j}^n \frac{W_{i,j+1}^n - W_{i,j}^n}{\Delta Y} = \frac{1}{R_e}\left[\bar{\mu}_{i,,j}^n \left(\frac{W_{i,j+1}^n - 2W_{i,j}^n + W_{i,j-1}^n}{\left(\Delta Y\right)^2}\right)\right]$$
$$+ \frac{1}{R_e}\left[\left(\frac{\bar{\mu}_{i,j+1}^n - \bar{\mu}_{i,j}^n}{\Delta Y}\right)\left(\frac{W_{i,j+1}^n - W_{i,j}^n}{\Delta Y}\right) - \frac{H_a^2}{1+m^2}\left(W_{i,j}^n - mU_{i,j}^n\right)\right] \tag{17}$$

$$\frac{\theta_{i,j}^{n+1} - \theta_{i,j}^n}{\Delta\tau} + U_{i,j}^n \frac{\theta_{i,j}^n - \theta_{i-1,j}^n}{\Delta X} + V_{i,j}^n \frac{\theta_{i,j+1}^n - \theta_{i,j}^n}{\Delta Y} = \frac{1}{P_r}\left(\frac{\theta_{i,j+1}^n - 2\theta_{i,j}^n + \theta_{i,j-1}^n}{\left(\Delta Y\right)^2}\right)$$
$$+ E_c\, \bar{\mu}_{i,j}^n \left[\left(\frac{U_{i,j+1}^n - U_{i,j}^n}{\Delta Y}\right)^2 + \left(\frac{W_{i,j+1}^n - W_{i,j}^n}{\Delta Y}\right)^2\right] + \frac{E_c\, H_a^2}{1+m^2}\left[\left(U_{i,j}^n\right)^2 + \left(W_{i,j}^n\right)^2\right] \tag{18}$$

$$\bar{\mu}_{i,j}^n = \left[1 + \left(\frac{\tau_D}{\sqrt{\left(\frac{U_{i,j+1}^n - U_{i,j}^n}{\Delta Y}\right)^2 + \left(\frac{W_{i,j+1}^n - W_{i,j}^n}{\Delta Y}\right)^2}}\right)^{1/2}\right]^2 \tag{19}$$

Here the subscripts i and j designate the grid points with X and Y coordinates respectively and the superscript n represents a value of time, $\tau = n\Delta\tau$ where

$n = 0, 1, 2, ...$ During any one time-step, the coefficients $U_{i,j}^{n}$ and $V_{i,j}^{n}$ appearing in equations (1)-(5) are treated as constants. At the end of any time-step $\Delta\tau$, the new temperature $T_{i,j}^{n+1}$, the new primary velocity $U_{i,j}^{n+1}$ and the new secondary velocity $W_{i,j}^{n+1}$ at all interior nodal points may be obtained by successive applications of equations (16), (17) and (18) respectively. This process is repeated in time and provided the time-step is sufficiently small $U_{i,j}^{n}$, $W_{i,j}^{n}$ and $\theta_{i,j}^{n}$ should eventually converge to values which approximate the steady-state solution of equations (8)-(12). Also the numerical values of the Local Shear Stress and Nusselt number are evaluated by five-point approximate formula for the derivative and Average Shear Stress and Nusselt number are evaluated by Simpson's $1/3$ integration rule.

To get the steady state solutions, the computations have been carried out upto $\tau = 2$. It has been observed that the results of the computations, however, show little changes after $\tau = 0.8$. Thus the solution for $\tau = 2$ are essentially steady state solutions. The graph for the steady state solution of velocity distribution are given below in Fig. 3;

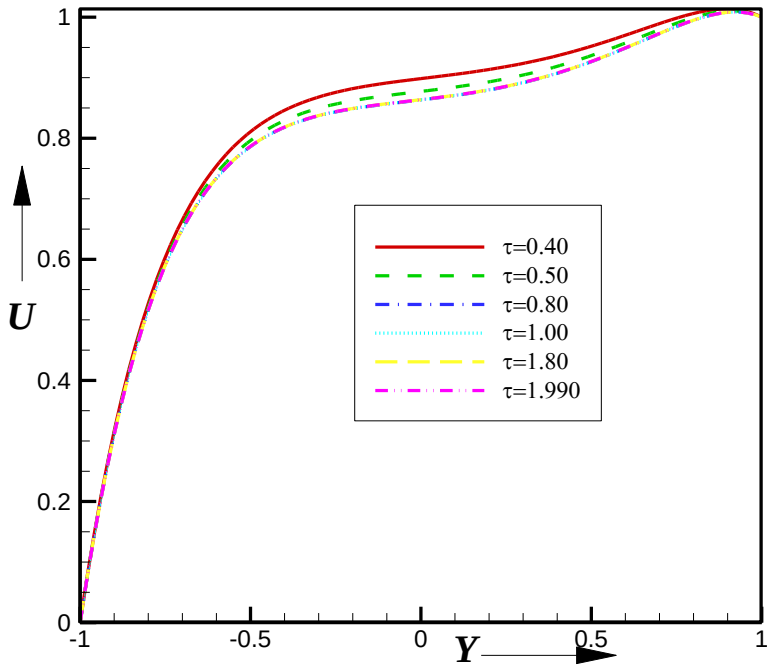

Fig. 3. Steady State solution for different values of τ

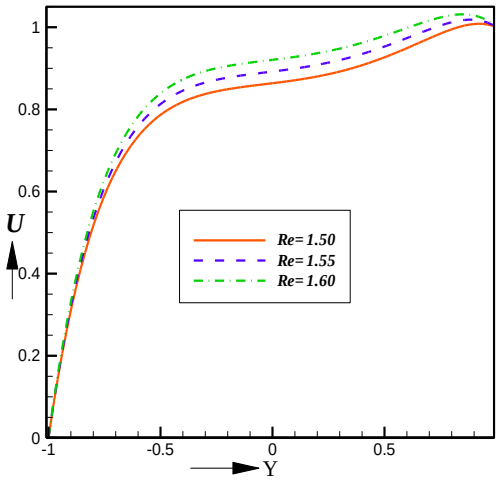

Fig. 4. Primary Velocity Profiles for different values of Reynolds Number R_e

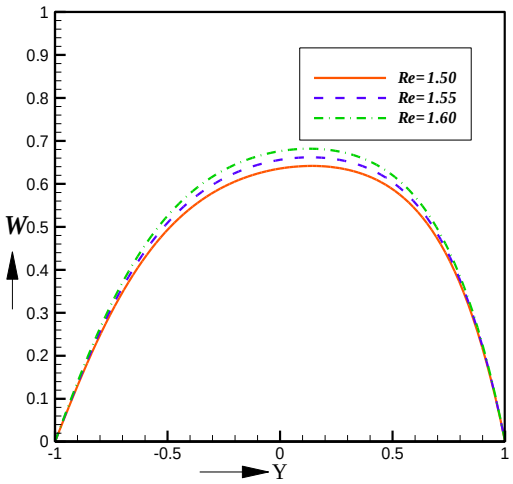

Fig. 5. Secondary Velocity Profiles for different values of Reynolds Number R_e

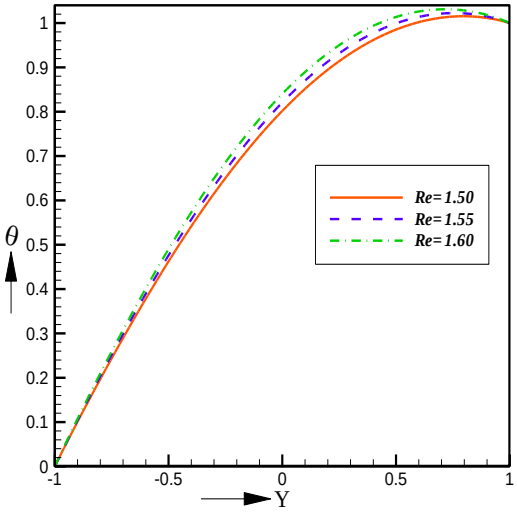

Fig. 6. Temperature Profiles for different values of Reynolds Number R_e

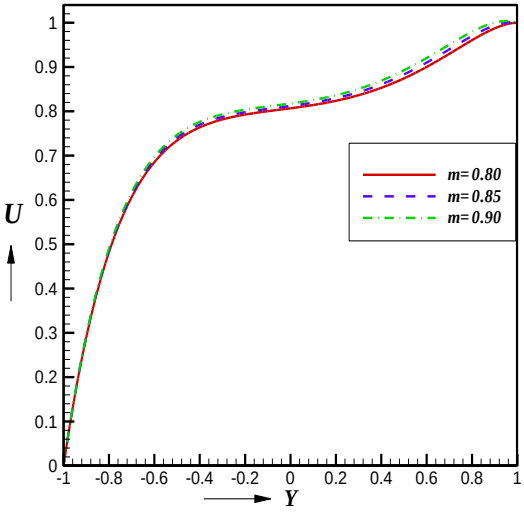

Fig. 7. Primary velocity Profiles for different values of Hall Parameter m

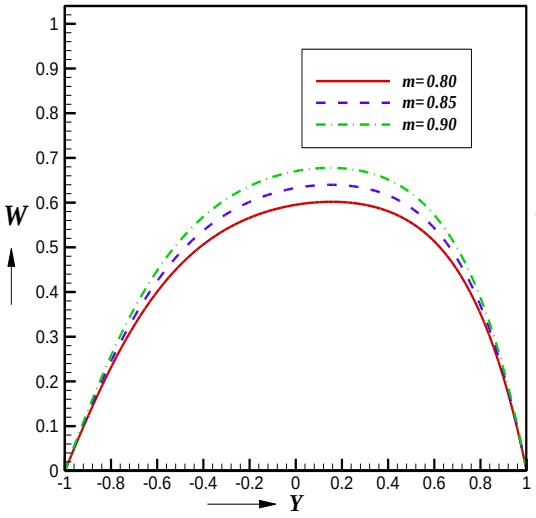

Fig. 8. Secondary velocity Profiles for different values of Hall Parameter m

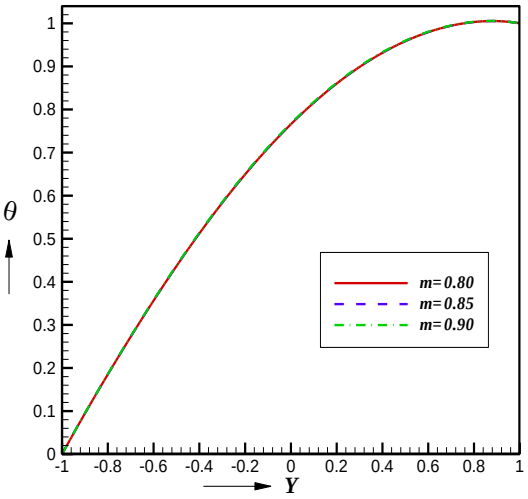

Fig. 9. temperature velocity Profiles for different values of Hall Parameter m

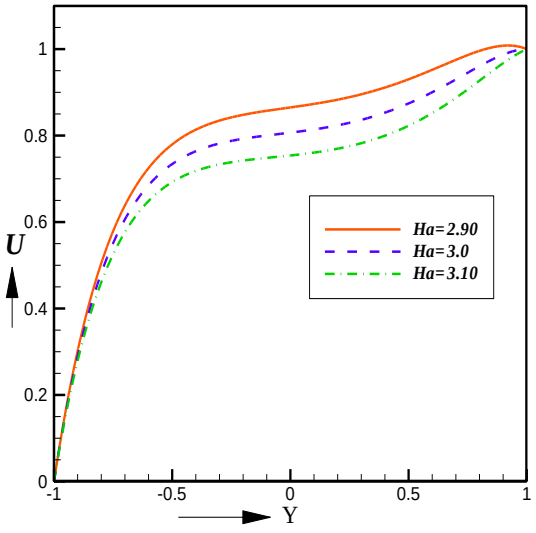

Fig. 10. Primary velocity Profiles for different values of Hall Parameter H_a

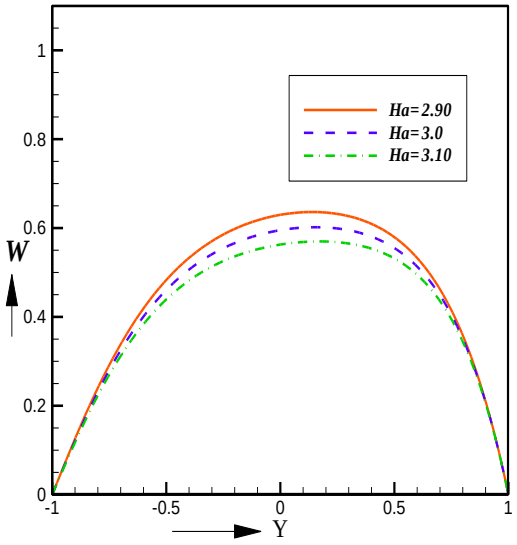

Fig. 11. Secondary velocity Profiles for different values of Hall Parameter H_a

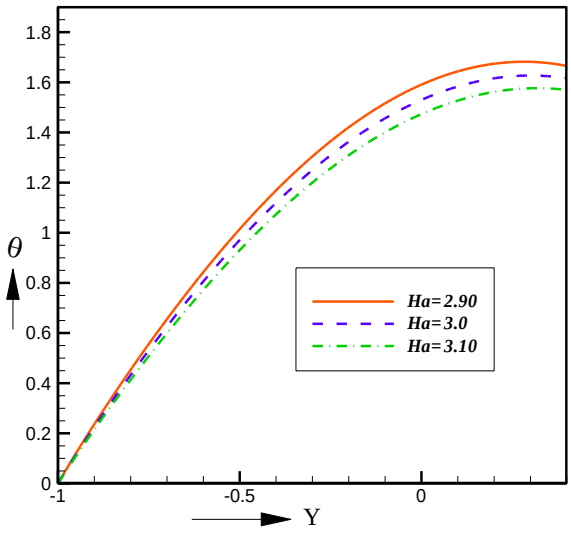

Fig. 12. Temperature Profiles for different values of Hall Parameter H_a

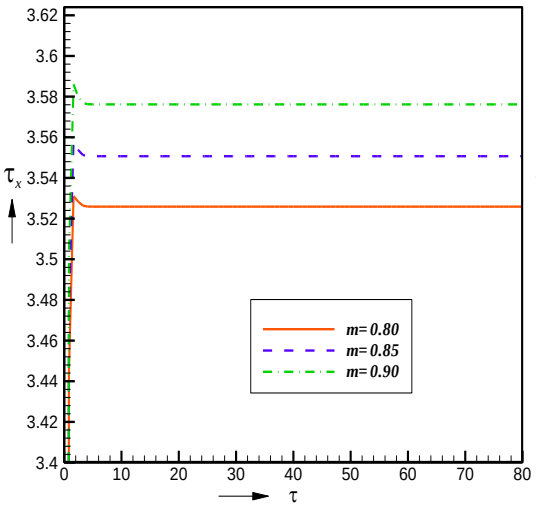

Fig. 13. Local Primary shear stress for different values of Hall Parameter m

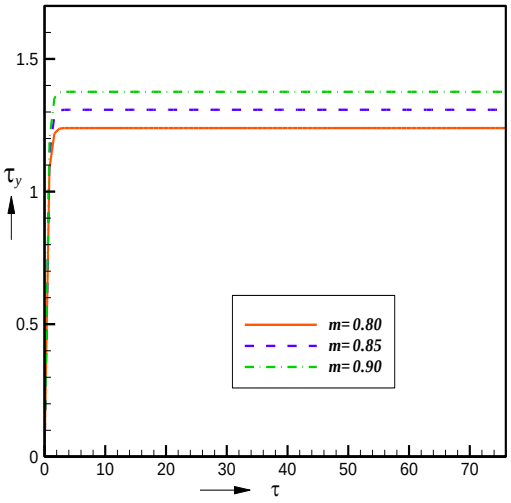

Fig. 14. Local Secondary shear stress for different values of Hall Parameter m

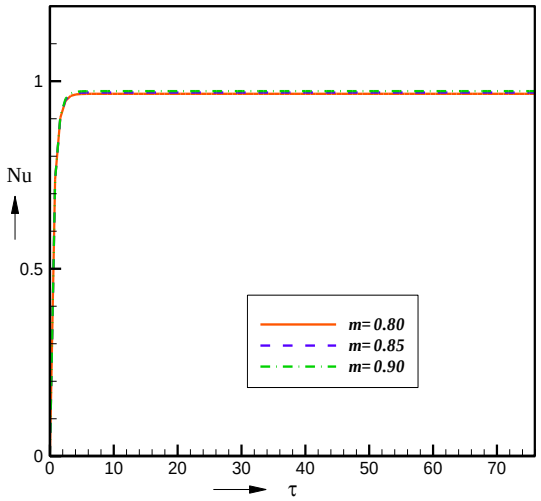

Fig. 15. Local Nusselt number for different values of Hall Parameter m

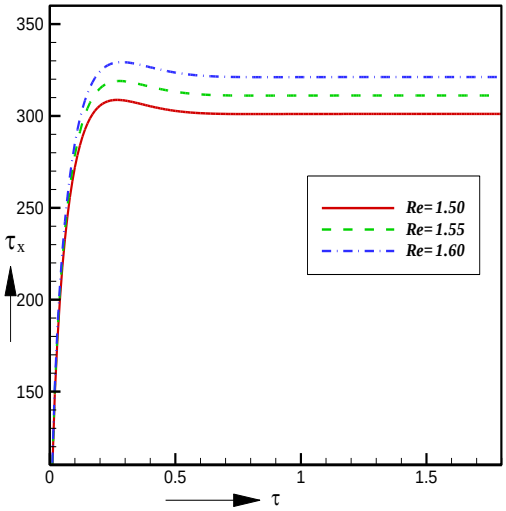

Fig. 16. Average Primary share stress for different values of Reynolds Number R_e

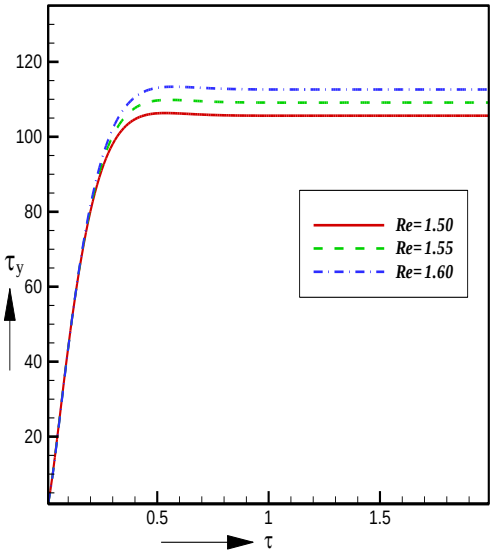

Fig. 17. Average secondary share stress for different values of Reynolds Number R_e

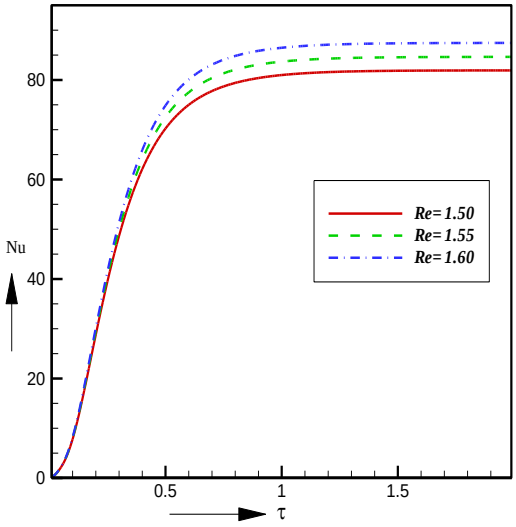

Fig. 18. Average Nusselt number for different values of Reynolds Number R_e

Results and Discussion

The results have been presented for various values of Reynolds number (R_e), Hall parameter (m) and Hartman number (H_a). Figs. 4-12 represented the velocity and temperature profile for different values of Reynolds number (R_e), Hall parameter (m) and Hartman number (H_a). Figs. 13-15 and 16-18 represented the Primary and secondary local and average shear stress and Nusselt number for different values of Reynolds number (R_e) and Hall parameter m. From this paper It has been observed that the primary velocity U, secondary velocity W, temperature distributions θ, primary average shear stress (τ_x), secondary average shear stress(τ_y) and average Nusselt number N_u have increased gradually as the rise of Reynold's number R_e as illustrated in Figs. 4 – 6 and 16-18 respectively. It has been observed that the primary velocity U and secondary velocity W increase with the increase of Hall parameter m as shown in Figs. 7-8 respectively. The primary local shear stress(τ_x), secondary local shear stress (τ_y) and local Nusselt number N_u have increased as the rise of Hall parameter m as illustrated in Figs. 13 – 15 respectively. The negligible effect of Hall parameter m on temperature distributions θ has been found with the increasing values of Hall parameter m shown in Figs. 8. The primary velocity U, secondary velocity W and temperature distributions θ decreases with the increase of Hartman number H_a as shown in Figs. 10-12 respectively.

Conclusion

In this work, MHD Casson fluid flow through a parallel plate is investigated by using explicit finite difference method for two dimensional Casson non-Newtonian fluid. The physical properties are discussed for different values of corresponding parameters. It has been observed that local and average primary and secondary shear stress and nusselt number gradually increase with the increases of Reynolds number and Hall Parameter.

References

Soundalgekar, V. M., Vighnesam, N.V. and Takhar, H.S. 1978. Hall and Ion-slip effects in MHD Couette flow with heat transfer. Institute of Electrical and Electronics Engineers (IEEE) Transactions on Plasma Science. **7**:178-182.

Attia, H. A. 2005. Unsteady Couette Flow with Heat transfer of a viscoelastic fluid considering the ion-slip. Journal of Korean Physical Society. **47:** 809-817.

Kanch, A. K. and Jana, R. N. 2001. Hall effects on Unsteady Couette Flow Under Boundary Approximation", Journal of Physical Science. **7**:74-86.

Sayed-Ahmed, M. E. and Attia, H. A. 1998. Magnetohydrodynamic Flow and Heat Transfer of a Non-Newtonian Fluid in an Eccentric Annulus. Canadian Journal of Physics. **76**:391-401.

Attia, H. A. 1998. Hall Current Effects on the Velocity and Temperature Fields of an Unsteady Hartmann Flow. Canadian Journal of Physics. **76**:739-746.

Attia, H. A. and Sayed-Ahmed, M. E. 2010. Transient MHD Couette Flow of a Casson Fluid between Parallel Plates with Heat Transfer. Italian Journal of pure and applied Mathematics. **27:**19-38.

Sayed-Ahmed, M. E., Attia, H. A. and Ewis, K. M. 2011. Time Dependent Pressure Gradient Effect on Unsteady MHD Couette Flow and Heat Transfer of a Casson Fluid. Canadian Journal of Physics. **3**:38-49.

Barishal University Journal Part 1, 6(1): 39-54 (2019) ISSN 2411-247X

LIMNOLOGICAL STUDIES OF CONSERVED MAN-MADE LAKE DURGASAGAR AT BARISHAL IN BANGLADESH AND ANGIOSPERMIC FLORAL DIVERSITY OF THE ADJACENT AREA

Md. Uzzal Hossain[*1], Laskar Ashikur Rahman[1], Mahmudul Hassan Suhag[2], Afroja Nasrin[3] and Md. Hasnat Jaman[4]

[1]*Department of Botany, University of Barishal, Bangladesh*
[2]*Department of Chemistry, University of Barishal, Bangladesh*
[3]*Department of Soil and Environmental Sciences, University of Barishal, Bangladesh*
[4]*Department of Geology and Mining, University of Barishal, Bangladesh*

Abstract

Limnological aspects Durgasagar (lake) and angiospermic floral diversity of the adjacent area were investigated during the year in 2019. A total of 153 angiosperms species belonging 127 genera and 63 families including exotic, wilds, cultivated and planted were recorded. Among the families, Asteraceae was the largest contributed family and represented 11 species followed by Solanaceae and Moraceae respectively. A total of 116 tree species and 126 terrestrial species were recorded. 38% of the recorded species has ethnomedicinal and pharmacological properties. Besides this, 29 fruits yielding species were also found in the survey. Physico-chemicals quality of air and water such as air temperature, humidity, water temperature, Secchi depth, pH, electrical conductivity (EC), total dissolved solids (TDS), dissolved oxygen (DO), Biological oxygen demand (BOD), alkalinity, PO_4-P and NO_3-N were studied and mean values of these are 24.63ºC, 64 % , 23.80ºC, 88.31 cm, 8.41, 66.72 µS/cm, 22.37 mg/l, 6.64 mg/l, 1.14 mg/l, 0.63 meq/l, 4.36 µg/l and 0.17 µg/l respectively. Frequent entrance of local people, tourists and weak infrastructure of boundary wall cause major damages to the vegetation of the area. Protection of biodiversity of this lake and adjacent area is essential to conserve this historically and man-made ecologically important lake.

Keywords: Limnology, Floral diversity, Physico-chemicals properties, Durgasagar and Barishal.

[*] *Corresponding author: muhossain@bu.ac.bd*

Introduction

Geographical location blesses Bangladesh with adequate freshwater reserve as a deltaic country and these include rivers, haors, baors, beels, lagoons, natural lakes, man-made lakes, ponds, floodplains and reservoirs. Among man-made lakes, Durgasagar locally known as Madhabpasha Dighi in Barishal is notable one and located at Madhabpasha under Babuganj upazilla in Barishal Sadar, existed between 22°76′N to 90°28'E having total area of about 2,500 hectares (Fig. 1). The lake is about 11 kilometers away from north of Barishal city. Besides this, in Bangladesh there are some artificial lake named Ramsagar in Dinajpur, Nilsagar in Nilphamari, Joysagar in Sirajganj and Dharmasagar in Cumilla. The words 'Sagar' (= sea) are the characteristic features of the aquatic ecosystems in many areas of Bangladesh and generally means large sized, perennial, pond-like water body and is a legendary of the Hindu landlord of the then Bengal under British India that has been purposefully dug-out for storing freshwater to meet the needs of domestic water use by the local people (Islam et al., 2012). Soil fertility, pH and humidity enrich the floral diversity of catchment areas of these lakes.

These aquatic ecosystems are legendary through their history, sustains age old and its interesting biodiversity makes it as a tourist spots. Due to increasing tendency of tourists and anthropogenic pressures, biodiversity of these protected areas like national parks, botanical gardens and eco-parks are decreasing rapidly (Rahman et al., 2012; Chowdhury et al., 2014). In order to conserve biodiversity of these protected areas, it is prerequisite to have precise data of present status of it. Taking into account of this prerequisite, Rahman and Hasan (1995); Uddin and Hassan (2010); Arefin et al., (2011); Dutta et al., (2014) and Rahaman et al., (2017) studied the angiospermic floral diversity of national parks named Bhawal (Gazipur), Lawachara (Maulvibazar), Satchari (Habiganj), Sitakunda (Chattogram) and Kuakata (Patuakhali) in Bnagladesh respectively whereas Rimi et al., (2013) assessed out the diversity of flora and fauna of Ramsagar at Dinajpur districts. But floral diversity particularly angiosperm diversity of remaining other conserved man-made lake is not check listed still. Furthermore, different exotic plant species has been planted for beautification purpose in the catchment area and these were listed (Hossain and Pasha, 2004).

Soil and water quality has a direct impact on both aquatic and terrestrial floral diversity of each area. In addition most of these man-made lakes are vulnerable so strongly by releasing excessive nutrients from decomposition of both liquid and solid wastes from tourists and local people that make the lakes eutrophic (Rahman et al.,

2017). Because of fresh water as an essential part of daily life, conservation of these freshwater resources is now national issue. For conservation and management strategy, a number of limnological investigations were carried out for Joysagar (Sirajganj), Nilsagar (Nilphamari), Ramsagar (Dinajpur) and Dharmasagar (Cumilla) by Nahar et al., (2010); Islam et al., (2012); Khondker et al., (2012); Bhuyan and Khondker (2017) respectively. But limnological aspects of Durgasar in Barishal is still not analyzed. Therefore, this study was conducted at Durgasagar and its adjacent area in Barishal with the following objectives: to assess physico-chemical qualities of water, to list angiospermic floral diversity, to evaluate the contribution of biodiversity to the local community and finally to depict a comprehensive management structure of ecotourism to protect the biodiversity.

Materials and Methods

Limnological study: The samples were collected mostly between 10:00 and 11:30 A.M. all the year round dividing it into four season named pre-monsoon, monsoon, post-monsoon and winter. Different portable field meters and chemicals purchased from Hanna Instruments, (Romania) were used to measure temperature (Model-HI98509), pH (Model-HI98107), electrical conductivity (Model-HI98304), alkalinity (Model-HI755), dissolved oxygen (Model-100T), humidity (Model-HI9564), total dissolved solids (Model-HI98301), PO_4-P (Model-5OT) and NO_3-N (Model-100T) *in-situ*. A Secchi disc was used to measure the depth of transparency. All physicals and chemicals analyses were performed according to mild modification of Khondker (1997).

Floral survey: The angiospermic floral survey was conducted during January to December, 2019 and twelve visits were done in each season of the year mentioned. The survey has covered all habitats of the study area including terrestrial and aquatic body. Maximum identification of the species observed was done at the field site and in case of confusion in authentic identification plant specimens were collected for herbarium preparation and photograph of each species was taken. Voucher specimens (Hyland, 1972) and photographs for species were preserved. Identification of the collected specimens were confirmed by consulting different floras such as Siddiqui et al., (2007); Ahmed et al., (2008-2009); Pasha and Uddin (2013). The updated nomenclature of the species was done according to Siddiqui et al., (2007) and Ahmed et al., (2008-2009).

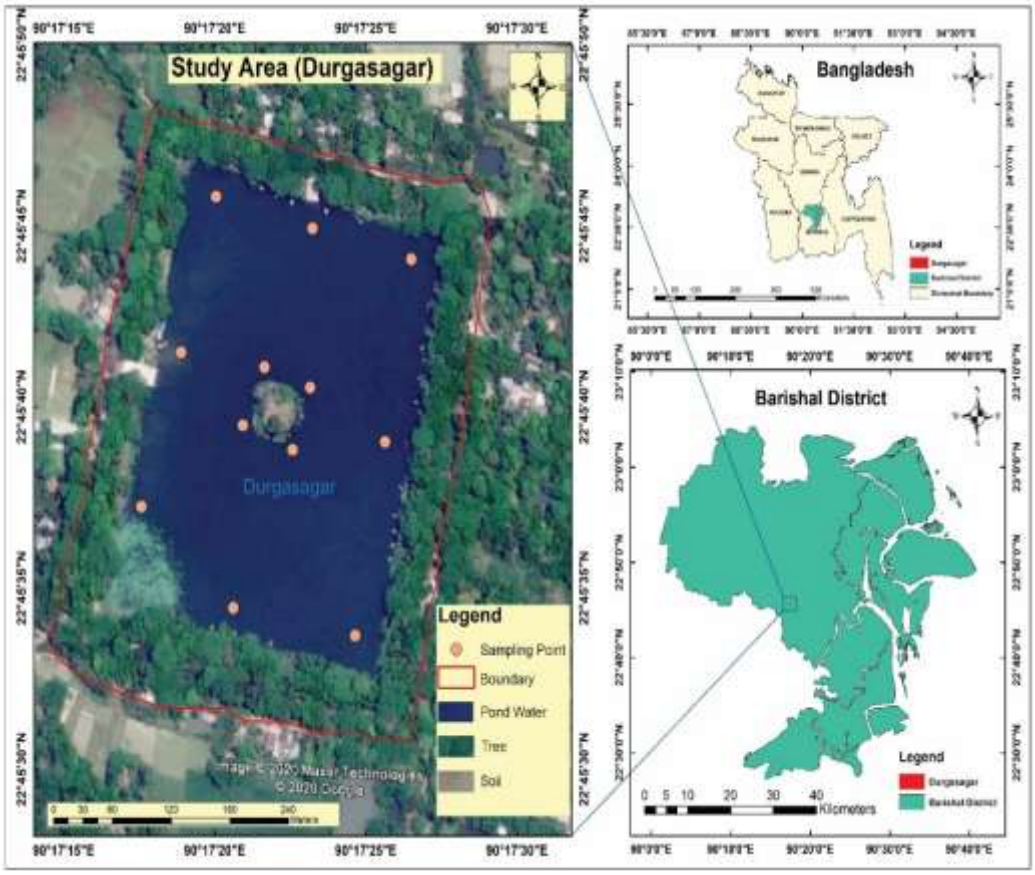

Fig 1. Location of study area of Durgasagar at Barishal, Bangladesh.

Results and Discussion

Limnological properties: All the physico-chemicals quality of water measured in present study are depicted in Table 1. Temperature of water plays a potential role on aquatic flora and fauna. Warm water contains less oxygen than that of cold water which may have fatal impact on aquatic flora and fauna. Mean water and air temperature were recorded 23.80°C and 24.63°C respectively (Table 1). Water temperature was found to be almost closed to the air temperature as desired with mild exceptions. Durve and Bal (1961); Oppenheimer et al., (1978); Chowdhury and Mazumder (1981) also found almost similar results in their previous study. During summer, a tendency of soaring up water temperature over surrounding air temperature was observed and this may be because of

thermal properties of water and air (Bhuiyan and Khondker, 2017). In this study, water temperature was slightly lower than that of air. In addition, Bhuiyan and Khondker (2017) also found same evidence in their study (Table 1). The mean of Secchi depth was recorded 88.31 cm (Table 1) which was highest among 5 man-made conserved lake in Bangladesh (Table 1). Total dissolved solids (TDS) represents the amount of total dissolved material in aquatic ecosystem and change in the runoff rate of surface chemicals from catchment area. High value of TDS makes the water turbid and results

Table 1. Comparative accounts of different physico-chemical parameters of five man-made lakes of Bangladesh (mean value).

Parameters	Unit	Name of the lake				
		Durgasagar (Present study)	Ramsagar (Khondker et al., 2012)	Nilsagar (Islam et al., 2012)	Joysagar (Nahar et al., 2010)	Dharmasagar (Bhuiyan and Khondker, 2017)
Air temp.	(°C)	24.63	20.48	19.27	29	32.58
Water temp.	(°C)	23.80	22.50	20.20	27.4	31.78
Secchi depth	(cm)	88.31	75	53	14.10	48
TDS	(mg/l)	22.37	10.66	32	-	130.44
Conductivity	(µS/cm)	66.72	73.66	126.33	109.20	502.50
p^H		8.41	6.73	6.96	7.4	7.67
DO	(mg/l)	6.64	7.99	11.64	-	7.59
BOD_5	(mg/l)	1.14	-	-	-	-
Alkalinity	(meq/l)	0.63	0.50	0.60	0.66	0.19
Humidity	(%)	64	-	-	-	-
NO_3-N	(µg/l)	0.17	0.007	0.19	97.5	41.95
PO_4-P	(µg/l)	4.36	3.16	6.80	79.87	4.61

- Represents not available

a fluctuation in abundance of aquatic flora and fauna. Average TDS was recorded 22.37 mg/l (Table 1) which is about two times more than Ramsagar (Khondker et al., 2012), but

about 1.5 times and 5.5 times lower than that of Nilsagar (Islam et al., 2012) and Dharmasagar (Bhuiyan and Khondker, 2017) respectively (Table 1).

In addition, Electrical conductivity (EC) indicates the concentration of electrolytes in the water body. The mean of EC was recorded 66.72 µS/cm (Table 1) which was lowest than those reported for Nilsagar (Islam et al., 2012), Ramsagar (Khondker et al., 2012), Joysagar (Nahar et al., 2012) and Dharmasagar (Bhuiyan and Khondker, 2017) (Table 1). pH of water describe the nature of water whether it is acidic, basic or neutral (Hasan and Bhuiyan, 2013). It regulates the biological environment and a sharp increase or decrease in pH of water body exerts a fatal impact on aquatic life. The average of pH of Durgasagar was 8.41 (Table 1). Compared to other studied water bodies it was found that Durgasagr is moderately alkaline in nature and just across of all the previous studies related to Nilsagar (Islam et al., 2012), Ramsagar (Khondker et al., 2012), Joysagar (Nahar et al., 2012) and Dharmasagar (Bhuiyan and Khondker, 2017) (Table 1). Dissolved oxygen (DO) is a regulator of metabolic process in aquatic ecosystem and an indicator of organic pollution (Hasan and Bhuiyan, 2013). Runoff of surface water with solid and/or liquid waste affects the DO of waterbody. The mean DO concentration recorded was 6.64 mg/l (Table 1) and lowest among the other compared lakes named Nilsagar (Islam et al., 2012), Ramsagar (Khondker et al., 2012), Joysagar (Nahar et al. 2012) and Dharmasagar (Bhuiyan and Khondker, 2017) (Table 1).

Taxonomic inventory and documentation of plant species: A total of 153 angiosperm species belonging to 127 genera and 63 families were recorded from the Durgasagar area (Table 2 and Table 4).

Table 2. List of angiospermic flora recorded from Durgasagar, Barishal

Serial	Scientific name	Local name	Family	Habitat	Habit	Medicinal value	Status
1.	*Abelmoscus moschata* (L.) Medic	Muskadana	Malvaceae	Terrestrial	Herb	No	Wild
2.	*Acacia auriculiformis* A. Cunn. ex Benth.& Hook.	Akashmoni	Mimosaceae	Terrestrial	Tree	No	Planted
3.	*Achyranthes aspera* L.	Apang	Amaranthaceae	Terrestrial	Herb	Yes	Wild
4.	*Acmella ciliata* (Kunth) Cass	Nakful	Asteraceae	Terrestrial	Herb	Yes	Wild
5.	*Actinoscirpus grossus* (L.f.) Goetgh & D.A. Simpson	Kesur	Cyperaceae	Amphibian	Herb	No	Wild
6.	*Aegle marmelos* (L.) Correa	Bell	Rutaceae	Terrestrial	Tree	Yes	Planted
7.	*Ageratum conyzoides* (L.) L.	Mukhra	Asteraceae	Terrestrial	Herb	Yes	Wild
8.	*Albizia lebbek* (L.) Benth.	Kalo sirish	Mimosaceae	Terrestrial	Tree	No	Planted
9.	*Albizia procera* (Roxb.) Benth.	Sada sirish	Mimosaceae	Terrestrial	Tree	No	Planted
10.	*Albizia richardiana* (Voigt) King & Prain	Gagon sirish	Mimosaceae	Terrestrial	Tree	No	Planted
11.	*Albizia saman* (Jacq.) Merr.	Raintree	Mimosaceae	Terrestrial	Tree	No	Planted
12.	*Alocasia acuminata* (Schott.) G. Don	Bonkochu	Araceae	Amphibian	Herb	Yes	Wild
13.	*Alstonia scholaris* (L.) R. Br.	Chatim	Apocynaceae	Terrestrial	Tree	Yes	Planted
14.	*Alternanthera phyloxeroides* (Mart.) Griseb.	Helenchna	Amaranthaceae	Amphibian	Herb	No	Wild
15.	*Amaranthus tricolor* L.	Lalshak	Amaranthaceae	Terrestrial	Herb	No	Cultivated
16.	*Annona reticulata* L.	Nona	Annonaceae	Terrestrial	Tree	No	Planted
17.	*Aphanamixis polystachya* (Wall.) R. Parker	Raina	Meliaceae	Terrestrial	Tree	Yes	Wild
18.	*Aponogeton crispus* Thunb	Gechu	Aponogetonaceae	Aquatic	Herb	No	Wild
19.	*Ardisia solanacea* (Poir.) Roxb.	Bonjam	Primulaceae	Terrestrial	Shrub	No	Wild
20.	*Areca catechu* L.	Supari	Arecaceae	Terrestrial	Tree	No	Planted
21.	*Artocarpus heterophyllus* Lam.	Kathal	Moraceae	Terrestrial	Tree	No	Planted
22.	*Artocarpus lakoocha* Buch.-Ham.	Deuya	Moraceae	Terrestrial	Tree	No	Planted
23.	*Averrhoa carambola* L.	Kamranga	Oxalidaceae	Terrestrial	Tree	No	Planted
24.	*Axonopus compressus* (Sw.) P.Beauv.	Balla ghash	Poaceae	Terrestrial	Herb	No	Wild
25.	*Azadirachta indica* A. Juss.	Neem	Meliaceae	Terrestrial	Tree	Yes	Planted
26.	*Bambusa bambos* (L.) Voss	Katabash	Poaceae	Terrestrial	Herb	No	Planted
27.	*Bischofia javanica* Blume	Kainjal	Euphorbiaceae	Terrestrial	Tree	Yes	Wild
28.	*Blumea lacera* (Burm.f.) DC.	Baro-Kuksim	Asteraceae	Terrestrial	Herb	No	Wild
29.	*Bombax ceiba* L.	Shimul	Bombacaceae	Terrestrial	Tree	No	Planted

Serial	Scientific name	Local name	Family	Habitat	Habit	Medicinal value	Status
30.	*Borassus flabellifer* L.	Tal	Arecaceae	Terrestrial	Tree	No	Planted
31.	*Breynia vitis-idaea* (Burm.f.) C. E. C. Fisher	Juli	Phyllanthaceae	Terrestrial	Shrub	Yes	Wild
32.	*Capsicum annuum* L.	Langka	Solanaceae	Terrestrial	Herb	Yes	Cultivated
33.	*Cardiospermum halicacabum* L.	Latafutki	Menispermaceae	Terrestrial	Climber	Yes	Wild
34.	*Carica papaya* L.	Pepe	Caricaceae	Terrestrial	Herb	Yes	Cultivated
35.	*Cassia fistula* L.	Badorlathi	Caesalpiniaceae	Terrestrial	Tree	Yes	Planted
36.	*Senna occidentalis* L.	Kolkasunda	Caesalpiniaceae	Terrestrial	Herb	Yes	Wild
37.	*Centella asiatica* (L.) Urb.	Thnakuni	Apiaceae	Terrestrial	Herb	Yes	Wild
38.	*Ceratophyllum demersum* L.	Sheola	Ceratophyllaceae	Aquatic	Herb	No	Wild
39.	*Ceratophyllum submersum* L.	Katajhanji	Ceratophyllaceae	Aquatic	Herb	No	Wild
40.	*Chromolaena odorata* (L.) King & Robinson	Assamlata	Asteraceae	Terrestrial	Herb	No	Wild
41.	*Chrysopogon aciculatus* (Retz.) Trin.	Premkata	Poaceae	Terrestrial	Herb	No	Wild
42.	*Citrus aurantifolia* (Christm.) Sw.	Patilebu	Rutaceae	Terrestrial	Shrub	No	Cultivated
43.	*Citrus grandis* Merr.	Batabilebu	Rutaceae	Terrestrial	Shrub	Yes	Cultivated
44.	*Clerodendrum viscosum* Vent.	Vait	Verbenaceae	Terrestrial	Herb	Yes	Wild
45.	*Coccinea grandis* (L.) Voigt	Telakucha	Cucurbitaceae	Terrestrial	Climber	Yes	Wild
46.	*Cocos nucifera* L.	Narikal	Arecaceae	Terrestrial	Tree	No	Cultivated
47.	*Codiaeum variegatum* (L.) A. Juss.	Patabahar	Euphorbiaceae	Terrestrial	Shrub	No	Planted
48.	*Coix lacryma-jobi* L.	Kaich	Poaceae	Amphibian	Herb	No	Wild
49.	*Colocasia esculenta* (L.) Schott	Janglikachu	Araceae	Amphibian	Herb	Yes	Wild
50.	*Commelina bengalensis* L.	Kanshira	Commelinaceae	Amphibian	Herb	No	Wild
51.	*Cordia myxa* L.	Bahubora	Boraginaceae	Terrestrial	Tree	No	Wild
52.	*Coriandrum sativum* L.	Dhonia	Apiaceae	Terrestrial	Herb	No	Cultivated
53.	*Costus speciosus* (Koenig ex Retz.) Smith	Keumul	Costaceae	Terrestrial	Herb	Yes	Wild
54.	*Cucurbita maxima* Duchesne	Kodu	Cucurbitaceae	Terrestrial	Herb	No	Cultivated
55.	*Curcuma longa* L.	Haldi	Zingiberaceae	Terrestrial	Herb	Yes	Cultivated
56.	*Curcuma zedoaria* (Christm.) Rosc.	Shati	Zingiberaceae	Terrestrial	Herb	Yes	Wild
57.	*Cynodon dactylon* (L.) Pers.	Durbaghash	Poaceae	Terrestrial	Herb	Yes	Wild
58.	*Cyperus rotandus* L.	Muthagash	Cyperaceae	Amphibian	Herb	No	Wild
59.	*Dalbergia sissoo* Roxb. ex DC.	Sisso	Fabaceae	Terrestrial	Tree	No	Cultivated
60.	*Delonix regia* (Hook.) Raf.	Krisnochura	Caesalpiniaceae	Terrestrial	Tree	No	Cultivated

Serial	Scientific name	Local name	Family	Habitat	Habit	Medicinal value	Status
61.	*Desmodium gangeticum* (L.) DC.	Shalpani	Fabaceae	Terrestrial	Herb	Yes	Wild
62.	*Dillenia indica* L.	Chalta	Dilleniaceae	Terrestrial	Tree	No	Planted
63.	*Dioscorea bulbifera* L.	Bonalu	Dioscoreaceae	Terrestrial	Climber	No	Wild
64.	*Diospyros peregrina* (Gaertn.) Gurke	Deshigab	Ebnaceae	Terrestrial	Tree	No	Wild
65.	*Dolichos lablab* L.	Sheem	Fabaceae	Terrestrial	Climber	No	Cultivated
66.	*Eclipta prostrata* (L.) L.	Kalokeshi	Asteraceae	Terrestrial	Herb	Yes	Wild
67.	*Eichhornia crassipes* (Mart.) Sloms	Kachuripana	Pontederiaceae	Aquatic	Herb	No	Wild
68.	*Enhydra fluctuans* Lour.	Helencha	Asteraceae	Aquatic	Herb	No	Wild
69.	*Ficus benghalensis* L.	Jhuribot	Moraceae	Terrestrial	Tree	No	Wild
70.	*Ficus hispida* L.f.	Kakdumur	Moraceae	Terrestrial	Tree	No	Wild
71.	*Ficus racemosa* L.	Jaggodumur	Moraceae	Terrestrial	Tree	Yes	Wild
72.	*Ficus religiosa* L.	Aswath	Moraceae	Terrestrial	Tree	Yes	Wild
73.	*Ficus rumphii* Blume	Gai Aswath	Moraceae	Terrestrial	Tree	No	Wild
74.	*Garcinia cowa* Roxb. ex Dc.	Kowa	Ebnaceae	Terrestrial	Tree	No	Planted
75.	*Glycosmis arborea* (Roxb.) DC.	Matkila	Rutaceae	Terrestrial	Shrub	Yes	Wild
76.	*Hibiscus rosa-sinensis* L.	Roktajaba	Malvaceae	Terrestrial	Shrub	No	Planted
77.	*Holarrhena antidysenterica* (L.) Wall. ex Decne.	Kurchi	Apocynaceae	Terrestrial	Tree	Yes	Planted
78.	*Ipomoea aquatica* Forssk.	Kalmi	Convolvulaceae	Amphibian	Herb	No	Wild
79.	*Ipomoea fistulosa* Mart. ex Choisy	Dholkalmi	Convolvulaceae	Terrestrial	Herb	Yes	Wild
80.	*Ixora coccinea* L.	Lalraggon	Rubiaceae	Terrestrial	Shrub	No	Planted
81.	*Justicia gendarussa* Burm.	Jagatmadan	Acanthaceae	Terrestrial	Herb	Yes	Wild
82.	*Lagenaria vulgaris* Ser.	Laow	Cucurbitaceae	Terrestrial	Herb	No	Cultivated
83.	*Lagerstroemia speciose* (L.) Pers.	Katajarul	Lythraceae	Terrestrial	Tree	No	Planted
84.	*Leea guineensis* G. Don	Phupharia	Vitaceae	Terrestrial	Shrub	No	Wild
85.	*Lepisanthes rubiginosa* (Roxb.) Leenh	Kakjam	Sapindaceae	Terrestrial	Shrub	No	Wild
86.	*Leucas aspera* (Willd.) Link	Dondokalas	Lamiaceae	Terrestrial	Herb	Yes	Wild
87.	*Lippia alba* (Mill.) N. E. Br. ex Britton & P.Wilson	Bonpisach	Verbenaceae	Terrestrial	Herb	No	Wild
88.	*Ludwigia adscendens* (L.) H. Hara	Kesordam	Onagraceae	Aquatic	Herb	No	Wild
89.	*Ludwigia octovalvis* (Jacq.) P. H. Raven	Bhuikura	Onagraceae	Amphibian	Herb	No	Wild
90.	*Ludwigia perennis* L.	Bonlobongo	Onagraceae	Amphibian	Herb	No	Wild
91.	*Luffa cylindrica* (L.) M. Roem.	Dhundal	Cucurbitaceae	Terrestrial	Climber	No	Cultivated
92.	*Lycopersicon esculentum* Mill.	Begoon	Solanaceae	Terrestrial	Herb	No	Cultivated

Serial	Scientific name	Local name	Family	Habitat	Habit	Medicinal value	Status
93.	*Malvaviscus arboreus* Cav.	Morichjoba	Malvaceae	Terrestrial	Shrub	No	Planted
94.	*Mangifera indica* L.	Aam	Anacardiaceae	Terrestrial	Tree	No	Planted
95.	*Melia azedarach* L.	Ghoraneem	Meliaceae	Terrestrial	Tree	Yes	Planted
96.	*Mikania cordata* (Burm.f.) B. L. Rob.	Rayotlata	Asteraceae	Terrestrial	Climber	Yes	Wild
97.	*Musa sapientum* L.	Kancha Kola	Musaceae	Terrestrial	Herb	No	Cultivated
98.	*Mussaenda erythrophylla* Scumach. & Thonn.	Nagballi	Rubiaceae	Terrestrial	Shrub	No	Planted
99.	*Nelumbo nucifera* Gaertn.	Poddmo	Nelumbonaceae	Aquatic	Herb	No	Planted
100.	*Neolamerckia cadamba* (Roxb.) Bosser	Kodom	Rubiaceae	Terrestrial	Tree	No	Planted
101.	*Nymphaea rubra* Roxb. ex Andr.	Lalshapla	Nymphaeaceae	Aquatic	Herb	No	Planted
102.	*Nymphoides cristata* (Roxb.) Kuntze	Chandmala	Menyanthaceae	Aquatic	Herb	No	Wild
103.	*Oroxylum indicum* (L.) Kurz	Kanaidhingi	Bignoniaceae	Terrestrial	Tree	Yes	Wild
104.	*Otellia alismoides* (L.) Pers.	Panikola	Hydrocharitaceae	Aquatic	Herb	No	Wild
105.	*Oxalis corniculata* L.	Aamrul	Oxalidaceae	Terrestrial	Herb	Yes	Wild
106.	*Peperomia pellucida* (L.) H. B. & K.	Luchipata	Piperaceae	Terrestrial	Herb	No	Wild
107.	*Persicaria hydropiper* (L.) Spach	Bishkatali	Polygonaceae	Amphibian	Herb	Yes	Wild
108.	*Phoenix sylvestris* (L.) Roxb.	Khejur	Arecacea	Terrestrial	Tree	No	Planted
109.	*Phyllanthus reticulatus* Poir. In Lamn.	Pankushi	Phyllanthaceae	Terrestrial	Shrub	No	Wild
110.	*Physalis minima* L.	Bontepari	Solanaceae	Terrestrial	Herb	No	Wild
111.	*Pilea microphylla* (L.) Liebrn.	Lotamorich	Urticaceae	Terrestrial	Herb	No	Wild
112.	*Piper longum* L.	Pipul	Piperaceae	Terrestrial	Herb	Yes	Wild
113.	*Piper nigrum* L.	Golmorich	Piperaceae	Terrestrial	Climber	Yes	Wild
114.	*Piper sylvestre* Lam.	Rupali pipul	Piperaceae	Amphibian	Herb	No	Wild
115.	*Polyalthia longifolia* (Sonn.) Thwaites	Debdaru	Annonaceae	Terrestrial	Tree	No	Planted
116.	*Potamogeton crispus* L.	Kokra	Potamogetonaceae	Aquatic	Herb	No	Wild
117.	*Pouzolzia zeylanica* (L.) Benn.	Kullaroki	Urticaceae	Amphibian	Herb	No	Wild
118.	*Raphanus sativus* (L.) Domin	Mula	Brassicaceae	Terrestrial	Herb	No	Cultivated
119.	*Rorippa indica* (L.) Hiern.	Bonsorisha	Brassicaceae	Amphibian	Herb	No	Wild
120.	*Rosa involucrata* Roxb. ex Lindl.	Golap	Rosaceae	Terrestrial	Shrub	No	Cultivated
121.	*Saccharum spontaneum* L.	Kashful	Poaceae	Terrestrial	Herb	No	Wild
122.	*Salvia plebeia* R. Br.	-	Lamiaceae	Terrestrial	Herb	No	Wild
123.	*Scoparia dulcis* L.	Bondhone	Scrophulariaceae	Terrestrial	Herb	Yes	Wild
124.	*Sida cordifolia* L.	Berella	Malvaceae	Terrestrial	Herb	Yes	Wild

Serial	Scientific name	Local name	Family	Habitat	Habit	Medicinal value	Status
125.	*Sida rhombifolia* L.	Sadaberella	Malvaceae	Terrestrial	Herb	No	Wild
126.	*Smilax macrophylla* Roxb.	Kumarilata	Smilacaceae	Terrestrial	Climber	Yes	Wild
127.	*Solanum americanum* Mill.	Titbegoon	Solanaceae	Terrestrial	Herb	No	Wild
128.	*Solanum indicum* L.	Katabegoon	Solanaceae	Terrestrial	Shrub	Yes	Wild
129.	*Solanum melongena* L.	Begoon	Solanaceae	Terrestrial	Herb	No	Cultivated
130.	*Solanum nigrum* L.	Unresolved	Solanaceae	Terrestrial	Herb	Yes	Wild
131.	*Solanum torvum* Sw.	Bunobegoon	Solanaceae	Terrestrial	Shrub	No	Wild
132.	*Solanum xanthocarpum* Schard. H & Wendl.	Kantikari	Solanaceae	Terrestrial	Herb	Yes	Wild
133.	*Spondias pinnata* (L.f.) Kurz	Aamra	Anacardiaceae	Terrestrial	Tree	No	Planted
134.	*Stephania japonica* (Thunb.) Miers	Akondilata	Menispermaceae	Terrestrial	Climber	Yes	Wild
135.	*Streblus asper* Lour.	Sheora	Moraceae	Terrestrial	Tree	Yes	Wild
136.	*Swietenia mahagoni* Jacq.	Mehogani	Meliaceae	Terrestrial	Tree	No	Planted
137.	*Symplocos racemosa* Roxb.	Loodpipul	Symplocaceae	Terrestrial	Tree	Yes	Wild
138.	*Synedrella nodiflora* (L.) Gaertn.	Sindrella	Asteraceae	Terrestrial	Herb	Yes	Wild
139.	*Syngonium podophyllum* Schott.	Hongsapod	Araceae	Terrestrial	Climber	No	Wild
140.	*Syzygium cumini* (L.) Skeels	Kalojam	Myrtaceae	Terrestrial	Tree	No	Planted
141.	*Syzygium fruticosum* DC.	Phutijam	Myrtaceae	Terrestrial	Tree	No	Wild
142.	*Syzygium jambos* (L.) Alston	Golabjam	Myrtaceae	Terrestrial	Tree	No	Planted
143.	*Syzygium malaccense* (L.) Merr. & L. M. Perry	Jamrul	Myrtaceae	Terrestrial	Tree	No	Planted
144.	*Tagetes erecta* L.	Gadha	Asteraceae	Terrestrial	Herb	Yes	Cultivated
145.	*Tamarindus indica* L.	Tetul	Caesalpiniaceae	Terrestrial	Tree	Yes	Planted
146.	*Terminalia arjuna* (Roxb. ex DC.) Wight & Arn.	Arjun	Combretaceae	Terrestrial	Tree	Yes	Planted
147.	*Tiliacora acuminata* (Lam.) Hook.f. & Thom.	Bhaglata	Menispermaceae	Terrestrial	Climber	Yes	Wild
148.	*Typha elephantiana* Roxb.	Hogla	Typhaceae	Amphibian	Herb	No	Wild
149.	*Urena lobata* L.	Bonokra	Malvaceae	Terrestrial	Herb	No	Wild
150.	*Vernonia cinerea* (L.) Less.	Shiallata	Asteraceae	Terrestrial	Herb	Yes	Wild
151.	*Vigna unguiculata var. sesquipedalis* (L.) Verdc.	Barboti	Fabaceae	Terrestrial	Climber	No	Cultivated
152.	*Wedelia chinensis* (Osbeck) Merr.	Bhimraj	Asteraceae	Terrestrial	Herb	Yes	Wild
153.	*Xanthosoma violaceum* Schott.	Dudhkachu	Araceae	Amphibian	Herb	Yes	Wild

- Represents not available

Among the families, Asteraceae contributed highest number of species (11 species) followed by Solanaceae (9 species), Moraceae (8 species), Malvaceae (6 species) and remaining other 119 angiosperm species were from different families (Table 2 and Table 3). Rimi et al., (2013) found 232 angiosperm species from Ramasagar area of Dinajpur among which Asteraceae contributed highest number of species (11 species) followed by Poaceae (29 species) (Table 3).

Table 3. List of comparative dominant families of two man-made lakes.

Family	Name of the lake	
	Durgasagar (Present study)	Ramsagar (Rimi et al., 2013)
Asteraceae	11	11
Solanaceae	9	9
Moraceae	8	6
Malvaceae	6	5
Poaceae	6	29
Mimosaceae	5	9
Araceae	4	3
Arecaceae	4	-
Caesalpiniaceae	4	8
Cucurbitaceae	4	1
Fabaceae	4	5
Meliaceae	4	5
Myrtaceae	4	6
Piperaceae	4	1
Rutaceae	4	3

- Represents not available

Moreover, among 153 species, 126 species are terrestrial in habitat, followed by amphibian and aquatic (Table 4). Plant species were classified into four different habit groups and among these 77 belong to herb, 48 to tree, 16 to shrub and 12 to climber. Rimi et al., (2013) also found that herb contributed maximum number (81 species) among 232 angiosperms followed by trees, shrubs and climbers consecutively (Table 5).

Table 4. Over view of angiospermic floral diversity of Duragasagar.

Categories	Investigated	Categories	Investigated
Number of family	63	Tree	48
Number of genus	127	Medicinal	58
Number of species	153	Nonmedicinal	95
Terrestrial	126	Timbers	13
Amphibian	16	Fruits	29
Aquatic	11	Ornamental	21
Climber	12	Cultivated and planted	61
Herb	77	Wild	92
Shrub	16	Weeds	83

Furthermore, about 38% of the 153 angiosperms species have ethnomedicinal and pharmacological potentiality (Table 2 and Table 6), whereas Rimi et al., (2013) found nearly 32% of the total angiospermic species as ethnomedicinal and pharmacological (Table 6

Table 5. Comparative plant species distribution of two man-made lakes area according habit.

Habit	Name of the lake	
	Durgasagar (Present study)	Ramsagar (Rimi et al., 2013)
Herb	77	81
shrub	16	61
Tree	48	78
Climber	12	12

Table 6. Comparative diversity (angiosperms) distribution of two man-made lake areas.

Categories	Name of the lake	
	Durgasagar (Present study)	Ramsagar (Rimi et al., 2013)
Timber plants	13	28
Fruits plants	29	19
Medicinal plants	58	75
Ornamental plants	21	6
Cultivated and planted plant	61	18
Wild plants	92	-
Weeds	83	57

- Represents not available

In the category of timber yielding species, Ramsagar contributed nearly 1.5 times than Durgasagar, but in case of fruit yielding species Durgasagar contributed almost 2.5 times than Ramsagar (Table 6). The reason for this difference may be that in Durgasagar about 3.5 times more planted species were found than that of found in Ramsagar. In addition, almost 3.5 times more ornamental and 1.6 times more weeds were recorded than that of Ramsagar (Table 6).

Study of physico-chemical quality of water and angiospermic floral diversity of adjacent area of Durgasagar is very important step for conservation and management. There is no significance of conservation of the biological resources including flora and fauna without assessment and documentation. The contribution of floral and faunal diversity to the local people in the study area was mainly for fruits, ethnomedicinal purpose and fodder. But increasing population pressure initiates the deforestation and deterioration. It is time to conserve this aquatic catchment treasure through increasing surveillance, annual development work and management plan, constructing well established demarcation boundary and miscellaneous works.

Acknowledgements

Authors would like to thank Research Cell, University of Barishal for financial support (BU/Reg./Research (Academic)/2018-19/424/1527(21)). Furthermore authors are grateful to Department of Botany, University of Barishal for all kind of technical supports.

References

Ahmed Z. U., Z. N. T. Begum, M. A. Hassan, M. Khondker, S. M. H. Kabir, M. Ahmad, A. T. A. Ahmed, A. K. A. Rahman and E. U. Haque (Eds). 2008 - 2009. Encyclopedia of Flora and Fauna of Bangladesh. **Vol**. (6-10). Angiosperms; Dicotyledons. Asiat. Soc. Bangladesh, Dhaka.

Ahmed Z. U., Z. N. T. Begum, M. A. Hassan, M. Khondker, S. M. H. Kabir, M. Ahmad, A. T. A. Ahmed, A. K. A. Rahman and E.U. Haque (Eds). 2008 - 2009. Encyclopedia of Flora and Fauna of Bangladesh. **Vol**. (12). Angiosperms; Dicotyledons. Asiat. Soc. Bangladesh, Dhaka.

Arefin M. K., M. M. Rahman, M. Z. Uddin and M. A. Hassan. 2011. Angiosperm flora of Satchari national park, Habiganj, Bangladesh. Bangladesh J. Plant Taxon. **18**(2): 117-140.

Banerjee S. M. 1967. Water quality and soil conditions of fish ponds in some states of India in relation to fish production. Indian J. Fish. **14**: 115-144.

Bhuiyan M. A. H. and M. Khondker. 2017. Seasonal variation of water quality of Dharma sagar of Comilla city. Bangladesh J. Bot. **46**(3): 971-978.

Chowdhury S. H and A. Mazumder. 1981. Limnology of Lake Kaptai. I. Physico-chemical features. Bangladesh J. Zool. **9**(1): 59-72.

Chowdhury M. S. H., N. Nazia, S. Izumiyama, N. Muhammed and M. Koike. 2014. Patterns and extent of threats to the protected areas of Bangladesh: The need for a relook at conservation strategies. The international journal of protected areas and conservation. **20**(1): 91-104.

Durve V. S. and D. V. Bal. 1961. Hydrobiology of the Kelwa Back Water and adjoining sea. J. Univ. Bombay. **29**(3-5): 39-48.

Dutta S., M. K. Hossain, M.A. Hossain and P. Chowdhury. 2014. Floral diversity of Sitakunda botanical garden and eco-park in Chittagong, Bangladesh. Indian J. Trop. Biodiv. **22**(2): 106-118.

Hasan M. K. and M. A. H. Bhuiyan. 2013. A comparative study of water quality in the peripheral rivers of Dhaka City. Indian J. Human. **3**(3): 1-9.

Hossain M. K. and M. K. Pasha. 2004. An account of the exotic flora of Bangladesh. Journal of forestry and environment. **2**: 99-115.

Hyland B. P. M. 1972. A technique for collecting botanical specimens in rain forest. Flora Malesiana Bulletin. **26**: 2038-2040.

Islam M. S., M. A. Gani, M. A. Alfasane and M. Khondker. 2012. Limnological notes on Nilsagar, Nilphamari, Bangladesh. Dhaka Univ. J. Biol. Sci. **22**(1): 75-78.

Khondker M., M. A. Alfasane, M. A. Gani and M. S. Islam. 2012. Limnological notes on Ramsagar, Dinajpur, Bangladesh. Bangladesh J. Bot. **41**(1): 119-121.

Khondker M. 1997. Baboharic limnology O mithapanir jalaj udvider parichiti. Dhaka University, Bangladesh. 1-251pp.

Nahar K., M. Khondker and M. Sultana. 2010. Seasonal succession and diversity of benthic diatom of two wetland ecosystems of Bangladesh. Bangladesh J. Bot. **39**(1): 29-36.

Oppenheimer J. R., M. G. Ahmed, K. A. Huq, A. K. M. A. Alam, K. M. S. Aziz, S. Ali and A. S. M. M. Haque. 1978. Limnological studies of three ponds in Dhaka, Bangladesh. Bangladesh J. Fish. **1**: 1-28.

Pasha M. K. and S. B. Uddin. 2013. Dictionary of Plant Names of Bangladesh (Vascular Plants). Janokalyan Prokashani. Chittagong, Dhaka, Bangladesh. pp. 1-434.

Rahman M. O. and M. A. Hassan. 1995. Angiospermic Flora of Bhawal National Park, Gazipur (Bangladesh). Bangladesh J. Plant Taxon. **2**(1 & 2): 47-79.

Rahaman M. A., M. A. Rahman and M. Z. Uddin. 2017. Diversity of angiosperm of Kuakata national park, Patuakhali district, Bangladesh. J. Asiat. Soc. Bangladesh, Sci. **43**(2): 143-159.

Rahman M. M., M. M. Rahman and M. K. Huda. 2017. Seasonal variations of chemical properties of water of the Kaptai lake, Rangamati, Bangladesh. Jahangirnagar University J. Biol. Sci. **6**(2): 11-17.

Rahman M. M., M. Y. Hossain, F. Ahamed, Fatematuzzhura, B. R. Subba, E. M. Abdallah and J. Ohtom. 2012. Biodiversity in the Padma Distributary of the Ganges River, Northwestern Bangladesh: Recommendations for Conservation. World Journal of Zoology **7** (4): 328-337.

Rimi R. H., F. Rahman and M. B. Latif. 2013. Biodiversity Status and its Management at Ramsagar National Park at Dinajpur in Bangladesh. J. Environ. Sci. & Natural Resources, **6**(1): 21 – 32.

Siddiqui K. U., M. A. Islam, Z. U. Ahmed, Z. N. T. Begum, M. A. Hassan, M. A. M. Khondker, M. M. Rahman, S. M. H. Kabir, M. Ahmad, A. T. A. Ahmed, A. K. A. Rahman and E. U. Haque (eds.). 2007. Encyclopedia of Flora and Fauna of Bangladesh. **11**. Angiosperms; Monocotyledons. Asiatic Society of Bangladesh, Dhaka.

Uddin M. Z. and M. A. Hassan. 2010. Angiosperm diversity of Lawachara national park (Bangladesh): a preliminary assessment. Bangladesh J. Plant Taxon. **17**(1).

Barishal University Journal Part 1, 6(1) : 55-68 (2019) ISSN 2411-247X

EXISTENCE OF A CLASS OF CAPUTO TYPE FRACTIONAL DIFFERENTIAL EQUATIONS WITH NONLOCAL BOUNDARY CONDITIONS INVOLVING RIEMANN-LIOUVILLE INTEGRAL

Samima Akhter*

Department of Mathematics, University of Barishal, Barishal-8200, Bangladesh.

Abstract

The objective of this paper is to represent the existence and uniqueness of solutions for Caputo type fractional differential equations with new nonlocal boundary conditions involving Riemann-Liouville integrals. The existence results are obtained by applying Banach's contraction principle, Scheafer's fixed point theorem, Krasnoselskii's fixed point theorem and Leray-Schauder's nonlinear alternative theorem. Some examples are illustrated to verify the result of the theorems.

Keywords: Caputo Fractional derivative, Riemann-Liouville integral equation, Boundary value problem, Fixed point theorems, Existence.

Introduction

Fractional calculus, a well known procedure to describe the calculus of non-integer order, that is a generalization of ordinary differentiation and integration to arbitrary order. The concept of fractional operations has been introduced by G.W. Leibniz and Marquis de l'Hospital in 1695 due to the question that arose to find the meaning and solution of $D^{\frac{1}{2}}$. This question grabbed the attention of many renowned mathematicians including Euler, Liouville, Laplace, Riemann, Grünwald, Letnikov and many others. Since then the theory of fractional calculus developed rapidly in various applied disciplines like Fractional Geometry, Fractional Differential Equations and Fractional Dynamics. Lately Fractional Differential Equations with different orders conducting a strong role in analyzing many phenomena related to physics, chemistry, biology, economics, control theory, signal and image processing, biophysics, blood flow phenomena, aerodynamics, fitting of experimental data, etc.(Podlubny 1999; Hilfer 2000; Kilbas, Srivastava and Trujillo 2006; Mainardi 2010; Ortigueira 2011; Petras 2011) and the reference given there in.

* *Corresponding author's e-mail: samima.akh13@gmail.com*

In mathematics the theory of boundary value problems for nonlinear fractional differential equations has received attention of the researchers (Ahmed 2010; Bai et al 2009; Han and Wang 2011; Rehman et al. 2010 etc.) and many aspects of this theory need to be explored.

In 2012 Sudsutad and Tariboon discussed boundary value problems for fractional differential equations with three-point fractional integral boundary conditions with some standard fixed point theorems. Ravi P. Agarwal et al in 2017 have studied existence of nonlinear fractional order boundary value problems with nonlocal multi point conditions involving Liouville-Caputo derivative. Faouzi Haddouchi (2018) considered existence results for a class of Caputo type fractional differential equations with Riemann-Liouville fractional integrals and Caputo fractional derivatives in boundary conditions by Banach contraction principle , Schaefer's and Krasnoselskii's fixed point theorems.

Motivated by the works of the mathematician mentioned above this article is concerned with the existence and uniqueness of solutions for a boundary value problem of nonlinear fractional differential equations with Riemann integral boundary conditions given by

$$^{c}D^{\alpha}x(t) = f(t, x(t)),\ t \in [0,1], 1 < \alpha \leq 2 \quad (1)$$

$$x(0) = \beta \int_0^{\mu} x(s)ds\ ,\ x'(T) = \varphi I^{q} x(\eta) \quad (2)$$

Where $^{c}D^{\alpha}$ is the Caputo fractional derivative of order α, with $1 < \alpha \leq 2$, $f: [0,1] \times \mathbb{R} \to \mathbb{R}$ is a given continuous function, I^{q} is the Riemann-Liouville fractional integral of order q with $0 < q \leq 1$ and $0 < \mu, \eta < 1$, as well as β, φ, T are real constants.

1. Preliminaries

Definition 1.1 (Kilbas, Srivastava and Trujilla, 2006) The Riemann-Liouville factional integer of order α for a continuous function x is defined as

$$I^{\alpha}x(t) = \frac{1}{\Gamma(\alpha)} \int_0^t \frac{x(s)}{(t-s)^{p-1}}\ ds,\ \ \alpha > 0$$

provided the integral exists and $\Gamma(\cdot)$ is the gamma function which is defined by $\Gamma(x) = \int_0^{\infty} t^{x-1} e^{-t} dt.$

Definition 1.2 (Kilbas, Srivastava and Trujilla, 2006) For at least nth continuously differentiable function $f: [0, \infty) \to \mathbb{R}$, the Caputo derivative of fractional order p is defined as

$$^{c}D^{\alpha}\ x(t) = \frac{1}{\Gamma(n-\alpha)} \int_0^t (t-s)^{n-\alpha-1}\, x^{n}(s) ds,\ \ n-1 < \alpha < n, n = [\alpha] + 1,$$

where $[\alpha]$ denotes the integer part of the real number α.

Lemma 1.1 (Kilbas, Srivastava and Trujilla, 2006) For $\alpha > 0$, the general solution of the fractional differential equation ${}^{c}D^{\alpha}\, x(t) = 0$ is given by

$$x(t) = c_0 + c_1 t + c_2 t^2 + \cdots \ldots \ldots + c_{n-1} t^{n-1},$$

For some $c_i \in \mathbb{R}, i = 0,1, \ldots, n-1 (n = [\alpha] + 1)$.

Lemma 1.2 For any $f \in C[0,1]$, the solution of the problems

${}^{c}D^{\alpha} x(t) = f(t, x(t)),\ t \in [0,1], 1 < \alpha \leq 2$

consisted with boundary conditions

$x(0) = \beta \int_0^{\mu} x(s)ds\ ,\ x'(T) = \varphi I^{q} x(\eta)$

has a unique solution as

$$x(t) = \frac{1}{\Gamma(\alpha)} \int_0^t (t-s)^{\alpha-1} f(s)ds + \left(\frac{\mu^2}{2(1-\mu)B} + \frac{t}{B}\right)\left\{\frac{\varphi\eta^{q}}{\Gamma(q+1)(1-\mu)} \int_0^{\mu}\int_0^{s} \frac{(t-s)^{\alpha-1}}{\Gamma(\alpha)} f(u)duds + \varphi \int_0^{\eta}\int_0^{t} \frac{(t-\tau)^{\alpha-1}(\tau-s)^{q-1}}{\Gamma(\alpha)\,\Gamma(q)} f(\tau)d\tau ds - \frac{1}{\Gamma(\alpha-1)} \int_0^{T} (T-s)^{\alpha-2} f(s)ds\right\} + \frac{1}{1-\mu}\int_0^{\mu}\int_0^{s} \frac{(t-s)^{\alpha-1}}{\Gamma(\alpha)} f(u)duds \quad (3)$$

Proof: The general solution of the fractional differential equations (1) and (2) can be written as

$$x(t) = c_0 + c_1 t + \int_0^t \frac{(t-s)^{\alpha-1}}{\Gamma(\alpha)} f(s)ds \quad (4)$$

where $c_0, c_1 \in \mathbb{R}$ are arbitrary constants.

Applying the given boundary conditions, we find that

$$c_0 = \frac{\mu^2}{2(1-\mu)B}\left[\frac{\varphi\eta^{q}}{\Gamma(q+1)(1-\mu)} \int_0^{\mu}\int_0^{s} \frac{(t-s)^{\alpha-1}}{\Gamma(\alpha)} f(u)duds + \varphi \int_0^{\eta}\int_0^{t} \frac{(t-\tau)^{\alpha-1}(\tau-s)^{q-1}}{\Gamma(\alpha)\,\Gamma(q)} f(\tau)d\tau ds - \frac{1}{\Gamma(\alpha-1)} \int_0^{T} (T-s)^{\alpha-2} f(s)ds\right]$$

$$c_1 = \frac{1}{B}\left[\frac{\varphi\eta^{q}}{\Gamma(q+1)(1-\mu)} \int_0^{\mu}\int_0^{s} \frac{(t-s)^{\alpha-1}}{\Gamma(\alpha)} f(u)duds + \varphi \int_0^{\eta}\int_0^{t} \frac{(t-\tau)^{\alpha-1}(\tau-s)^{q-1}}{\Gamma(\alpha)\,\Gamma(q)} f(\tau)d\tau ds - \frac{1}{\Gamma(\alpha-1)} \int_0^{T} (T-s)^{\alpha-2} f(s)ds\right]$$

where B is given by $B = \left[1 - \frac{\mu^2 \varphi \eta^q}{\Gamma(q+1)(1-\mu)} - \frac{\varphi \eta^{q+1}}{\Gamma(q+2)}\right] \neq 0$.

Inserting the values c_0 and c_1 in (4), we get (3). This completes the proof of the Lemma 1.2.

2. Main Results

In this section we embed the conditions for the existence of the problems (1) and (2) using some fixed point theorems.

Let $\mathfrak{D} = C([0,1], \mathbb{R})$ denote the Banach space of all continuous function from [0,1] to $\mathbb{R}$ endowed with the norm defined by $\|x\| = \sup\{|x(t)|, t \in [0,1]\}$. It is evident that the problems (1) and (2) has solutions if and only if the operator $\mathcal{H}$ has fixed points.

As in Lemma 1.2, we define an operator $\mathcal{H}: \mathfrak{D} \to \mathfrak{D}$ such that

$$(\mathcal{H}x)(t) = \frac{1}{\Gamma(\alpha)} \int_0^t (t-s)^{\alpha-1} f(s, x(s)) ds + \left(\frac{\mu^2}{2(1-\mu)B} + \frac{t}{B}\right)\left\{\frac{\varphi \eta^q}{\Gamma(q+1)(1-\mu)} \int_0^\mu \int_0^s \frac{(t-s)^{\alpha-1}}{\Gamma(\alpha)} f(r, x(r)) dr ds + \varphi \int_0^\eta \int_0^t \frac{(t-\tau)^{\alpha-1}(\tau-s)^{q-1}}{\Gamma(\alpha)\Gamma(q)} f(\tau, x(\tau)) d\tau ds - \frac{1}{\Gamma(\alpha-1)} \int_0^T (T-s)^{\alpha-2} f(s, x(s)) ds\right\} + \frac{1}{1-\mu} \int_0^\mu \int_0^s \frac{(t-s)^{\alpha-1}}{\Gamma(\alpha)} f(r, x(r)) dr ds \quad (5)$$

For computational requirement set Δ as

$$\Delta = \frac{1}{\Gamma(p+1)} + \left(\frac{|\mu^2|}{2|(1-\mu)|\,|B|} + \frac{1}{|B|}\right)\left[\frac{|\varphi|\,|\eta^q|}{\Gamma(q+1)\,|(1-\mu)|} \frac{\mu^{\alpha+1}}{\Gamma(\alpha+2)} + |\varphi| \frac{\eta^{\alpha+q}}{\Gamma(\alpha+q+1)} - \frac{T^{\alpha-1}}{\Gamma(\alpha)}\right] + \frac{1}{|(1-\mu)|} \frac{\mu^{\alpha+1}}{\Gamma(\alpha+2)} \quad (6)$$

Now we are in a state to present the main result of our paper. The first part is associated with the existence and uniqueness of solutions for (1) and (2) by using Banach's contraction principle.

Theorem 2.1 Let $f: [0,1] \times \mathbb{R} \to \mathbb{R}$ be a continuous function satisfying the Lipschitz condition:

(I) $\quad |f(t,x) - f(t,y)| \leq m|x-y|, m > 0 \ \forall\, t \in [0,1], x, y \in \mathbb{R}.$

Then the problems (1) and (2) has a unique solution on [0,1] provided that $\Delta m < 1$, where Δ is given by Eq.(6).

Proof: Consider $sup_{t\in[0,1]}\,|f(t,0)| = \vartheta$. We show that the the operator $\mathcal{H}$ defined by (5) satisfies the relation $\mathcal{H}B_r \subset B_r$, where $B_r = \{x \in \mathfrak{D}: \|x\| \leq r\}$ and $r \geq \Delta\vartheta(1-\Delta m)^{-1}$.

For $x \in B_r$, $t \in [0,1]$ using assumption (I) we get ,

$$\begin{aligned}|f(t,x(t))| &= \left|f\big(t,x(t)\big) - f(t,0) + f(t,0)\right| \\ &\leq \left|f\big(t,x(t)\big) - f(t,0)\right| + |f(t,0)| \\ &\leq m\|x\| + \vartheta \;\; \leq mr + \vartheta \end{aligned} \tag{7}$$

With the aid of Eq. (6) and (7), we get,

$$\begin{aligned}\|(\mathcal{H}x)\| \leq sup_{t\in[0,1]}\Bigg\{&\frac{1}{\Gamma(\alpha)}\int_0^t (t-s)^{\alpha-1}f(s,x(s))ds \\ &+\left(\frac{\mu^2}{2(1-\mu)B} + \frac{t}{B}\right)\Bigg\{\frac{\varphi\eta^q}{\Gamma(\mathrm{q}+1)(1-\mu)}\int_0^\mu\int_0^s \frac{(t-s)^{\alpha-1}}{\Gamma(\alpha)}f(r,x(r))drds \\ &+\varphi\int_0^\eta\int_0^t \frac{(t-\tau)^{\alpha-1}\,(\tau-s)^{\mathrm{q}-1}}{\Gamma(\alpha)\,\Gamma(\mathrm{q})}f(\tau,x(\tau))d\tau ds \\ &-\frac{1}{\Gamma(\alpha-1)}\int_0^T (T-s)^{\alpha-2}f(s,x(s))ds\Bigg\} \\ &+\frac{1}{1-\mu}\int_0^\mu\int_0^s \frac{(t-s)^{\alpha-1}}{\Gamma(\alpha)}f(r,x(r))drds\Bigg\}\end{aligned}$$

$$\begin{aligned}&\leq (mr+\vartheta)sup_{t\in[0,1]}\left\{\frac{1}{\Gamma(\mathrm{p}+1)} + \left(\frac{|\mu^2|}{2|(1-\mu)|\,|\mathrm{B}|} + \frac{1}{|B|}\right)\left[\frac{|\varphi|\,|\eta^q|}{\Gamma(\mathrm{q}+1)\,|(1-\mu)|}\frac{\mu^{\alpha+1}}{\Gamma(\alpha+2)} + \right.\right. \\ &\left.\left. |\varphi|\frac{\eta^{\alpha+\mathrm{q}}}{\Gamma(\alpha+\mathrm{q}+1)} - \frac{\mathrm{T}^{\alpha-1}}{\Gamma(\alpha)}\right] + \frac{1}{|(1-\mu)|}\frac{\mu^{\alpha+1}}{\Gamma(\alpha+2)}\right\} \\ &\leq (mr+\vartheta)\Delta \leq \mathrm{r}.\end{aligned}$$

This shows that $\mathcal{H}B_r \subset B_r$.

Now for any $x, y \in \mathfrak{D}$ and $t \in [0,1]$, we obtain

$$\|\mathcal{H}x - \mathcal{H}y\| \leq sup_{t\in[0,1]} \left\{ \int_0^t \frac{(t-s)^{\alpha-1}}{\Gamma(\alpha)} \left|f\big(s,x(s)\big) - f(s,y(s))\right| ds \right.$$
$$+ \left(\frac{\mu^2}{2(1-\mu)B} \right.$$
$$\left. + \frac{t}{B} \right) \left\{ \frac{\varphi\eta^q}{\Gamma(\mathrm{q}+1)(1-\mu)} \int_0^\mu \int_0^s \frac{(t-s)^{\alpha-1}}{\Gamma(\alpha)} \left|f\big(r,x(r)\big)\right.\right.$$
$$\left. - f(r,y(r))\right| drds$$
$$+ \varphi \int_0^\eta \int_0^t \frac{(t-\tau)^{\alpha-1}\,(\tau-s)^{\mathrm{q}-1}}{\Gamma(\alpha)\,\Gamma(\mathrm{q})} |f(\tau,x(\tau)) - f(\tau,y(\tau)))| d\tau ds$$
$$\left. - \frac{1}{\Gamma(\alpha-1)} \int_0^T (T-s)^{\alpha-2} \left|f\big(s,x(s)\big) - f(s,y(s))\right| ds \right\}$$
$$\left. + \frac{1}{1-\mu} \int_0^\mu \int_0^s \frac{(t-s)^{\alpha-1}}{\Gamma(\alpha)} \left|f\big(r,x(r)\big) - f(r,y(r))\right| drds \right\}$$

$$\leq m\Delta|\mathrm{x}-\mathrm{y}|$$

Since $m\Delta < 1$, by the given condition, it shows that $\mathcal{H}$ is a contraction. Thus, by Banach contraction mapping principle, there exists a unique solution for the problems (1) and (2). This completes the proof.

Our next result is based on Schaefer's fixed point theorem.

Theorem 2.2 Let $f:[0,1]\times\mathbb{R}\to\mathbb{R}$ be a continuous function which satisfies (I). In addition we assume that

(II) There exists a constant $l>0$ such that $|f(t,x)|\leq l$ for all $t\in[0,1], x,y\in\mathbb{R}$. Then the BVP (1) and (2) has at least one solution on [0,1].

Proof: We prove that the operator $\mathcal{H}$ has a fixed point by using Schaefer's fixed point theorem. The proof is divided into several steps.

Firstly we show that the operator $\mathcal{H}$ is continuous.

Let x_n be a sequence in $\mathfrak{D}$ such that $x_n\to x$. Then for each $t\in[0,1]$ we obtain,

$|(\mathcal{H}x_n) - (\mathcal{H}x)| \leq$

$\left\{\frac{1}{\Gamma(\alpha)} \int_0^t (t-s)^{\alpha-1} ds + \left(\frac{\mu^2}{2(1-\mu)B} + \frac{t}{B}\right) \left\{\frac{\varphi\eta^q}{\Gamma(q+1)(1-\mu)} \int_0^\mu \int_0^s \frac{(t-s)^{\alpha-1}}{\Gamma(\alpha)} dr ds + \varphi \int_0^\eta \int_0^t \frac{(t-\tau)^{\alpha-1}(\tau-s)^{q-1}}{\Gamma(\alpha)\Gamma(q)} d\tau ds - \frac{1}{\Gamma(\alpha-1)} \int_0^T (T-s)^{\alpha-2} ds\right\} + \frac{1}{1-\mu} \int_0^\mu \int_0^s \frac{(t-s)^{\alpha-1}}{\Gamma(\alpha)} dr ds\right\} \times \|f(.,x_n(.)) - f((.,x(.))\|$

$$\leq \Delta \, \|f(.,x_n(.)) - f((.,x(.))\|$$

Since f is continuous, then $|(\mathcal{H}x_n) - (\mathcal{H}x)| \to 0$ as $n \to \infty$. Therefore $\mathcal{H}$ is continuous.

In this step we will show $\mathcal{H}$ maps bounded sets into $\mathfrak{D}$.

For any positive r, let $B_r = \{x \in \mathcal{H}: \|x\| \leq r\}$ be a bounded set in $\mathfrak{D}$.

$$\begin{aligned}|(\mathcal{H}x)(t)| \leq \Bigg\{ & \frac{1}{\Gamma(\alpha)} \int_0^t (t-s)^{\alpha-1} |f(s,x(s))| ds \\ & + \left(\frac{\mu^2}{2(1-\mu)B} \right. \\ & \left. + \frac{t}{B}\right)\left\{\frac{\varphi\eta^q}{\Gamma(q+1)(1-\mu)} \int_0^\mu \int_0^s \frac{(t-s)^{\alpha-1}}{\Gamma(\alpha)} |f(r,x(r))| dr ds \right. \\ & + \varphi \int_0^\eta \int_0^t \frac{(t-\tau)^{\alpha-1}(\tau-s)^{q-1}}{\Gamma(\alpha)\Gamma(q)} |f(\tau,x(\tau))| d\tau ds \\ & \left. - \frac{1}{\Gamma(\alpha-1)} \int_0^T (T-s)^{\alpha-2} |f(s,x(s))| ds \right\} \\ & + \frac{1}{1-\mu} \int_0^\mu \int_0^s \frac{(t-s)^{\alpha-1}}{\Gamma(\alpha)} |f(r,x(r))| dr ds \Bigg\}\end{aligned}$$

$$\leq l\Delta = \vartheta, \; x \in B_r$$

Here we will show that $\mathcal{H}(B_r)$ is equicontinuous in B_r . Let $0 < t_1 < t_2 < 1$ and $x \in B_r$, then we get the following enumeration,

$$
\begin{aligned}
&|(\mathcal{H}x)(t_2) - (\mathcal{H}x)(t_1)| \\
&\leq \frac{1}{\Gamma(\alpha)} \int_0^{t_1} (t_2 - s)^{\alpha-1} - (t_1 - s)^{\alpha-1} \left|f\big(s, x(s)\big)\right| ds \\
&+ \int_{t_1}^{t_2} \frac{(t_2 - s)^{\alpha-1}}{\Gamma(\alpha)} \left|f\big(s, x(s)\big)\right| ds \\
&+ \frac{(t_2 - t_1)}{B} \left\{ \frac{\varphi \eta^q}{\Gamma(\mathrm{q}+1)(1-\mu)} \int_0^{\mu} \int_0^{s} \frac{(u - s)^{\alpha-1}}{\Gamma(\alpha)} |f(r, x(r))| dr ds \right. \\
&+ \varphi \int_0^{\eta} \int_0^{s} \frac{(\eta - s)^{\mathrm{q}-1} (s - \tau)^{\alpha-1}}{\Gamma(\alpha)\,\Gamma(\mathrm{q})} |f(\tau, x(\tau))| d\tau ds \\
&\left. - \frac{1}{\Gamma(\alpha - 1)} \int_0^{T} (T - s)^{\alpha-2} \left|f\big(s, x(s)\big)\right| ds \right\}
\end{aligned}
$$

$$
\leq m \left\{ \frac{1}{\Gamma(\alpha+1)} [(t_2^{\alpha} - t_1^{\alpha}) + 2(t_2 - t_1)^{\alpha}] + \frac{t_2 - t_1}{|B|} \left[\frac{|\varphi|\,|\eta^q|}{\Gamma(\mathrm{q}+1)\,|(1-\mu)|} \frac{\mu^{\alpha+1}}{\Gamma(\alpha+2)} + |\varphi| \frac{\eta^{\alpha+\mathrm{q}}}{\Gamma(\alpha+\mathrm{q}+1)} - \frac{\mathrm{T}^{\alpha-1}}{\Gamma(\alpha)} \right] \right\}
$$

As $t_2 \to t_1$, the right hand side tends to zero independently of $\mathrm{x} \in B_r$. Hence by the Arzela-Ascoli theorem, the operator $\mathcal{H}$ is completely continuous.

Finally $\mathcal{H}$ priori bounds. Now we will show that the set $V = \{x \in \mathfrak{D} : x = \varepsilon \mathcal{H}x, 0 < \varepsilon < 1\}$ is bounded.

Let $x \in V$, then $x = \varepsilon \mathcal{H}x$ for some $0 < \varepsilon < 1$. Thus for some $t \in [0,1]$, we have $x(t) =$

$$
l \left[\frac{1}{\Gamma(\alpha)} \int_0^{t} (t - s)^{\alpha-1} f(s, x(s)) ds + \left(\frac{\mu^2}{2(1-\mu)B} + \frac{t}{B} \right) \left\{ \frac{\varphi \eta^q}{\Gamma(\mathrm{q}+1)(1-\mu)} \int_0^{\mu} \int_0^{s} \frac{(t-s)^{\alpha-1}}{\Gamma(\alpha)} f(r, x(r)) dr ds + \varphi \int_0^{\eta} \int_0^{t} \frac{(t-\tau)^{\alpha-1} (\tau-s)^{\mathrm{q}-1}}{\Gamma(\alpha)\,\Gamma(\mathrm{q})} f(\tau, x(\tau)) d\tau ds - \frac{1}{\Gamma(\alpha-1)} \int_0^{T} (T - s)^{\alpha-2} f(s, x(s)) ds \right\} + \frac{1}{1-\mu} \int_0^{\mu} \int_0^{s} \frac{(t-s)^{\alpha-1}}{\Gamma(\alpha)} f(r, x(r)) dr ds \right]
$$

which implies that using $\varepsilon < 1$, we get, $|x(t)| = \varepsilon |(\mathcal{H}x)(t)| \leq l\Delta = \vartheta$. Thus V is bounded. Schaefer's fixed point theorem implies that (1) and (2) has at least one solution. This completes the proof of the theorem.

The existence and uniqueness of the problem will be established by using Krasnoselskii's fixed point theorem.

Theorem 2.3 Let $f: [0,1] \times \mathbb{R} \to \mathbb{R}$ be continuous function satisfying (I) and (II). Further we assume that

(III) $\quad |f(t,x)| \leq \delta(t),\ \forall\ (t,x) \in [0,1] \times \mathbb{R}$, and $\delta \in C([0,1] \times \mathbb{R}^+)$.

Then the problem (1) and (2) has at least one solution on [0,1], if $l\left(\Delta - \frac{1}{\Gamma(\alpha+1)}\right) < 1$ where Δ is given by Eq. (6).

Proof: Let us define $B_r = \{x \in \mathfrak{D}: \|x\| \leq r\}$ with $r \geq \Delta\|\delta\|$. Consider two operators K_1 and K_2 on B_r as follows

$$(K_1x)(t) = \frac{1}{\Gamma(\alpha)} \int_0^t (t-s)^{\alpha-1} f(s,x(s))ds$$

$$(K_2x)(t) = \left(\frac{\mu^2}{2(1-\mu)B} + \frac{t}{B}\right)\left\{\frac{\varphi\eta^q}{\Gamma(q+1)(1-\mu)} \int_0^\mu \int_0^s \frac{(t-s)^{\alpha-1}}{\Gamma(\alpha)} f(r,x(r))drds + \varphi \int_0^\eta \int_0^t \frac{(t-\tau)^{\alpha-1}\,(\tau-s)^{q-1}}{\Gamma(\alpha)\,\Gamma(q)} f(\tau,x(\tau))d\tau ds - \frac{1}{\Gamma(\alpha-1)} \int_0^T (T-s)^{\alpha-2} f(s,x(s))ds\right\} + \frac{1}{1-\mu} \int_0^\mu \int_0^s \frac{(t-s)^{\alpha-1}}{\Gamma(\alpha)} f(r,x(r))drds$$

For $x, y \in B_r$, we have

$\|K_1x + K_2y\| \leq \delta\Delta \leq r$. Thus $K_1x + K_2y \in B_r$.

$$\begin{aligned}
\|(K_2x) - (K_2y)\| &\leq sup_{t\in[0,1]}\left(\frac{\mu^2}{2(1-\mu)B} + \frac{t}{B}\right)\left\{\frac{\varphi\eta^q}{\Gamma(q+1)(1-\mu)} \int_0^\mu \int_0^s \frac{(t-s)^{\alpha-1}}{\Gamma(\alpha)} \left|f\big(r,x(r)\big) - f(r,y(r))\right| drds \right. \\
&\quad + \varphi \int_0^\eta \int_0^t \frac{(t-\tau)^{\alpha-1}\,(\tau-s)^{q-1}}{\Gamma(\alpha)\,\Gamma(q)} |f(\tau,x(\tau)) - f(\tau,y(\tau)))| d\tau ds \\
&\quad \left. - \frac{1}{\Gamma(\alpha-1)} \int_0^T (T-s)^{\alpha-2} \left|f\big(s,x(s)\big) - f(s,y(s))\right| ds\right\} \\
&\quad + \frac{1}{1-\mu} \int_0^\mu \int_0^s \frac{(t-s)^{\alpha-1}}{\Gamma(\alpha)} \left|f\big(r,x(r)\big) - f(r,y(r))\right| drds \\
&\leq l\left(\Delta - \frac{1}{\Gamma(\alpha+1)}\right)\|x-y\|
\end{aligned}$$

It follows from the assumption that K_2 is a contraction mapping.

Continuity of f implies K_1 is continuous. Also K_1 is uniformly bounded on B_r as

$$\|K_1 x\| \leq \frac{\|\delta\|}{\Gamma(\alpha+1)}$$

We prove the compactness of the operator K_1. Let $t_1, t_2 \in [0,1]$ with $t_1 < t_2$. Define $sup_{t\in[0,1]\times B_r}|f(t,x)| = f_m$ and we obtain

$$\begin{aligned}|(K_1x)(t_2) - (K_1x)(t_1)| &= \frac{1}{\Gamma(\alpha)}\left|\int_0^{t_1}[(t_2-s)^{\alpha-1} - (t_1-s)^{\alpha-1}]f\big(s,x(s)\big)ds \right.\\ &\left. + \int_{t_1}^{t_2}(t_2-s)^{\alpha-1}f(s,x(s))ds\right|\\ &\leq \tfrac{f_m}{\Gamma(\alpha+1)}\,|t_1^{\alpha} - t_2^{\alpha}|.\end{aligned}$$

Which is independent of x. Thus K_1 is equicontinuous. So K_1 is relatively compact on B_r. Hence by the Arzela-Ascoli theorem K_1 is compact on B_r. Thus all the assumption of theorem 2.3 are satisfied. So the conclusion of theorem 2.3 implies that boundary value problems (1) and (2) has at least one solution on [0,1].

Finally the proof of the problems (1) and (2) will be presented by Leray-Schauder's nonlinear alternative**.**

Lemma 2.4 Let E be a Banach space, E_1 be a closed, convex subset of E, U be an open subset of $E_1$and $0 \in U$. Suppose that $F: \overline{U} \to E_1$ is a continuous, compact (that is, $F(\overline{U})$ is a relatively compact subset of E_1) map. Then either

(i) F has a fixed point in $\overline{U}$, or

(ii) There is a $u \in \partial U$(the boundary of U in E_1) and $\tau \in (0,1)$ with $u = \tau F(u)$.

Theorem 2.5 Assume that Let $f: [0,1] \times \mathbb{R} \to \mathbb{R}$ be continuous function which satisfies the conditions stated below.

(IV) there exists a continuous nondecreasing function $\rho : [0,\infty) \to (0,\infty)$ and a function $g \in (\mathfrak{D}[0,T], \mathbb{R}^+)$ such that $|f(t,x)| \leq \rho(t)g(\|x\|)$ for each $(t,x) \in [0,1] \times \mathbb{R}$

(V) there exists a constant $W > 0$ such that $\frac{W}{g(W)\|\rho\|\Delta}$>1

Then the boundary value problems (1.1) and (1.2) has at least one solution on [0,1].

Proof: Let us consider the operator $\mathcal{H}:\mathfrak{D}\to\mathfrak{D}$ defined by (5) and prove that $\mathcal{H}$ maps bounded sets into bounded in $\mathfrak{D}$. As $B_r=\{x\in\mathfrak{D}:\|x\|\le r\}$ we have

$$
\begin{aligned}
(\mathcal{H}x)(t)\le\Bigg[&\frac{1}{\Gamma(\alpha)}\int_0^t(t-s)^{\alpha-1}g(s)\rho(\|x\|)ds\\
&+\left(\frac{\mu^2}{2(1-\mu)B}\right.\\
&\left.+\frac{t}{B}\right)\left\{\frac{\varphi\eta^q}{\Gamma(q+1)(1-\mu)}\int_0^\mu\int_0^s\frac{(t-s)^{\alpha-1}}{\Gamma(\alpha)}g(s)\rho(\|x\|)drds\right.\\
&+\varphi\int_0^\eta\int_0^t\frac{(t-\tau)^{\alpha-1}(\tau-s)^{q-1}}{\Gamma(\alpha)\,\Gamma(q)}g(s)\rho(\|x\|)d\tau ds\\
&\left.-\frac{1}{\Gamma(\alpha-1)}\int_0^T(T-s)^{\alpha-2}g(s)\rho(\|x\|)ds\right\}\\
&+\frac{1}{1-\mu}\int_0^\mu\int_0^s\frac{(t-s)^{\alpha-1}}{\Gamma(\alpha)}g(s)\rho(\|x\|)drds\Bigg]
\end{aligned}
$$

$$\le g\|r\|\|\rho\|\,\Delta$$

As in the proof of the previous result for $0<t_1<t_2<1$ and $x\in B_r$. We have the operation $\mathcal{H}$ is continuously continuous. Thus it follows that $\mathcal{H}$ maps bounded sets into equicontinuous sets of $\mathfrak{D}$.

Let x be a solution for the given problem. Then for $\tau\in(0,1)$ as before, we obtain,

$|x(t)|=\|\tau(\mathcal{H}x)(t)\|\le g\|x\|\|\rho\|\,\Delta$

which on taking the norm for $t\in[0,1]$ yields $\frac{\|x\|}{g\|x\|\|\rho\|\,\Delta}\le 1$.

In view of (V) , there exists W such that $\|x(t)\|\neq W$. Let us set

$W_1=\{u\in\mathfrak{D}:\|x(t)\|<W+1\}$.

Note that the operator $\mathcal{H}:\overline{W_1}\to\mathfrak{D}$ is continuous and completely continuous. From the choice of W_1, there is no $u\in\partial W_1$ such that $u=\tau\mathcal{H}u$ for some $\tau\in(0,1)$. Consequently, by the nonlinear alternative of Leray-Schauder type, we deduce that $\mathcal{H}$ has a fixed point $u\in\overline{W_1}$ which is a solution of problems (1) and (2). This completes the proof of the theorem.

3. Examples

In this section we will give some illustrative examples to verify the results that are proved in section 2.

Example 3.1 Consider the following fractional differential equation with integral conditions:

$$ {}^{c}D^{\frac{3}{2}}x(t) = \frac{e^{-2t}\,2\cos(\sin x + t^2)}{11 + e^{-\cos t}}, \qquad t \in [0,1] $$

$$ x(0) = \int_0^{1/6} x(s)ds, \quad x'(2) = \frac{1}{3} I^{\frac{1}{2}} x(\tfrac{1}{4}) $$

Set $\alpha = \frac{3}{2}$, $q = \frac{1}{2}$, , $T = 2$, $\mu = \frac{1}{6}$, $\varphi = \frac{1}{3}$, $\eta = \frac{1}{4}$ and $f(x,t) = \frac{e^{-2t}\,2\cos(\sin x + t^2)}{11+e^{-\cos t}}$.

Since $|f(t,x) - f(t,y)| \le \frac{1}{6}|x-y|$, where $m = \frac{1}{6}$. Thus

$$ m\Delta = \frac{1}{6}\left[\frac{1}{\Gamma(\alpha+1)} + \left(\frac{|\mu^2|}{2|(1-\mu)|\,|\mathrm{B}|} + \frac{1}{|B|}\right)\left[\frac{|\varphi|\,|\eta^q|}{\Gamma(\mathrm{q}+1)\,|(1-\mu)|}\frac{\mu^{\alpha+1}}{\Gamma(\alpha+2)} + |\varphi|\frac{\eta^{\alpha+\mathrm{q}}}{\Gamma(\alpha+\mathrm{q}+1)} - \frac{\mathrm{T}^{\alpha-1}}{\Gamma(\alpha)}\right] + \frac{1}{|(1-\mu)|}\frac{\mu^{\alpha+1}}{\Gamma(\alpha+2)}\right] $$

$$ \cong .127302571 < 1 $$

Hence by theorem 2.1, boundary value problems has unique solution in [0,1].

Example 3.2 Consider the following fractional differential equation with some specific boundary conditions

$$ {}^{c}D^{\frac{4}{3}}x(t) = \frac{t^2(x^2 + e^{t/2})}{(3+t^2)(e^{-x}+4) + \sqrt{t+17}}, \qquad t \in [0,1] $$

$$ x(0) = \int_0^{1/7} x(s)ds, \quad , \quad x'(1) = \frac{1}{13} I^{\frac{4}{5}} x(\tfrac{3}{5}) $$

Set $\alpha = \frac{4}{3}$, $q = \frac{4}{5}$, , $T = 1$, $\mu = \frac{1}{7}$, $\varphi = \frac{1}{13}$, $\eta = \frac{3}{5}$ and $f(x,t) = \frac{t^2(x^2+e^{t/2})}{(3+t^2)(e^{-x}+4)+\sqrt{t+17}}$.

Here, $|f(x,t)| \le \left|\frac{t^2(x^2+e^{t/2})}{(3+t^2)(e^{-x}+4)+\sqrt{t+17}}\right| \le \frac{1}{24}$

Then $l\left(\Delta - \frac{1}{\Gamma(\alpha+1)}\right) \cong 0.078357 < 1$.

Hence all the conditions of theorem 2.3 are satisfied and consequently the problem has at least one solution in [0, 1].

Example 3.3 Consider the following fractional differential equation with integral boundary conditions:

$$ {}^{c}D^{\frac{7}{6}}x(t) = \frac{x^3 \sin(\frac{\pi x}{2})}{\pi\sqrt{11+t}} + \frac{(t+1)^2 e^{-3x}}{8+x^2}, \qquad t \in [0,1] $$

$$ x(0) = \int_0^{1/2} x(s)ds \quad , \quad x'\left(\frac{5}{2}\right) = \frac{1}{15}\, I^{\frac{7}{8}} x(\tfrac{1}{9}) $$

Here, $= \frac{7}{6}$, $q = \frac{7}{8}$, $, T = 5/2,\ \mu = \frac{1}{2},\ \varphi = \frac{1}{15}, \eta = \frac{1}{9}$ and $f(x,t) = \frac{x^3 \sin(\frac{\pi x}{2})}{\pi\sqrt{11+t}} + \frac{(t+1)^2 e^{-3x}}{7+x^2}$

$$ |f(t,x))| \leq \left|\frac{x^3 \sin(\frac{\pi x}{2})}{\pi\sqrt{11+t}} + \frac{(t+1)^2 e^{-3x}}{7+x^2}\right| \leq \left(\frac{\|x^3\|}{12\pi} + \frac{2e^{-3x}}{8}\right)(t+1)^2. $$

$$ \frac{W}{\rho(\|W\|)g\Delta} \cong \frac{2.356}{1.236} \cong 1.906 > 1 $$

Hence all the conditions of theorem 2.5 are satisfied and consequently the problem has at least one solution.

Conclusion

In this paper we represented the existence and uniqueness of solutions for Caputo type fractional differential equations with new nonlocal boundary conditions involving Riemann-Liouville integrals. The problem was solved in Lemma 1.2 with the help of Lemma 1.1 and definitions. The existence results were proved by applying Banach's contraction principle, Scheafer's fixed point theorem, Krasnoselskii's fixed point theorem and Leray-Schauder's nonlinear alternative theorem. Here we showed three consecutive examples based on Banach's contraction principle, Scheafer's fixed point theorem and Leray-Schauder's nonlinear alternative theorem.

References

Ahmad, B. 2010. Existence of solutions for irregular boundary value problems of nonlinear fractional differential equations. Applied Mathematics Letters. **23**: 390-394.

Bai, Z. and Qiu, T. 2009. Existence of positive solution for singular fractional differential equation. Applied Mathematics and computation. **215**: 2761-2767.

Faouzi, H. 2018. Existence results for a class of Caputo type fractional differential equations with Riemann-Liouville fractional integrals and Caputo fractional derivatives in Boundary conditions. arXiv: Classical Analysis and ODEs.: n.pag.

Han, X. and Wang, T. 2011. The existence of solutions for a nonlinear fractional multi-point boundary value problem at resonance. International Journal of Differential Equations**:** 1-14.

Hilfer, R. 2000. Fractional Calculus in Physics. World Scientific, Singapore.

Kilbas, AA. Srivastava, HM. Trujillo, JJ. 2006. Theory and Applications of Fractional Differential Equations. Elsevier. Amsterdam.

Mainardi, F. 2010. Fractional Calculus and Waves in Linear Viscoelasticity: An Introduction to Mathematical Models. Imperial College Press. Singapore.

Ortigueira, MD. 2011. Fractional Calculus for Scientists and Engineers. Springer. Heidelberg.

Petras, I. 2011. Fractional-Order Nonlinear Systems: Modeling, Analysis and Simulation. Springer. Berlin.

Podlubny, I. 1999. Fractional Differential Equations. Academic Press, San Diego.

Ravi, p. A. Ahmed A. Alaa A. and And Bashir A. 2017. On nonlinear fractional-order boundary value problems with nonlocal multi point conditions involving Liouville-Caputo derivative. Differential Equations and Applications. **2:** 147-160.

Rehman, MU. Khan, RA. 2010. Existence and uniqueness of solutions for multi-point boundary value problems for fractional differential equations. Applied Mathematics Letters. **23**: 1038-1044.

Sudsutad, W. and Tariboon, J. 2012. Boundary value problems for fractional differential equations with three-point fractional integral boundary conditions. Advances in Difference Equations. 93.

Barishal University Journal Part 1, 6(1): 69-81 (2019) ISSN 2411-247X

Review Paper

AN OVERVIEW OF ANTIBACTERIAL DRUG DISCOVERY

Halima Bagum*

Department of Chemistry, University of Barishal-8200, Bangladesh

Abstract

Antibacterial drug discovery have received a significant attraction with the aim to develop a library of bioactive compounds using organic synthesis. This work elaborately outlined different synthetic approaches and models to a variety of antibacterial drugs.

***Keywords*:** Antibacterial drugs, Antibiotic resistance, Drug discovery, Synthesis, Semi-synthesis, Natural products.

Introduction

Antibacterial drugs represent chemical substances that are able to inhibit or destroy the growth of bacteria. These are derived from bacteria or molds or produced by chemical synthesis.

The first breakthrough in antimicrobial drug discovery was the treatment of malaria with the fully synthetic thiazine dye, methylene blue (Guttmann et al. 1891). The gradual development of drug discovery is depicted in Fig. 1 (Wright et al. 2014). Later, Bertheim, Ehrlich and co-workers contributed to the discovery of the first antibacterial drug, salvarsan (Lloyd et al. 2005), which was found to be effective for the treatment of syphilis (Bosch et al. 2008). Further investigation led to the discovery of the red dye, prontosil, and a number of sulfadrugs (Lesch, 2006). Noteworthy, the first two clinically used antibiotic classes were fully synthetic molecules.

In 1928, the discovery of penicillin (Fleming, 1929) was arguably the most exciting scientific development of the 20th century, which was isolated from the fungus *Penicillium chrysogenum* but the true significance of the discovery took another decade to realise. Further investigation revealed even crude or partially-purified penicillin had

* *Corresponding Author's Email: halimaju35@gmail.com*

dramatic results against streptococcal (Chain et al. 1940) and staphylococcal infections (Abraham et al. 1941).

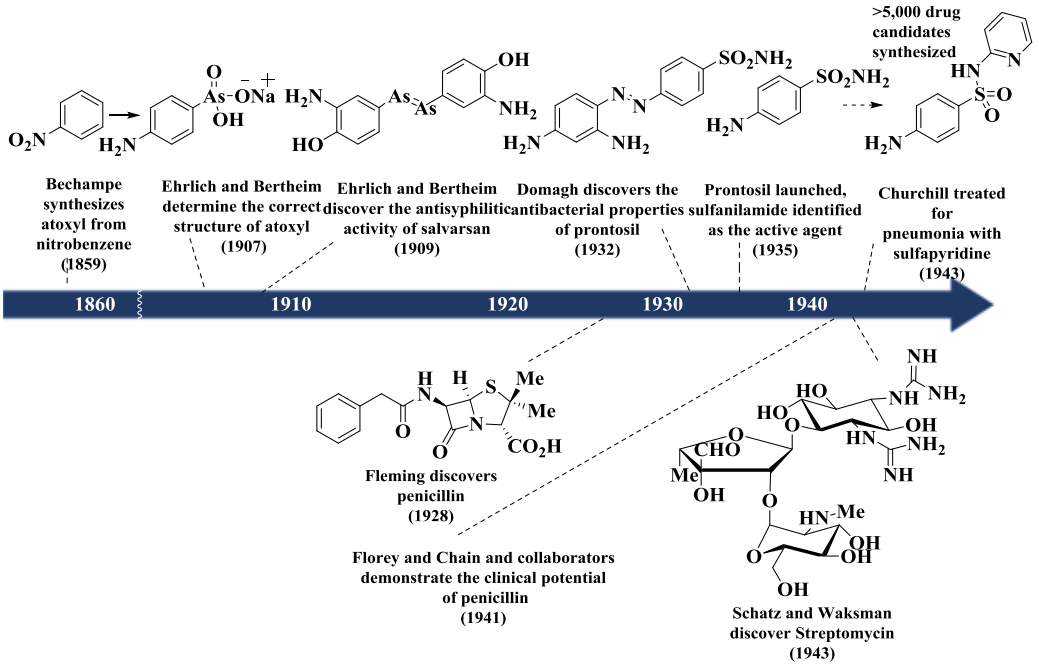

Fig. 1: Early history of antibiotic drug discovery

Different Classes of Antibacterials

According to large-scale manufacturing process, antibiotics can be categorised (Wright et al. 2014) into three classes (Fig. 2). This to some extent reflects their chronology of discovery and development.

Fig. 2: Three distinct categories of antibacterials

In 1941, the British government exhorted American pharmaceutical companies to consider the mass production of penicillin by fermentation. Four chemical and pharmaceutical companies, including Pfizer, responded to this call for large-scale production of the therapeutic compound penicillin. In 1944, Pfizer opened the world's first large penicillin factory, soon after Jasper Cane and co-workers achieved a landmark advance by implementing their deep-tank fermentation techniques for the production of penicillin (Stone, 1977). Production began with a sterile culture of the *Penicillinium* bacteria, which was then propagated and moved to massive fermenter tanks containing microbe fodder, chiefly corn steep liquor, milk sugar, salts and minerals. The mould was allowed to grow for two to four days. Subsequently, penicillin was extracted from the broth, purified and bottled in sterile rooms to avoid contamination. Finally, the bottles were moved through a freezing apparatus and then into a vacuum drier to dehydrate the drug. This remarkable development made Pfizer the leading supplier of the drug during World War II. Later, the scientists improved the method that removed yellow impurities of the originally found penicillin. The crystallisation method yielded white penicillin, stable at ambient temperature and potent for two years. Pfizer applied the fermentation techniques to the manufacture of other antibiotics including streptomycin (Schatz et al. 2005; Waksman, 2010) and terramycin (Finlay et al. 1950).

All efforts towards the development of a fully synthetic route towards penicillin failed during World War II (Sheehan, 1982; Parascandola, 1983; du Vigneaud et al. 1946; Chain, 1948; Robinson, 1949). John Sheehan solved the problem of finding fully synthetic pathways to penicillin. In 1950, Sheehan and co-workers (Sheehan et al. 1950) reported the total synthesis of methyl 5-phenyl-(2-carbomethoxyethyl)-penicillinate, a 5-phenylsubstituted penicillin derivative (Scheme 1). Although this analogue was inactive, this work was an important step forward. In 1955, Sheehan and Hess (Sheehan et al. 1955) invented an extremely mild method for the formation of amide bonds directly from the amine and carboxyl components, using carbodiimide reagents.

This chemical transformation was the key step in the first fully synthetic route to a natural penicillin, penicillin V (phenoxymethylpenicillin) (Sheehan et al. 1957). A few years after this key discovery, Sheehan and Logan (Sheehan et al. 1959) reported the synthesis of 6-aminopenicillanic acid (6-APA) by both semisynthetic and synthetic routes. In the same year, Batchelor (Batchelor et al. 1959) reported the isolation of 6-APA from penicillin fermentation broths and this then became the dominant precursor for the production of semisynthetic structural analogues of penicillin.

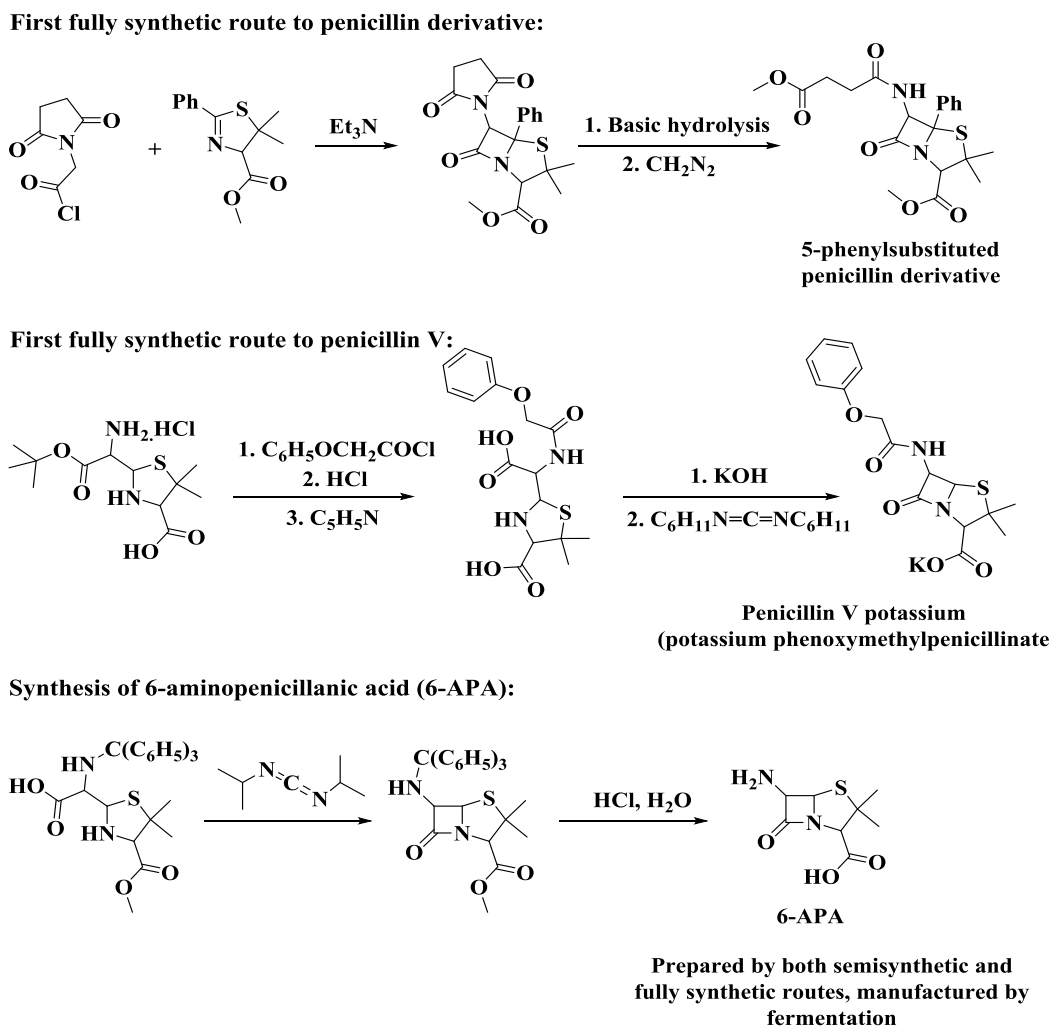

Scheme 1: Fully synthetic approaches to penicillin V and 6-aminopenicillanic acid

Semisynthesis became a key route in antibacterial drug discovery when dihydrostreptomycin (Bartz et al. 1946; Peck et al. 1946), a product found by catalytic hydrogenation of streptomycin, exhibited similar antibacterial properties with greater chemical stability. Using the semisynthetic approach, a broad-spectrum of β-lactam (Newton et al. 1955; Abraham et al. 1961; Chauvette et al. 1962; O'Callaghan et al. 1976; Verbist et al. 1980; Kessler et al. 1985; Garau et al. 1997), tetracycline (McCormick et al. 1960; Chubch et al. 1971; Sum et al. 1994; Sum et al. 1999) and macrolide (Morimoto et al. 1984; Morimoto et al. 1990) antibiotics (Fig. 3) were then synthesised.

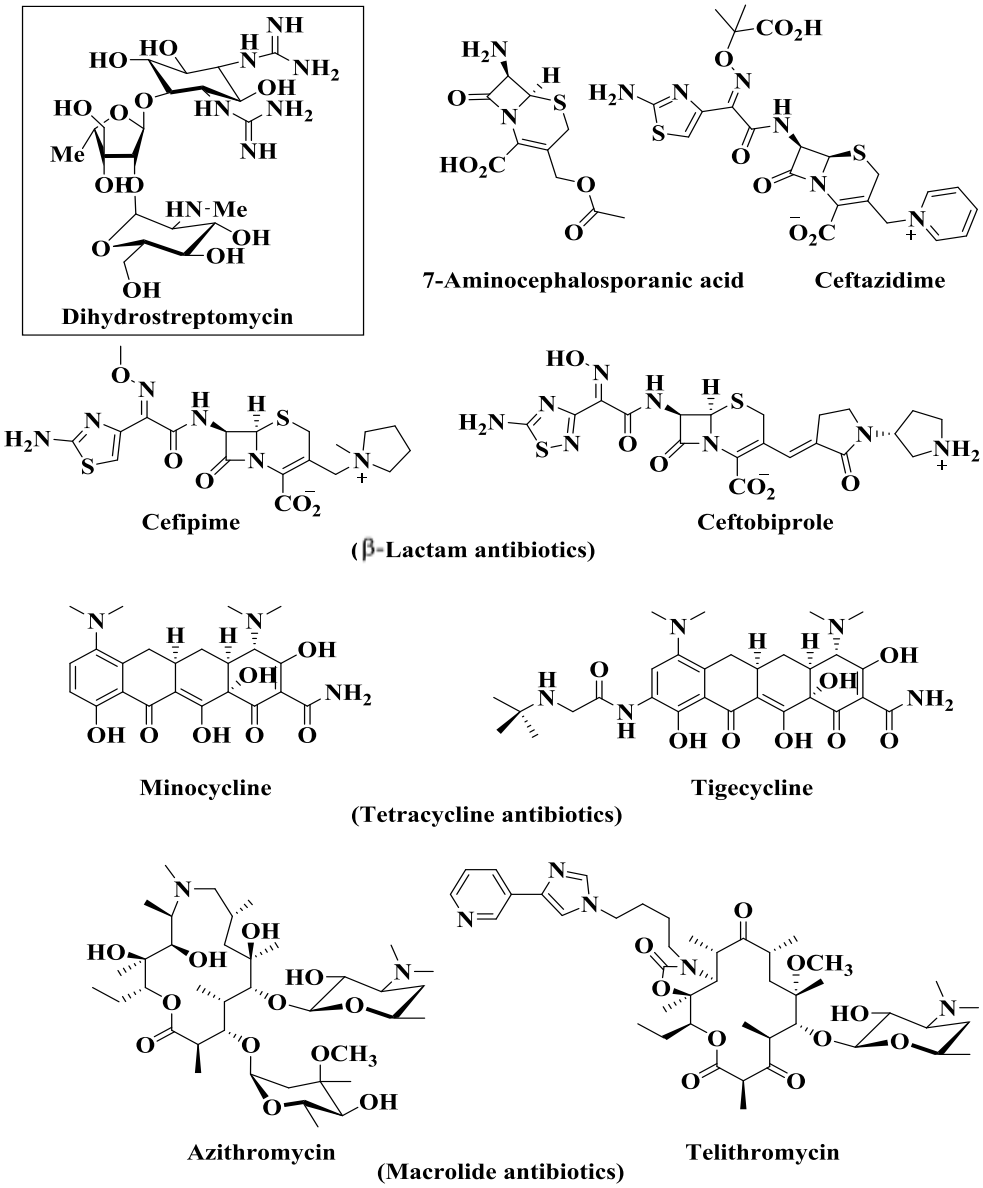

Fig. 3: Some examples of antibacterial drug developed by semisynthetic approach

In addition to the continued widespread application of semisynthesis in the development of antibiotics, fully synthetic approaches led to a large number of drugs (Fig. 4) including chloramphenicol (Controulis et al. 1949), metronidazole (Günay et al. 1999), trimethoprim (Fowle et al. 1968; Darrell et al. 1968), fosfomycin (Zhang et al. 2008; Estebanez et al. 2009), quinolones (Domagala et al. 1986; Hayakawa et al. 1986),

carbapenems (Melillo et al. 1986; Breuer et al. 1981) and oxazolidinones (Barbachyn et al. 2003).

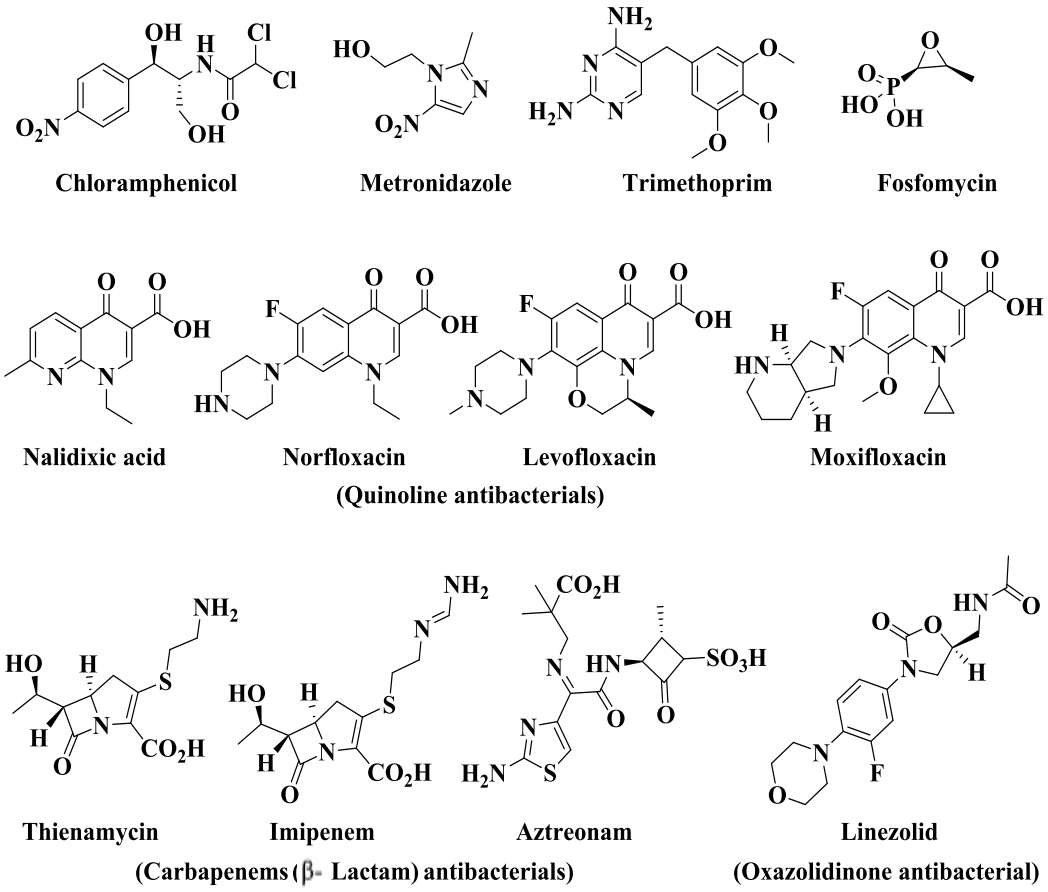

Fig. 4: Some examples of fully synthetic antibacterials

Antibiotic Resistance

Unfortunately, many existing drugs are becoming less effective as a consequence of resistance in pathogenic bacteria. The phenomenon of antibacterial resistance is not new, having been observed as early as 1940, when some bacteria had already acquired resistance to sulfa drugs (Aminov, 2010; Abraham et al. 1988). Resistance, however, has now become much more widespread, and has increased to the stage that it is a global threat which will limit treatment options for patients. Antibiotic resistance results in part from high consumption, and a recent report (Klein et al. 2018) on antibiotic resistance shows an increase of global antibiotic consumption by 65% between 2000-2015 (Fig. 5).

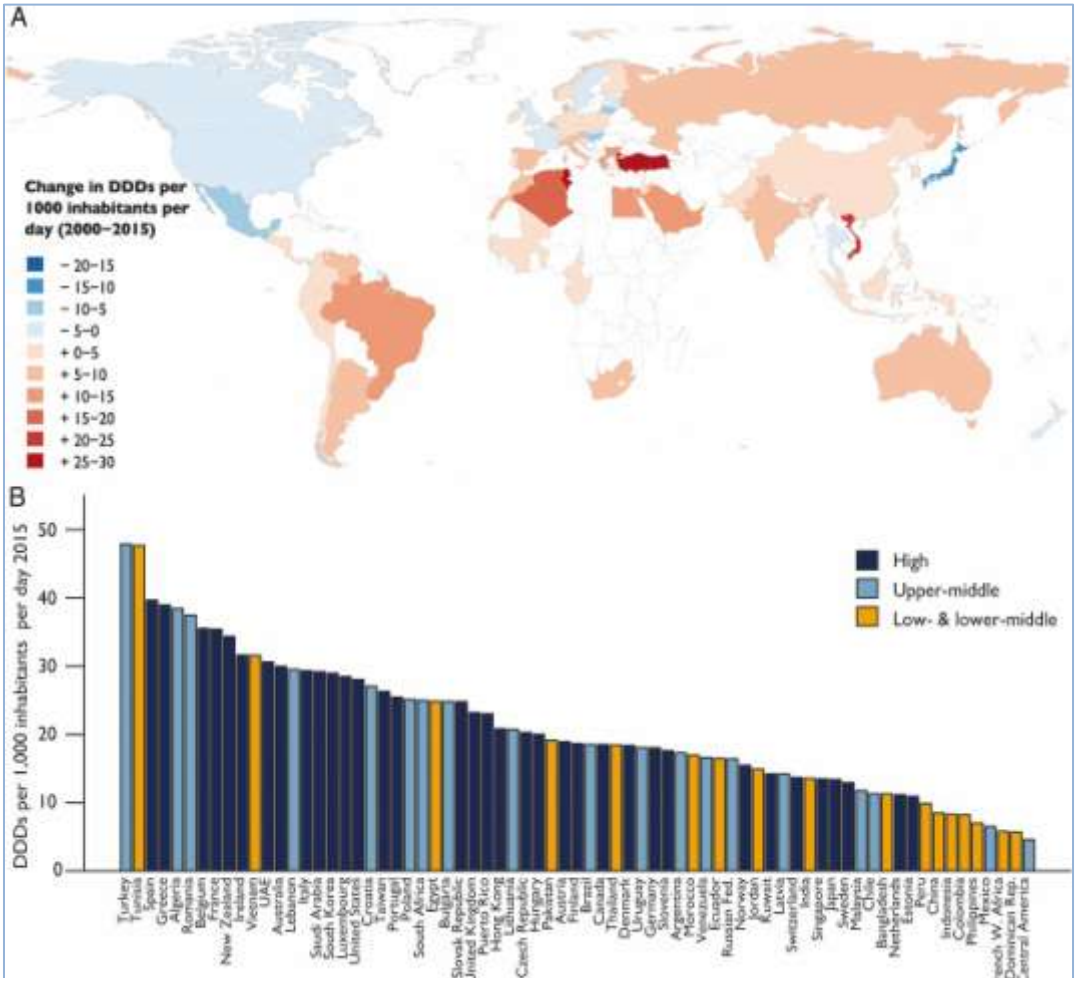

Fig. 5: Global antibiotic consumption by country: 2000-2015. (A) Change in the national antibiotic consumption rate between 2000 to 2015 in DDDs per 1000 inhabitants per day. For Vietnam, Bangladesh, The Netherlands, and Croatia, change was calculated from 2005, and for Algeria from 2002 as data for those years from those countries were not available. (B) Antibiotic consumption rate by country for 2015 in DDDs per 1000 inhabitants per day. Source: IQVIA MIDAS, 2000-2015, IQVIA Inc. (www.pnas.org/cgi/doi/10.1073/pnas.1717295115; accessed on June 2018)

Modern Antibacterial Drug Discovery

The past and future of antibiotic drug discovery (Brown et al. 2016) can be illustrated as a timeline (Fig. 6), showing the prevalent manoeuvres of each era. Most of the antibiotic

drugs currently in use were discovered in the "Golden Era". Pharmacological and toxicological limitations and resistance to early antibiotics led to the development of next period of antibiotic drug discovery, the Medicinal Chemistry era. This involved the synthesis of derivatives of the natural scaffolds which had been found in the golden era of antibiotic discovery, and which contributed to the improved application of antibiotics until the early 1990s. The emergence of new discovery methods then became essential due to the rise of antibiotic resistance.

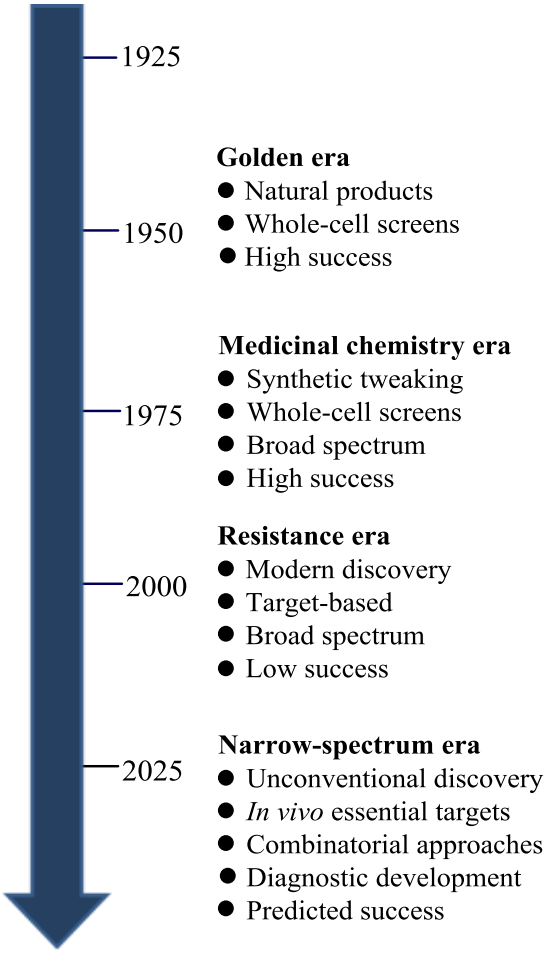

Fig. 6: Models of antibiotic drug discovery and development

With the help of modern technology, a target-based approach was initiated, but no new antibacterial medicines have been found by this approach. When confronted with the increasing resistance in this era, the failure of the development of new antibiotics for

more than two decades, coupled with over-prescription, has become a major concern. A careful investigation and understanding of antibiotics and their mode of action may now be required for the development of new medicines that will be able to tackle resistant bacteria.

Conclusion

This review explored the background of antibacterials and the synthetic utility of a library of compounds. It has shown the extensive use and importance of synthetic and semisynthetic approach in the development of new antibacterial drugs. Throughout this review, the earlier strategies towards antibacterial drug discovery, different categories of antibacterials, global antibiotic resistance and models of antibiotic drug discovery have discussed in a broad spectrum.

Acknowledgements

I take the opportunity to thank the Commonwealth Scholarship Commission in the UK for the award (BDCS-2015-52), and the University of Oxford for the contribution to carry out the research.

References

Guttmann P., P. Ehrlich. 1891. Ueber die wirkung des methylenblau bei malaria. Berlin Klin Wochenschr; **28**:953–956.

Wright P. M., I. B. Seiple, A. G. Myers. 2014. The evolving role of chemical synthesis in antibacterial drug discovery. Angew Chemie Int Ed. **53(34)**:8840-8869.

Lloyd N. C., H. W. Morgan, B. K. Nicholson, R. S. Ronimus. 2005. The composition of ehrlich's salvarsan: Resolution of a century-old debate. Angew Chemie Int Ed. **44(6)**:941-944.

Bosch F., L. Rosich. 2008. The contributions of paul ehrlich to pharmacology: A tribute on the occasion of the centenary of his nobel prize. Pharmacology. **82(3)**:171-179.

Lesch J. E. 2006. The first miracle drugs: How the sulfa drugs transformed medicine. Oxford University Press, New York.

Fleming A. 1929. On the Antibacterial action of cultures of a penicillium, with special reference to their use in the isolation of B. influenzæ. BrJ Exp Pathol. **10**:226-236.

Chain E, H. W. Florey, A. D. Gardner. 1940. Penicillin as a chemotherapeutic agent. Lancet. **2**:226-228.

Abraham E. P., E. Chain, C. M. Fletcher. 1941. Further observations on penicillin. Lancet. **238(6155)**:177-189.

Stone G. 1977. Penicillin production through deep-tank fermentation - national historic chemical landmark - American Chemical Society. https://www.acs.org/content/acs/en/education/whatischemistry/landmarks/penicillin.html. Accessed on June 23, 2018.

Schatz A., E. Bugie, S. A. Waksman. 2005. Streptomycin, a substance exhibiting antibiotic activity against gram-positive and gram-negative bacteria. 1944. Clin Orthop Relat Res. **(437)**:3-6.

Waksman S. A. 2010. Antibiotic substances-contribution of the microbiologist. Ann N Y Acad Sci. **1213(1)**:107-111.

Finlay A. C., G. L. Hobby, P'An SY. 1950. Terramycin, a new antibiotic. *Science (80-)*. **111(2874)**:85.

Sheehan J. C. 1982. The enchanted ring : The untold story of penicillin. MIT Press. https://mitpress.mit.edu/books/enchanted-ring. Accessed on June 24, 2018.

Parascandola J. 1983. The enchanted ring: The untold story of penicillin . John C. Sheehan. Isis. **74(2)**:280-281.

du Vigneaud V., F. H. Carpenter, R. W. Holley, A. H. Livermore, J. R. Rachele. 1946. Synthetic penicillin. Science (80-). **104(2706)**:431-450.

Chain E. 1948. The chemistry of penicillin. Annu Rev Biochem. **17(1)**:657-704.

Robinson F. A. 1949. The chemistry of penicillin, edited by Hans T. Clarke, John R. Johnson and Sir Robert Robinson. Pp. 1042 and Appendix. Princeton University Press, New Jersey (London: Geoffrey Cumberlege) 1949, J Pharm Pharmacol. **1(1)**:634-635.

Sheehan J. C., E. L. Buhle, E. J. Corey, G. D. Laubach, J. J. Ryan. 1950. The total synthesis of a 5-phenyl penicillin: methyl 5-phenyl-(2-carbomethoxyethyl)-penicillinate. J Am Chem Soc. **72(8)**:3828-3829.

Sheehan J. C., G. P. Hess. 1955. A new method of forming peptide bonds. J Am Chem Soc. **77(4)**:1067-1068.

Sheehan J. C., K. R. Henery-Logan 1957. The total synthesis of penicillin V. J Am Chem Soc. **79(5)**:1262-1263.

Sheehan J. C., K. R. H. Logan. 1959. A general synthesis of the penicillins. J Am Chem Soc. **81(21)**:5838-5839.

Batchelor F. R., F. P. Doyle, J. H. C. Nayler, G. N. Rolinson. 1959. Synthesis of penicillin: 6-aminopenicillanic acid in penicillin fermentations. Nature. **183(4656)**:257-258.

Bartz Q. R., J. Controulis, H. M. Crooks, M. C. Rebstock. 1946. Dihydrostreptomycin 1. J Am Chem Soc. **68(11)**:2163-2166.

Peck R. L., C. E. Hoffhine, Folkers K. 1946. Streptomyces antibiotics. IX. dihydrostreptomycin. J Am Chem Soc. **68(7)**:1390-1391.

Newton G. G. F., E. P. Abraham, C. Cephalosporin. 1955. A new antibiotic containing sulphur and D-α-aminoadipic acid. Nature. **175(4456)**:548-548.

Abraham E. P., G. G. F. Newton. 1961. The structure of cephalosporin C. Biochem J. **79(2)**:377-393.

Chauvette R. R., E. H. Flynn, B. G. Jackson. 1962. Chemistry of cephalosporin antibiotics. II. Preparation of a new class of antibiotics and the relation of structure to activity. J Am Chem Soc. **84(17)**:3401-3402.

O'Callaghan C. H., R. B. Sykes, A. Griffiths, J. E. Thornton. 1976. Cefuroxime, a new cephalosporin antibiotic: activity in vitro. *A*ntimicrob Agents Chemother. **9(3)**:511-519.

Verbist L., J. Verhaegen. 1980. GR-20263: A new aminothiazolyl cephalosporin with high activity against *Pseudomonas* and *Enterobacteriaceae*. Antimicrob Agents Chemother. **17(5)**:807-812.

Kessler R. E., M. Bies, R. E. Buck. 1985. Comparison of a new cephalosporin, BMY 28142, with other broad-spectrum beta-lactam antibiotics. Antimicrob Agents Chemother. **27(2)**:207-216.

Garau J., W. Wilson, M. Wood, J. Carlet. 1997. Fourth-generation cephalosporins: a review of in vitro activity, pharmacokinetics, pharmacodynamics and clinical utility. Clin Microbiol Infect. **3**:S87-S101.

McCormick J. R. D., E. R. Jensen, P. A. Miller, A. P. Doerschuk. 1960. The 6-deoxytetracyclines. 1 further studies on the relationship between structure and antibacterial activity in the tetracycline series. J Am Chem Soc. **82(13)**:3381-3386.

Chubch R. F. R., R. E. Schaub, M. J. Weiss. 1971. Synthesis of 7-dimethylamino-6-demethyl- 6-deoxytetracycline (Minocycline) via 9-Nitro-6-demethyl-6-deoxytetracycline. J Org Chem. **36(5)**:723-725.

Sum P-E, V. J. Lee, R. T. Testa. 1994. Glycylcyclines. 1. A new generation of potent antibacterial agents through modification of 9-aminotetracyclines. *J Med Chem*. **37(1)**:184-188.

Sum P-E, P. Petersen. 1999. Synthesis and structure-activity relationship of novel glycylcycline derivatives leading to the discovery of GAR-936. Bioorg Med Chem Lett. **9(10)**:1459-1462.

Morimoto S., Y. Takahashi, Y. Watanabe, S. Omura. 1984. Chemical modification of erythromycins. I. Synthesis and antibacterial activity of 6-O-methylerythromycins A. J Antibiot (Tokyo). **37(2)**:187-189. http://www.ncbi.nlm.nih.gov/pubmed/6706855. Accessed on June 24, 2018.

Morimoto S, Y. Misawa, T. Adachi, T. Nagate, Y. Watanabe, S. Omura. 1990. Chemical modification of erythromycins. II. Synthesis and antibacterial activity of O-alkyl derivatives of erythromycin A. J Antibiot (Tokyo). **43(3)**:286-294.

Controulis J., M. C. Rebstock, H. M. Crooks. 1949. Chloramphenicol (Chloromycetin). 1 V. Synthesis. J Am Chem Soc. **71(7)**:2463-2468.

Günay N. S., G. Çapan, N. Ulusoy, N. Ergenç, G. Ötük, Kaya D. 1999. 5-Nitroimidazole derivatives as possible antibacterial and antifungal agents. Farm. **54(11-12)**:826-831.

Fowle A. S. 1968. Trimethoprim. Br Med J. **2(5604)**:557. http://www.ncbi.nlm.nih.gov/pubmed/4302077. Accessed on June 24, 2018.

Darrell J. H., L. P. Garrod, P. M. Waterworth. 1968. Trimethoprim: laboratory and clinical studies. J Clin Pathol. **21(2)**:202-209. http://www.ncbi.nlm.nih.gov/pubmed/5697054. Accessed on June 24, 2018.

Zhang Z., J. Tang, X. Wang, H. Shi. 2008. Chiral ketone- or chiral amine-catalyzed asymmetric epoxidation of cis-1-propenylphosphonic acid using hydrogen peroxide as oxidant. J Mol Catal A Chem. **285(1-2)**:68-71.

Estebanez A., R. Pascual, V. Gil, O F. rtiz, M. Santibáñez, C. Pérez Barba. 2009. Fosfomycin in a single dose versus a 7-day course of amoxicillin–clavulanate for the treatment of asymptomatic bacteriuria during pregnancy. Eur J Clin Microbiol Infect Dis. **28(12)**:1457-1464.

Domagala J. M., L. D. Hanna, C. L. Heifetz. 1986. New structure-activity relationships of the quinolone antibacterials using the target enzyme. The development and application of a DNA gyrase assay. J Med Chem. **29(3)**:394-404.

Hayakawa I., S. Atarashi, S. Yokohama, M. Imamura, K. Sakano, M. Furukawa. 1986. Synthesis and antibacterial activities of optically active ofloxacin. Antimicrob Agents Chemother. **29(1)**:163-164.

Melillo D. G., R. J. Cvetovich, K. M. Ryan, M. Sletzinger. 1986. An enantioselective approach to (+)-thienamycin from dimethyl 1,3-acetonedicarboxylate and (+)-.alpha.-methylbenzylamine. J Org Chem. **51(9)**:1498-1504.

Breuer H., C. M. Cimarusti, T. Denzel, W. H. Koster, W. A. Slusarchyk, U. D. Treuner. 1981. Monobactams--structure-activity relationships leading to SQ 26,776. J

Antimicrob Chemother. **8** Suppl E:21-28. http://www.ncbi.nlm.nih.gov/pubmed/7199044. Accessed on June 24, 2018.

Barbachyn M. R., C. W. Ford. 2003. Struktur-Wirkungs-Beziehungen von oxazolidinonen: grundlage der entwicklung von linezolid. Angew Chemie. **115(18)**:2056-2070.

Aminov R. I. 2010. A brief history of the antibiotic era: lessons learned and challenges for the future. Front Microbiol. **1**:1-7.

Abraham E. P., E. Chain. 1988. An enzyme from bacteria able to destroy penicillin. **10(4)**:677-678.

Klein E. Y., T. P. Van Boeckel, E. M. Martinez. 2018. Global increase and geographic convergence in antibiotic consumption between 2000 and 2015. Proc Natl Acad Sci. **115(15)**:E3463-E3470. doi:10.1073/pnas.1717295115.

Brown E. D., G. D. Wright. 2016. Antibacterial drug discovery in the resistance era. Nature. **529(7586)**:336-343.

BARISHAL UNIVERSITY JOURNAL PART 1

ISSN 2411-247X

Volume 6 **Issue 2** **December 2019**

CONTENTS

Full Article

Barishal University Journal Part 1, 6(2): 1-7 (2019) ISSN 2411-247X

APPLICATION OF MAIN-CHAIN CHIRAL POLYMERIC ORGANOCATALYST IN ASYMMETRIC EPOXIDATION OF TRANS-CHALCONE

Md. Masud Parvez[*1], Md. Alauddin[2] and Shinichi Itsuno[3]

[1]*Department of Chemistry, University of Barishal, Bangladesh*
[2]*Department of Theoretical and Computational Chemistry, University of Dhaka, Bangladesh*
[3]*Department of Environmental and Life Sciences, Toyohashi University of Technology, Japan*

Abstract

Main-chain chiral ionic polymers have been applied as chiral polymeric organocatalyst in asymmetric epoxidation of trans-chalcone. These polymeric organocatalysts showed catalytic activity (up to 100% conversion and 51% ee), when applied in asymmetric epoxidation of trans-chalcone. They work more efficiently when used with the surfactant "Triton X-100" (5 mol%).

***Keywords*:** Polymeric organocatalyst, Main-chain chiral polymers, Asymmetric epoxidation, Cinchona alkaloids.

Introduction

Optically active epoxides have become one of the major fields of interest, since the first report (Katsuki et al. 1980) on the asymmetric epoxidation of allylic alcohol. Ever since, many approaches have been proposed for the epoxidation of both un functionalized olefins and electron-deficient enones (Portal et al. 2002). Among the approaches, chiral phase transfer catalysis (PTC) is one of the widely used method, applied to the asymmetric epoxidation of electron-deficient olefins. Enantioselective epoxidation of electron deficient olefins under PTC conditions catalyzed by quaternized cinchona alkaloids pioneered by (Helder et al. 1976) Later (Lygo et al. 1998) and (Corey et al. 1999) improved the method. Dimeric cinchona derived catalysts with the addition of surfactants was reported by (Jew et al. 2005) and very high enantioselectivity was obtained with shorter reaction time. Non-Cinchona-derived species, such as spiro ammonium salts (Oi et al. 2004), polyamino acids (Juliá et al. 1980), lanthanoid-binaphthol complexes (Shibasaki et al. 1997) and chiral crown ethers derived from D-glucose, D-galactose, and D mannitol (Bako et al. 2004) have also been used in this kind

[*] *Corresponding author's email: masud.chdu@yahoo.com*

of asymmetric epoxidation. Moreover, polymer-supported cinchona derived phase transfer catalyst (Lv et al. 2006) in asymmetric epoxidation of chalcones. Although several works have done with the monomeric, dimeric and polymer-supported cinchona derived quaternary ammonium salts, there is almost no report on the application of main-chain chiral polymeric organocatalyst in the asymmetric epoxidation of chalcones.

In our previous work, we synthesized some main-chain chiral polymers and applied in asymmetric benzylation of glycine derivative (Parvez et al. 2012). In this work, we applied the same main-chain chiral ionic polymer in asymmetric epoxidation of *trans*-chalcone.

Experimental Section

Materials and Methods

All reagents were purchased from Sigma-Aldrich, Wako Pure Chemical Industries, Ltd., or Tokyo Chemical Industry Co., Ltd. at the highest available purity and used as is unless noted otherwise. Reactions were monitored by thin-layer chromatography (TLC) using Merck precoated silica-gel plates (Merck 5554, 60F254). ^{1}H (300 MHz or 400 MHz) and ^{13}C NMR (75 MHz or 100 MHz) spectra were measured on Mercury 300 or Jeol ECS 400 spectrometer. HPLC analyses were performed with a JASCO HPLC system comprising a three-line degasser DG-980-50, an HPLC pump PV-980, and a CO-965 column oven equipped with a chiral column (CHIRALPAC AD, Daicel). A UV detector (JASCO UV-975 for JASCO HPLC system) was used for peak detection.

Synthesis of Main-chain Chiral Polymers

We have utilized some main-chain chiral polymers synthesized in our previous work (Scheme 2) (Parvez et al. 2012). A solution of cinchona derived dimeric quaternary ammonium salt 2 (1 mmol,) in 10 mL CH_3OH and a solution of disulfonic acid-disodium salt 3 (1 mmol) in 8 mL water were mixed together and stirred vigorously at room temperature for 24 hours. Then it was filtered and washed with water and hexane to obtain the resulting ionic polymer. The yields of the products were in the range 80~90%.

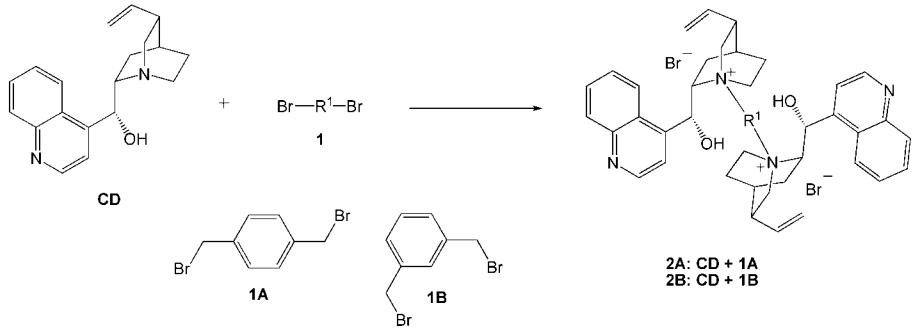

Scheme 1 Synthesis of dimer **2** from cinchonidine **CD** (Jew et al. 2001)

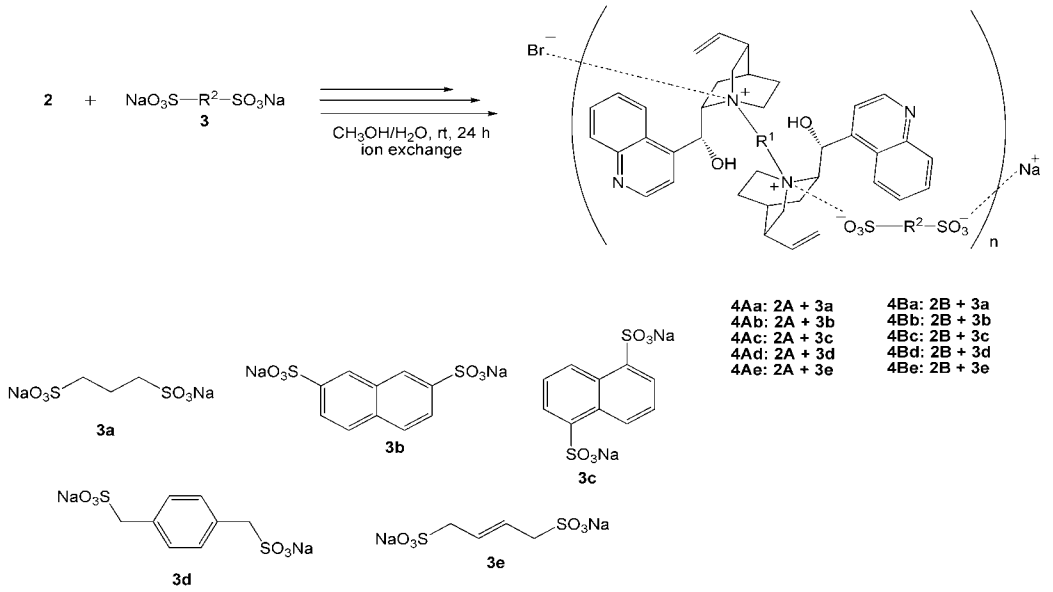

Scheme 2 Synthesis of main-chain chiral ionic polymer **4** (Parvez et al. 2012)

General Procedure for Asymmetric Epoxidation of *Trans*-chalcone

Aqueous hydrogen peroxide (30%, 0.27 mL; 2.4 mmol) and 50 wt % aqueous KOH (0.027 mL, 0.24 mmol) were added to a mixture of chalcone **5** (50 mg, 0.24 mmol), **catalyst** (5 mol%) and Triton-X 100 (5 mol%) in $^{i}Pr_2O$ (0.8 mL), and the reaction mixture was stirred vigorously at room temperature until the starting material had been consumed. The resulting suspension was diluted with ether (10 mL), washed with water (2×5 mL), dried over $MgSO_4$, filtered, and concentrated in vacuo to get the desired product 6 as a white solid. The enantioselectivity was determined by chiral HPLC analysis (DAICEL CHIRALPAC AD, Daicel), hexane/ethanol=90:10, flow rate=1.0 mL min^{-1}, 23°C, λ=254 nm; retention times: 16.6 min (minor), 24.0 min (major). The absolute configuration was determined by comparison of the HPLC retention time with reported data (Lygo et al. 1998).

Results and Discussion

Application of Main-Chain Chiral Polymers

Cinchona derived quaternary ammonium salts are quite effective in asymmetric epoxidation of *trans*-chalcones. So, the polymers containing cinchonidium unit in the

polymer main-chain should show catalytic activity in asymmetric epoxidation of *trans*-chalcones. Several groups have reported the asymmetric epoxidation of chalcone and their derivatives using cinchona derived quaternary ammonium salts using different types of oxidants, solvents, bases to obtain chiral epoxides. The reaction is very sensitive towards the catalyst structure, oxidant, solvent and base. So, it was quite challenging to apply main-chain chiral polymeric oraganocatalyst and obtain an optimized condition for the asymmetric epoxidation of chalcones.

We arbitrarily started with the optimization of the reaction with different dimeric and polymeric catalysts, oxidants, solvents and bases (Scheme 3, Table 1). But unfortunately, most of the cases racemic product was obtained.

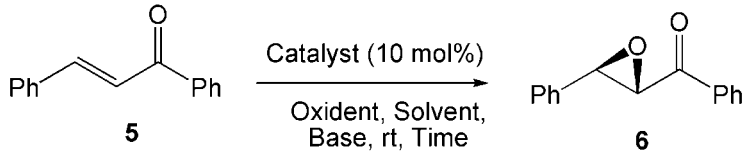

Scheme 3 Asymmetric epoxidation of Chalcone **5**

Table 1. Asymmetric epoxidation of *trans*-chalcone using various main-chain chiral polymeric Organocatalysts at different reaction conditions

Entry	Catalyst	Oxidant	Solvent	Base (1 equiv.)	Time (h)	Conv. ((%) [a]	Ee (%)[b]
1	**2A**	NaOCl	Toluene	------	24	0	ND
2	**2A**	^{t}BuOOH	DCM	50 wt% KOH	120	95	53
3	**4Ac**	H_2O_2	Toluene	LiOH (Solid)	48	48	Racemic
4	**4Ac**	H_2O_2	Bu_2O	LiOH (Solid)	48	60	Racemic
5	**4Ad**	NaOCl	Toluene	------	72	0	ND
6	**4Bb**	H_2O_2	Bu_2O	LiOH. H_2O (Solid)	48	50	6
7[c]	**4Bb**	H_2O_2	Bu_2O	LiOH. H_2O (Solid)	96	60	5
8	**4Bc**	NaOCl	Toluene	------	72	0	ND

[a]Determined by ^{1}H NMR. [b]Determined by HPLC (CHIRALPAC AD, Daicel). [b](αS, βR) major product. [c]Carried out at 0 ^{o}C. [d]Opposite configuration was obtained.

When dimer **2A** was applied, it showed no catalytic activity (Table1, entry 1). Changing the oxidant, solvent and addition of 50 wt% KOH (1 equiv.) increases the catalytic activity but rate was too low (entry 2). Using polymer **4Ac** racemic product was obtained (entry 3 and 4). The results were not satisfactory, in case of **4Bb** and **4Bc** (entry 6 to 7). Then, we turned our attention to the addition of surfactant "Span 20" to the reaction

mixture. Asymmetric epoxidation of chalcones using surfactant surprisingly the rate of reaction increased and high enantioselectivity was obtained (Jew et al. 2005). We also tried to apply the main-chain chiral ionic polymer **4A(a~e)** in asymmetric epoxidation of chalcones in presence of 1 mol% of span 20, diisopropyl ether as solvent and 30% H_2O_2 as an oxidant and the results are summarized in Table 2.

In this case, we noticed that polymer containing *p*-xylene moiety in the main-chain **4A (a~e)** employed in asymmetric epoxidation of chalcones also did not show good catalytic activity and sometime racemic products were obtained (Table 2, entry 3 and 5). Although the conversion of **5** to **6** and rate of reactions were fair.

Table 2. Asymmetric epoxidation of *trans*-chalcone using main-chain chiral polymeric Organocatalyst **4A(a~e)** with the addition of surfactant "Span 20".

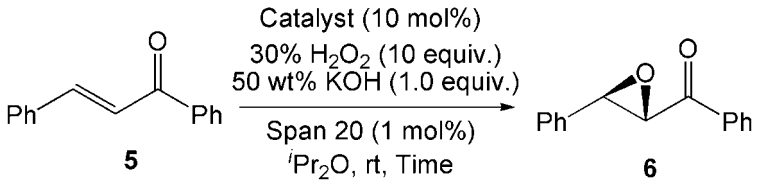

Entry	Catalyst	Time (h)	Conv. (%) [a]	Ee (%) [b]
1[d]	**4Aa**	24	68	3
2	**4Ab**	24	52	8
3	**4Ac**	24	88	Racemic
4[d]	**4Ad**	24	59	2
5	**4Ae**	24	100	Racemic

[a]Determined by ^{1}H NMR. [b]Determined by HPLC (CHIRALPAC AD, Daicel).
[b](αS, βR) major product. [d]Opposite configuration was obtained.

When polymeric organocatalyst **4B(a~e)** containing *m*-xylene moiety in the main-chain were employed in asymmetric epoxidation of *trans*-chalcone better results were obtained, compare to the results obtained with **4A(a~e)**. The results are summarized in Table 3. Polymeric catalyst **4Ba** showed some catalytic activity, when Span 20 was used as surfactant (Table 3, entry 1), whereas 4**Bb** and **4Bc** gave racemic product (entry 2 and 3).

After changing the surfactant from "Span 20" to "Triton-X 100" the enantioselectivity increased. We used 5 mol% catalyst and 5 mol% of "Triton-X 100" as surfactant and improved enantioselectivities were obtained (Table 3, entry 4 to 6).

Table 3. Asymmetric epoxidation of *trans*-chalcone using main-chain chiral polymeric Organocatalyst **4B(a~e)** with the addition of different types of surfactants.

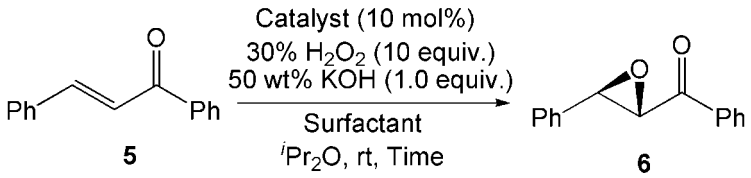

Entry	Catalyst	Surfactant (mol%)	Time (h)	Conv. (%)[a]	Ee (%)[b]
1	**4Ba**	Span 20, (1 mol %)	24	100	26
2	**4Bb**	Span 20, 1 mol %)	24	99	Racemic
3	**4Bc**	Span 20, 1 mol %)	24	100	Racemic
4	**4Ba**	**Triton X-100 (5 mol%)**	**16**	**100**	**38**
5	**4Bd**	**Triton X-100 (5 mol%)**	**16**	**100**	**51**
6	**4Be**	**Triton X-100 (5 mol%)**	**16**	**100**	**33**

[a]Determined by ^{1}H NMR. [b]Determined by HPLC (CHIRALPAC AD, Daicel). [b](αS, βR) major product.

Conclusion

Asymmetric epoxidation of *trans*-chalcone has been carried out using various main-chain chiral polymeric organocatalyst. Several types of main-chain chiral polymers have been utilized. The reaction is sensitive to the catalyst structure, oxidant, solvent, temperature and base. After screening all the polymeric catalyst and optimization of the reaction condition, polymeric organocatalyst **4Ba**, **4Bd** and **4Bd** showed 38% to 51% enantioselectivity and 100% conversion in presence of Triton X-100 (5 mol%), when applied in asymmetric epoxidation of *trans*-chalcone.

Acknowledgement

This work was done in the Laboratory of Professor Shinichi Itsuno, Department of Environmental and life Sciences, Toyohashi University of Technology, Japan 441-8122.

References

Katsuki T., K. B. Sharpless. 1980. The first practical method for asymmetric epoxidation. J. Am. Chem. Soc. **102**: 5974-5976.

Porter M. J., J. Skidmore. 2002. Asymmetric epoxidation of electron-deficient olefins. Chem. Commun. 1215- 1225.

Helder R., J. C Hummelen, R. W. P. M Laane, J. S Wiering, H. Wynberg. 1976. Catalytic asymmetric induction in oxidation reactions. The synthesis of optically active epoxides.Tetrahedron Lett. **17**:1831–1834.

Lygo B., P. G. Wainwright. 1998. Asymmetric phase-transfer mediated epoxidation of α, β-unsaturated ketones using catalysts derived from *Cinchona* alkaloids Tetrahedron Lett. **39**: 1599-1602.

Corey E. J., F.-Y. Zhang. 1999. Mechanism and Conditions for Highly Enantioselective Epoxidation of α,β-Enones Using Charge-Accelerated Catalysis by a Rigid Quaternary Ammonium Salt. Org. Lett. **1**: 1287– 1290.

Jew S.-S., J.-H. Lee, B.-S. Jeong, M.-S. Yoo, M.-J., Kim, Y.-J. Lee, S.-H Choi, K. Lee, M. S Lah, H.-G. Park. 2005**.** Highly Enantioselective Epoxidation of 2,4-Diarylenones by Using Dimeric Cinchona Phase-Transfer Catalysts: Enhancement of Enantioselectivity by Surfactants. Angew. Chem. Int. Ed. **44**: 1383–1385.

Juliá S., J. Masana, J. C. Vega. 1980. "Synthetic Enzymes". Highly Stereoselective Epoxidation of Chalcone in a Triphasic Toluene-Water-Poly[(S)-alanine] System. Angew. Chem. Int. Ed. Engl. **19**: 929–933.

Shibasaki M., H. Sasai, T. Arai. 1997. Asymmetric Catalysis with Heterobimetallic Compounds. Angew. Chem. Int. Ed. **36**: 1236–1256.

Bakó T., P. Bakó, G. Keglevich, P. Bombicz, M. Kubinyi. 2004. Phase-transfer catalyzed asymmetric epoxidation of chalcones using chiral crown ethers derived from D-glucose, D-galactose, and D-mannitol. Tetrahedron: Asymmetry. **15**: 1589–1595.

Lv J., X. Wang, J. Liu, L. Zhang, Y. Wang. 2006. Catalytic asymmetric epoxidation of chalcones under poly(ethylene glycol)-supported Cinchona ammonium salt catalyzed conditions. Tetrahedron Asymmetry**. 17**: 330-335.

Parvez M. M., N. Haraguchi, S. Itsuno. 2012. Molecular design of chiral quaternary ammonium polymers for asymmetric catalysis applications. Org. Biomol. Chem., **10**: 2870-2877.

Barishal University Journal Part 1, 6(2): 9-22 (2019) ISSN 2411-247X

GENERALIZATIONS OF THE TERNARY CANTOR SET

Hena Rani Biswas* and Md. Monirul Islam Sumon

Department of Mathematics, University of Barishal, Barishal- 8200, Bangladesh

Abstract

In this paper we present some basic concepts of ternary Cantor set. We have proved several interesting lemmas, theorems, and propositions relating to Cantor set and discussed the general Cantor set and the universal Cantor set. The principle aim of this paper is introduce a generator of finite subsets of the basic ternary Cantor set and its generalization to the Cantor *n*-ary set. We also have proved that the Cantor set $C_{1/3}$ and $C_{1/2}$ are measurable set and have measure zero. Finally, we have proved the homeomorphism between the general and the universal Cantor sets.

Keywords: Cantor set, Topology, Measure, Universal Cantor sets, Homeomorphism.

Introduction

Cantor set was discovered by German mathematician George Cantor (1845–1918) in the last part of the nine-tenth century. In 1883, he wrote a series of papers that contained the first systematic treatment of the point set topology of real line in which he raised some problems and attracted interest of researchers to the field of set theory. One of these is the classical Cantor set which he forwarded as an example of a perfect, nowhere dense subset of $\mathbb{R}$. A considerable stir was created in the mathematical community since the properties of the Cantor set were found to be counter intuitive. For example, it is hard to imagine points in the Cantor set other than the end points of the intervals which are removed in the process of its construction, yet we know that they must exist. Throughout much of the twentieth century, Cantor set was considered to be a little more than mathematical curiosity. However, the work of Stephen Smale in the 1960s demonstrated that Cantor sets play an important role in dynamical systems (Gautam Choudhury, et al., 2019).

The Cantor set plays a very important role in many branches of mathematics, above all in set theory, chaotic dynamical systems and fractal theory. Cantor sets can be constructed

* *Corresponding Author's Email: biswas.hena@yahoo.com*

geometrically by continuous removal of a portion of the closed unit interval $[0,1]$ infinitely. The set of points remained in the unit interval after this removal process is over is called the Cantor set. Cantor set can be understood geometrically by imagining the continuous removal of a set portion of a shape in such a way that at every stage of removal, the chucks of the shape that remain each have the same percentage removed from their centers. If this removal process continues infinitely, then the tiny bits of the shape that remains from a Cantor set. The Cantor set has many definitions and many different constructions. Although Cantor originally provided a purely abstract definition, the most accessible is the Cantor 'middle-thirds' or ternary set construction. Now we will briefly describe how to construct this set. Let $I = [0,1]$ be the closed interval then remove the open third segment $\left(\frac{1}{3},\frac{2}{3}\right)$ and let $A_1 = \left[0,\frac{1}{3}\right] \cup \left[\frac{2}{3},1\right]$ now remove the open third segments in each part. Let $A_2 = \left[0,\frac{1}{9}\right] \cup \left[\frac{2}{9},\frac{1}{3}\right] \cup \left[\frac{2}{3},\frac{7}{9}\right] \cup \left[\frac{8}{9},1\right]$. Continue in this way removing the middle third of each segment to get A_3, A_4 ... . Note that $A_1 \supseteq A_2 \supseteq A_3 \supseteq \cdots$. And for each $k \in \mathbb{N}$, A_k is the union of 2^k closed intervals, each of length 3^{-k}. This process is visible in the Fig. 1.

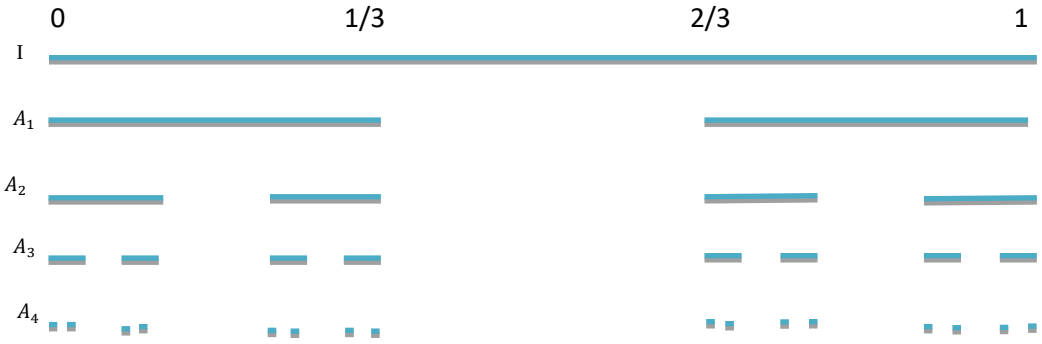

Fig.1. The first five sets formed in the construction of the Cantor Ternary set.

Finally, we define the Cantor ternary set as follows: $C = \bigcap_{i=1}^{\infty} A_i$.

In section 2 of this paper we describe the mathematical preliminaries which are requirements for the subsequent chapters. In section 3 we discuss some basic theorems and properties of the ternary Cantor set. In section 4 we solve some problems about Cantor set such as, the Cantor set $C_{1/3}$ when added to itself give the interval $[0,2]$ and the Cantor set $C_{1/3}$ and $C_{1/2}$ are measurable set and have measure zero. In this section we also prove the homeomorphism between the general and the universal Cantor sets.

Mathematical Preliminaries

In this section we are giving some definitions, lemmas and propositions needed for the main results. We start with some elementary definitions.

Definition 2.1 (Cantor Set)

A nonempty set $C \subset \mathbb{R}$ is called a Cantor set if

(i) C is closed and bounded.

(ii) C contains no intervals.

(iii) Every point in C is an accumulation point of C.

Definition 2.2 (Cantor-like set (Stettin R., 2017))

Any subset of the real line R which is compact, totally disconnected and perfect is called Cantor-like set or imply Cantor set.

Definition 2.3 (Cantor Middle third set $C_{\frac{1}{3}}$):

Beginning with the unit interval $I = [0,1]$, define closed subsets $A_1 \supset A_2 \supset \cdots$ in I as follows : we obtain A_1 by removing the interval $\left(\frac{1}{3}, \frac{2}{3}\right)$ from I, A_2 is then obtained by removing from A_1 the open intervals $\left(\frac{1}{9}, \frac{2}{9}\right)$ and $\left(\frac{7}{9}, \frac{8}{9}\right)$. In general, having A_{n-1}, A_n is obtained by removing the open middle thirds from each of the 2^{n-1} closed intervals that make up A_{n-1}. The Cantor middle third set is the subspace $C_{1/3} = \bigcap A_n$ of I.

Definition 2.4 (Cantor Middle Half set $C_{\frac{1}{2}}$):

Start with the unit interval $F_0 = [0,1]$. Remove the (open) middle half-resulting in $F_1 = [0,1/4] \cup [3/4,1]$. Then repeat the process removing the middle half of each of the intervals that remain. At stage n we get a set F_n that is the union of 2^n intervals each being of length 4^{-n}. These are nested: $F_0 \supset F_1 \supset F_2$ ..., so their intersection $C_{\frac{1}{2}} = \bigcap_{n=0}^{\infty} F_n$ is called the Cantor middle half set.

Definition 2.5 (Ternary Representation of Numbers):

For any $x \in [0,1], x$ can be represented in the scale of some integer $b > 1$ as $x = (0.a_1a_2a_3 \ldots)_b$, where every a_i is one of the integers $0, \ldots . b-1$. Also x can be represented by a convergent series as: $x = \sum_{i=1}^{\infty} \frac{a_i}{b^i} : a_i \in \{0, \ldots, \mathrm{b}-1\}$ for every $i = 1,2, \ldots$. The integer b is called the base of the scale. For $b = 2$ it is called a binary expansion; and for $b = 3$ it is called a ternary expansion.

Definition 2.6 (Ternary Rational):

Let $x \in [0,1]$ then there exist a sequence $< x_n >$, where $x_n \in \{0,1,2\}$, and $x = \sum_{i=1}^{\infty} \frac{x_i}{3^i}$. If the expansion of x ends in a sequence of zeros, then there exists $m \in N$ such that $x_i = 0$ for all $i > m$, hence $x = \sum_{i=1}^{m} \frac{x_i}{3^i} : x_i \in \{0,1,2\}$.

So $x = \left(\sum_{i=1}^{m-1} \frac{x_i}{3^i}\right) + \left(\sum_{i=m+1}^{\infty} \frac{2}{3^i}\right) + \left(\frac{x_m - 1}{3^m}\right)$.

Therefore x has two possible ternary expansions one ending in asserting of $0's$ and the other ending in asserting of $2's$. In this case we will say that x is ternary rational.

Definition 2.7 (Projection Function (Abdelmonem S. M., 2012)):

Let $\{X_i\}_{i \in A}$ be a sequence of nonempty sets for some $A \subseteq \mathbb{N}$. Define the set X as the product $X = \prod_{i \in A} X_i$, where any point $x \in X$ can be presented as $x = (x_1, x_2, \dots, x_i, \dots)$.

Then, the projection function $\pi_i : X \to X_i$ is defined for all $x \in X$ by $\pi_i(x) = x_i \in X_i$.

Definition 2.8 (Product Topology (Abdelmonem S. M., 2012**)):**

If (X_i, τ_i) is a topological space for all $i \in A$, then the product topology τ on $X = \prod_{i \in A} X_i$ is the smallest topology on X for which all the projection functions π_i are continuous. It is worth mentioning that the set $O = \prod_i O_i \subset X$ is basis if and only if each O_i is open in X_i and $O_i = X_i$ except for finitely many.

Definition 2.9 (General Cantor Set (Abdelmonem S. M., 2012**)):**

A set E is called a general Cantor set if and only if E can be written in the form $E = \bigcap_{n=1}^{\infty} E_n$, where E_n consists of k^n mutually disjoint non-empty connected compact sets $I_{i_1,\dots,i_n}$,

$$E_n = \bigcup_{i_1,\dots,i_n} I_{i_1,\dots,i_n}$$

and $i_1, \dots, i_n \in \{1, \dots, k\}$ for a positive integer $k \geq 2$ such that

(i) $I_{i_1,\dots,i_n,i_{n+1}} \subset I_{i_1,\dots,i_n}$ and $i_1, \dots, i_n, i_{n+1} \in \{1, \dots, k\}$.

(ii) There exists A and B real numbers, $0 < A, B < 1$ such that

$$\left|I_{i_1,\dots,i_n,i_{n+1}}\right| \geq A\left|I_{i_1,\dots,i_n}\right|,$$

and for $t \neq s$, $\rho(I_{i_1,\dots,i_n,s}, I_{i_1,\dots,i_n,t}) \geq B\left|I_{i_1,\dots,i_n}\right|$, where ρ is the distance function for any two sets A and B. $\rho(A,B) = \inf\{|a-b| : a \in A \text{ and } b \in B\}$. Indeed, $I_{i_1,\dots,i_n}$ is called a fundamental interval for any possible sequence $i_1, \dots, i_n \in \{1, \dots, k\}$, also a fundamental

system, F, of E is a finite disjoint collection of fundamental intervals whose union covers E. A very important concept is the level of the fundamental interval; the level of $I_{i_1,\dots,i_n}$ is n, in other words, the level gives the stage during the construction of the Cantor set in which the interval $I_{i_1,\dots,i_n}$ appears. So, the upper and lower orders of a fundamental system are the maximum and minimum values of the level of fundamental intervals in F. Moreover, if F consists of fundamental intervals of the same level, then it shall be called E_n i. e. a fundamental system of level n.

Definition 2.10 (Universal Cantor Set (Abdelmonem S. M., 2012**)):**

Let U be the space of all sequences $x = (x_1, x_2, \dots)$ in which each x_j for all j can take one of the values in $\{0,1\}$. The set U is called the universal Cantor set. The universal Cantor set is uncountable. Assume that U is countable. Then U can be written in the form $U = \{u_1, u_2, \dots, u_n, \}$, where

$$u_1 = (u_1^1, u_2^1, \dots),$$
$$u_2 = (u_1^2, u_2^2, \dots),$$
$$\vdots$$
$$u_n = (u_1^n, u_2^n, \dots),$$
$$\vdots$$

Now choose a sequence $y = (y_1, y_2, \dots)$ such that for all $j \in \mathbb{N}, y_j \in \{0,1\}$ and $y_j \neq u_j^j$. Then $y \in U$ but $y \neq \{u_1, u_2, \dots, u_n, \}$. Hence, U is uncountable. But U has a countable subset $U_0 = \{x \in U :$ such that $\exists\, n$ for which $x_n = x_{n+1} = \cdots\}$ i. e. U_0 contains the sequences have constant tails.

Let $U^m = \{x \in U : x_m = x_{m+1} = \cdots\}$, then U^m consists of exactly 2^{m} elements. Therefore, $U_0 = \bigcup_{m=1}^{\infty} U^m$ is countable because it is a union of countable set. Also the set U is the infinite product space $\prod_{n=1}^{\infty} U_n$, where each U_n is the discrete space {0, 1} which is the discrete topology. This means that U can be given the product topology defined as follows:

$$\mathcal{B} = \left\{ \prod_{l=1}^{\infty} O_l : O_l \text{ open in } U_l \text{ and } O_l = U_l \text{ except for finitely many } l \right\} \dots\dots\dots (2.1)$$

Lemma 2.1: (Abdelmonem S. M., 2012**)**

If we define $\delta_n = max\left|I_{i_1,\dots,i_n}\right|$, then for any general Cantor set $\delta_n \to 0\ as\ n \to \infty$, where the maximum is defined on all the possible sequences $i_1, \dots, i_n \in \{1, \dots, k\}$ for the fixed level n.

Lemma 2.2: (Abdelmonem S. M., 2012**)**

For all $k \in \mathbb{N}$. The universal Cantor set U is homeomorphic to $\prod_{n=1}^{\infty}\{1,2,\dots,k\}$. It is worth mentioning that $\prod_{n=1}^{\infty}\{1,2,\dots,k\}$, equivalently, the base k representation of real numbers in the interval $[0,1]$.

Proposition 2.1: (Goodson G. R., 2015) The Cantor set C is compact.

Some Basic Theorems and Properties of Ternary Cantor set

In this section we will discuss some basic theorems and properties of ternary cantor set which is helpful for main results of this paper.

Proposition 3.1: (Stettin R., 2017**)** The ternary Cantor set is nonempty.

Proposition 3.2: Cantor middle third set $C_{\frac{1}{3}}$ is (i) closed (ii) Dense in itself (iii) no interior.

Proof:

(i) Cantor middle third set is closed

From the construction of the Cantor middle third $set\ C_{\frac{1}{3}} = \cap A_n$, Since each sets A_n can be written as a finite union of 2^n closed intervals, each of which has a length of $\frac{1}{3^n}$, as follows:

- $A_0 = [0,1]$
- $A_1 = \left[0,\frac{1}{3}\right] \cup [\frac{2}{3}, 1]$
- $A_2 = \left[0,\frac{1}{9}\right] \cup \left[\frac{2}{9},\frac{3}{9}\right] \cup \left[\frac{6}{9},\frac{7}{9}\right] \cup [\frac{8}{9}, 1]$

  … … …

Since A_n is a finite union of closed sets, A_n is a closed set for all $n \in N$, then $C_{\frac{1}{3}}$ is an intersection of closed sets, therefore $C_{\frac{1}{3}}$ is a closed set.

(ii) Cantor middle third set is dense in itself

All endpoints of every subinterval will be contained in $C_{\frac{1}{3}}$. Take any $x \in C_{\frac{1}{3}} = \cap A_n$ then x is in A_n for all n, so x must be contained in one of the 2^n intervals that comprise the $set\ A_n$. Define x_n to be the left endpoint of that subinterval (if x is equal to that endpoint, then let x_n be the right endpoint of that subinterval). Since each subinterval has length $1/3^n$, we have:

$|x - x_n| < 1/3^n$. Hence, the sequence (x_n) converges to x and since all endpoints of the subintervals are contained in the Cantor set, we have found a sequence of numbers not equal to x contained in $C_{\frac{1}{3}}$ that converges to x. Therefore, x is a limit point $of\ C_{\frac{1}{3}}$. But since x was arbitrary, every point of $C_{\frac{1}{3}}$ is a limit point of it. Thus $C_{\frac{1}{3}}$ is dense in itself.

(iii) $C_{\frac{1}{3}}$ has no interior point

Assume that there exists $x \in int(C_{\frac{1}{3}})$, then there exists an $\varepsilon > 0$ such that $(x - \varepsilon, x + \varepsilon) \subset C_{\frac{1}{3}}$. Choose $n \in N$ such that $3^{-n} < \varepsilon$, then $(x - \varepsilon, x + \varepsilon) \not\subset A_n$.

Therefore, $(x - \varepsilon, x + \varepsilon) \not\subset C_{\frac{1}{3}}$, and this contradicts that

$x \in \text{int}C_{\frac{1}{3}}$. Therefore $C_{\frac{1}{3}}$ has no interior point.

Proposition 3.3: The Cantor middle third set is precisely the set of points in the interval I having a ternary expansion without $1's$.

Proof: Let's focus on the ternary representations of the decimals between 0 and 1. Since, in base three, 1/3 is equivalent to 0.1 and $2/3$ is equivalent to 0.2. We see that in the first stage of the construction (when we removed the middle third of the unit interval) we actually removed all of the real numbers whose ternary decimal representation have a 1 in the first decimal place, except for 0.1 itself. (Also 0.1 is equivalent to 0.0222 .... in base three, so if we choose this representation we are removing all the ternary decimals with 1 in the first decimal place.) In the same way, the second stage of the construction removes all those ternary decimals that have a 1 in the second decimal place. The third stage removes those with a 1 in the third decimal place, and so on. (By noticing that 1/9 is equivalent to 0.01 and $2/9$ is equivalent to 0.02 in base three.) Thus after every thing has been removed, the numbers that are left- that is, the numbers making up the cantor set- are precisely those whose ternary decimal representations consist entirely of $0's$ and $2's$. Then the Cantor middle third set $\boldsymbol{C_{\frac{1}{3}}}$ is precisely the set of points in the interval I having a ternary expansion without $1's$ i.e. $x = \sum_{i=1}^{\infty} \frac{x_i}{3^i} :\ x_i = 0, 2$ for all i.

Theorem 3.1: The total length of the subintervals removed in the derivation of $C_{\frac{1}{3}}$ is one.

Proof: At each stage $n > 0$ there are 2^{n-1} open subintervals removed and each of these subintervals has length $\left(\frac{1}{3}\right)^n$. The total length removed is then represented by the infinite geometric series $\sum_{n=1}^{\infty} 2^{n-1} \frac{1}{3^n}$. From Calculus we know if $|r| < 1$, then $\sum_{n=0}^{\infty} a.r^n = \frac{a}{1-r}$. Thus

$$\sum_{n=1}^{\infty} 2^{n-1}\frac{1}{3^n} = \frac{1}{3} + 2\left(\frac{1}{9}\right) + 4\left(\frac{1}{27}\right) + \cdots = \frac{\frac{1}{3}}{1-\frac{2}{3}} = 1.$$

Theorem 3.2: (Dylan R. N., 2017) The Ternary Cantor set has length of 0.

Proposition 3.4: (Goodson G. R., 2015**)** The Cantor middle one-third set C is totally disconnected.

Proposition 3.5: (Goodson G. R., 2015**)**The Cantor set C is uncountable.

Proposition 3.6: (Goodson G. R., 2015) The Cantor set $C_{1/3}$ when added to itself gives the interval [0,2].

Results and Discussions

In this section, we discuss generalizations of Cantor set. We can easily generalize this one-dimensional idea to any length other than 1/3, excluding of course the degenerate cases of 0 and 1. We show that $C_{\frac{1}{3}}$ and $C_{\frac{1}{2}}$ are measurable and have measure zero. In this section we also discuss a special subset A of $C_{\frac{1}{3}}$ that has measure zero with non-measurable sum.

Definition 4.1 We say that $B \subseteq X$ is a Bernstein set (in X) provided B and $X\backslash B$ intersect every non-empty perfect subset of X.

One-dimensional generalization of the Cantor set:

For this construction first fix a length $\delta \in \left(0, \frac{1}{2}\right)$. From [0, 1] remove the open middle interval I_0 of length $(1-2\delta)$ such that $[0,1] - I_0 = [0,\delta] \cup [1-\delta, 1]$ where $I_0 = (\delta, 1-\delta)$. Next, from $[0,\delta]$ and $[1-\delta, 1]$ remove the open middle intervals $I_{1,1}$ and $I_{1,2}$ each of length $(\delta - 2\delta^2)$.Call their union I_1, giving $I_1 = (\delta^2, \delta-\delta^2) \cup (1-(\delta-\delta^2), 1-\delta^2)$ with the length of I_1equal to $(2\delta - 4\delta^2)$. What remains is then $[0,1] - (I_0 \cup I_1)$ of length$1-(1-4\delta^2) = 4\delta^2$. Proceeding in this manner, we construct sequences of open sets I_n, each the finite union of disjoint open intervals.

Definition 4.2. The generalized Cantor set C_δ is then defined as $C_\delta = [0,1] - \cup_{i=0}^{\infty} I_i$.

We can see that setting $\delta = \frac{1}{3}$ returns the standard middle-thirds Cantor set. This form of the Cantor set, for any $\delta \in \left(0, \frac{1}{2}\right)$, shares the same properties of the ternary Cantor set, namely it is a compact, non-empty, perfect, totally disconnected, and uncountable metric space.

We generalize the construction of the Cantor ternary set:

Let $n = 2m + 1,\ m = 1,2,3, \ldots$. We start with the closed real interval $k_0 = [0,1]$ and divide it into *n* equal subintervals.

Remove the open intervals $\left(\frac{1}{n}, \frac{2}{n}\right), \left(\frac{3}{n}, \frac{4}{n}\right), \ldots \left(\frac{n-2}{n}, \frac{n-1}{n}\right)$ such that $k_1 = \left[0, \frac{1}{n}\right] \cup \left[\frac{2}{n}, \frac{3}{n}\right] \cup \ldots \cup \left[\frac{n-1}{n}, \frac{n}{n}\right]$.

We subdivide each of these $(m + 1)$ remaining intervals into *n* equal subintervals and form each remove the 2nd, 4th, … ,$(2m)^{th}$ open subinterval and continue in the previous manner.

In this way we obtain a sequence of closed intervals $\{M_k\}$-one in the zero step, $(m + 1)$ after the first step, $(m + 1)^2$ after the second step, etc. $(m + 1)^k$ intervals of length $\left(\frac{1}{n}\right)^k$ after the k^{th} step.

The Cantor *n*-ary set is defined by the formula $C(n) = \bigcap_{k=0}^{\infty} M_k$,we construct a sequence $(C_k(n))_{k=0}^{\infty}$of numbers of the Cantor *n*-ary set such that

$C_0(n) = \{0, 1\}$

$|C_0(n)| = 2 = 2.(m + 1)^0$

$C_1(n) = \left\{0, \frac{1}{n}, \frac{2}{n}, \ldots, \frac{n}{n}\right\} = \bigcup_{j=0}^{n} \left(\frac{j}{n}\right)$

$|C_1(n)| = n + 1 = 2m + 2 = (m + 1)|C_0(n)| = 2(m + 1)^1$

$$C_k(n) = \bigcup_{j=0}^{n} \bigcup_{i_1=0}^{(m-1)} \ldots \bigcup_{i_{k-1=0}}^{(m-1)} \frac{j + 2\left(n^{(k-1)} i_{k-1} + \cdots + n i_1\right)}{n^k}$$

$$\begin{aligned} |C_k(n)| &= |C_k(2m + 1)| \\ &= (m + 1)|C_{k-1}(n)| \\ &= (m + 1)2(m + 1)^{k-1} \\ &= 2(m + 1)^k \end{aligned}$$

If $|C_k(n)| = x$ then $k = \frac{ln(x/2)}{ln(m+1)}$.

The sum of the lengths of the removed intervals is equal to 1, because

$$m\left(\frac{1}{n}\right)+m(m+1)\left(\frac{1}{n}\right)^2+m(m+1)^2\left(\frac{1}{n}\right)^3+\cdots+m(m+1)^{k-1}\left(\frac{1}{n}\right)^k$$

$$=\sum_{k=1}^{\infty}(m+1)^{k-1}\left(\frac{1}{n}\right)^k$$

$$=\frac{m}{n}\frac{1}{1-\frac{m+1}{n}}=1$$

The Lebesgue measure of the Cantor set $C(n)$ is zero for every $n=2m+1, m=1,2,....$

Lemma 4.1: (Stettin R., 2017) The total length removed in each iteration of C_i to create $C_{i+1}\ is\ \frac{(n-1)^i}{n^{i+1}}$.

Lemma 4.2: (Stettin R., 2017) The total length removed in each iteration of C_i to make $C_{i+1}\ is\ \frac{n-1}{n^{i+1}}$.

Theorem 4.1: The $\frac{1}{n}-ary$ Cantor set has length 0.

Proof: This can be proven by looking at everything that is being removed from C. Recall by Lemma 4.1 that $\frac{(n-1)^i}{n^{i+1}}$ is removed during each iteration of C_i. This means that during C_0, $\frac{1}{n^1}$ is removed, during C_1, $\frac{(n-1)}{n^2}$ is removed and during C_2, $\frac{(n-1)^2}{n^3}$ is removed. This pattern continues and total length removed can be written as

$$=\sum_{j=o}^{\infty}\frac{(n-1)^j}{n^{j+1}}$$

$$=\frac{\frac{1}{n}}{1-\frac{n-1}{n}}$$

$$=\frac{\frac{1}{n}}{\frac{n}{n}-\frac{n-1}{n}}=\frac{\frac{1}{n}}{\frac{1}{n}}=1$$

This means that the total length of 1 is removed. The length of C_0 is the length of the initial interval, [0,1] which is 1. Therefore, the length of C is $1-1=0$.

Theorem 4.2: The $\frac{n-1}{n}-ary$ Cantor set has length 0.

Proof: This can be proven by looking at everything that is being removed from C. Recall by Lemma 4.2 that $\frac{n-1}{n^{j+1}}$ is removed during each iteration of C_i. This means that during $C_0, \frac{n-1}{n^1}$ is removed, during $C_1, \frac{n-1}{n^2}$ is removed, and during $C_2, \frac{n-1}{n^3}$ is removed. This pattern continues and the total length removed can be written as $\sum_{j=o}^{\infty} \frac{n-1}{n^{j+1}} = 1$.

This means that a length of 1 is removed. The starting length of C is the length of the initial interval, $[0,1] = 1$. Therefore, the length of $C = 1 - 1 = 0$.

Cantor Set in Measure theory:

Lemma 4.3. Let U be the set of elements of [0,1] that use only zero's and two's in one of its base four expansions, and let V be the set of elements that use only zero's and one's. Then $U + V = [0,1]$.

Proposition 4.1: The Cantor set $C_{\frac{1}{3}}$ is measurable and has measure zero.

Proof: Since $C_{\frac{1}{3}} = \bigcap A_n$, then $C_{\frac{1}{3}}$ is a countable intersection of closed sets, therefore $C_{\frac{1}{3}}$ is a Borel set, so $C_{\frac{1}{3}}$ is measurable. From the construction of $C_{\frac{1}{3}}$ we have for every stage $n > 0$ we remove 2^{n-1} disjoint intervals from each previous set each having length $\frac{1}{3^n}$.Therefore we will remove a total length of $\sum_{n=1}^{\infty} 2^{n-1} \frac{1}{3^n} = \frac{1}{3}\sum_{n=1}^{\infty}(2/3)^{n-1} = 1$

From the unit interval [0,1]. Then $C_{\frac{1}{3}}$ is obtained by removing a total length 1 from the unit interval [0,1], so $\mu\left(I \setminus C_{\frac{1}{3}}\right) = 1$. Since $\mu(I) = \mu\left(C_{\frac{1}{3}}\right) + \mu\left(I \setminus C_{\frac{1}{3}}\right)$, then $\mu\left(C_{\frac{1}{3}}\right)$

$$= \mu(I) - \mu\left(I \setminus C_{\frac{1}{3}}\right)$$

$$= 1 - 1 = 0$$

Therefore, the set $C_{\frac{1}{3}}$ is measurable and has zero measure.

Proposition 4.2: The Cantor set $C_{\frac{1}{2}}$ is measurable and has measure zero.

Proof: Since $C_{\frac{1}{2}} = \bigcap A_n$, then $C_{\frac{1}{2}}$ is a countable intersection of closed sets, therefore $C_{\frac{1}{2}}$ is a Borel set, so $C_{\frac{1}{2}}$ is measurable. From the construction of $C_{\frac{1}{2}}$ we have for every stage $n > 0$ we remove 2^{n-1} disjoint intervals from each previous set each having length $\left(\frac{2}{4}\right)^n$. Therefore we will remove a total length of

$$\sum_{n=1}^{\infty} 2^{n-1} \frac{2}{4^n} = \frac{2}{4}\sum_{n=1}^{\infty}(2/4)^{n-1} = 1$$

From the unit interval $[0,1]$. Then $C_{\frac{1}{2}}$ is obtained by removing a total length 1 from the unit interval [0,1], and $\mu\left(I \setminus C_{\frac{1}{2}}\right) = 1$. Then $\mu\left(C_{\frac{1}{2}}\right) = \mu(I) - \mu\left(I \setminus C_{\frac{1}{2}}\right) = 1 - 1 = 0$

Therefore the set $C_{\frac{1}{2}}$ is measurable and has zero measure.

Proposition 4.3. (Ciesielski K., H. Fejzic, C. Freiling., 2001)There is a set $A \subseteq C_{1/3}$ such that $A + A$ is Bernstein in $[0,2] = C_{1/3} + C_{1/3}$, hence $A + A$ is non-measurable.

Theorem 4.3: For $k \in \mathbb{N}$ fixed, there is a natural homeomorphism ϕ From U to a general Cantor set E constructed as in Definition (2.10), and this homeomorphism is defined for each $x = (x_1, x_2, \dots)$ by :

$$\phi(x) = \bigcap_{n=1}^{\infty} \left\{ I_{i_1,i_2,\dots,i_n} / x \in I_{i_1,i_2,\dots,i_n} \right\}$$

Proof: First show that ϕ is bijection. Assume that there exist two distinct points x and z in U such that $\phi(x) = \phi(z)$. Then

$$\phi(x) = \phi(z),$$

$$\Rightarrow \bigcap_{\substack{n=1 \\ x \in I_{i_1,i_2,\dots,i_n}}}^{\infty} I_{i_1,i_2,\dots,i_n} = \bigcap_{\substack{n=1 \\ z \in I_{i_1,i_2,\dots,i_n}}}^{\infty} I_{i_1,i_2,\dots,i_n}$$

$$\Rightarrow \lim_{\substack{n\to\infty \\ x \in I_{i_1,i_2,\dots,i_n}}} I_{i_1,i_2,\dots,i_n} = \lim_{\substack{n\to\infty \\ z \in I_{i_1,i_2,\dots,i_n}}} I_{i_1,i_2,\dots,i_n}$$

which contradicts that $x \neq z$, because, there exists an integer m for which $x \in I_{i_1,i_2,\dots,i_n,l}$ and $z \in I_{i_1,i_2,\dots,i_n,t}$ for some $l, t \in \{0,1\}$ and $l \neq t$, therefore, ϕ is a bijection. It is obvious that x is given by the representation $x = (i_1, i_2, \dots, i_n, \dots)$, where for all n integer, $x \in I_{i_1,i_2,\dots,i_n}$. Recalling that U is the product topology given by Equation (2.1) and E has the Euclidean topology given by

$T = \{E \cap (a,b) : (a,b) \subset \mathbb{R}\}$,

Now to show that ϕ and ϕ^{-1} are continuous. Let $(a,b) \cap E \in T$ for some $0 < a < b < 1$. Then

$$\phi^{-1}\left((a,b) \cap E\right) = \{x \in U : \phi(x) \in (a,b) \cap E\}$$

$$= \left\{ x \in U : \bigcap_{\substack{n=1 \\ x \in I_{i_1,i_2,\dots,i_n},}}^{\infty} I_{i_1,i_2,\dots,i_n}, \in (a,b) \cap E \right\}$$

$= \{x \in U : \text{there exists } m \text{ such that } x \in I_{i_1,i_2,\ldots,i_m} \subset (a,b) \cap E\}$,

$== \{x \in U : x \in \{i_1(x)\} \times \{i_2(x)\} \times \ldots \times \{i_m(x)\} \times \prod_{n=1}^{\infty} U_n\}$

For some sequence $\{i_1(x)\}_1^{\,m}$ and an integer m

So $\phi^{-1}((a,b) \cap E)$ is open for any arbitrary open $((a,b) \cap E \in T)$ which implies that ϕ is continuous. Now to show that ϕ^{-1} is continuous. We need to show that the image of each open set in $\mathcal{B}$ is also open $in\ \tau$. Pick an open set $\prod_{l=1}^{\infty} O_l \in \mathcal{B}$. Then there exists a sequence $j_1, j_2, \ldots, j_d \in \{0,1\}$ for some integer d such that

$$\prod_{l=1}^{\infty} O_l = \{j_1\} \times \{j_2\} \times \ldots \times \{j_d\} \times \prod_{n=1}^{\infty} U_n$$

This implies

$$\phi(\prod_{l=1}^{\infty} O_l) = \{y \in E : y \in I_{j1,j2,\ldots,jd}\}$$

$$= \{y \in E : y \in (a-\delta, b+\delta)\} \text{ for some } \delta > 0,$$

$$= \{y \in (a-\delta, b+\delta) \cap E\},$$

where a and b are the left and right end points for the interval $I_{j1,j2,\ldots,jd}$ respectively. So, ϕ^{-1} is continuous. Hence, ϕ is a homeomorphism.

Conclusion

The Cantor set is an interesting example of an uncountable set of measure zero and has many interesting properties and consequences in the fields of set theory, topology, and fractal theory. The cantor set, originally constructed purely under mathematical investigation, lately turned into near perfect models for a host of phenomena in the real world-from strange attractors of nonlinear dynamical systems to the distribution of galaxies in the universe. Cantor set, now, finds celebrated place in mathematical analysis and its applications among others. The general cantor set which is one of the early fractals appear in the worlds of mathematics, engineering, dynamical systems, physics and computer science. The universal cantor set is another point of view for the general cantor set; one of the other methods to represent the cantor set points by using the infinite sequence of indexes of the fundamental intervals.

In this paper we have solved some problems about cantor set such as, the cantor set $C_{1/3}$ when added to itself gives the interval $[0,2]$ and the cantor set $C_{1/3}$ and $C_{1/2}$ are measurable set and have measure zero. In the last section we have proved the homeomorphism between the general and the universal cantor sets.

References

Abdelmonem S. M. 2012. Hausdorff Dimension of Cantor Sets. African Institute for Mathematical Sciences (AIMS) Thesis for: Diploma in Mathematical Science. DOI: 10.13140/RG.2.1.2160.7920.

Bhaumik I., Binayak S. C. 2010. A Note On The Generalized Shift Map. Gen.Math. Notes. **1(2)**: 159-165.

Cantor, G. 1883. Über unendliche, lineare Punktmannigfaltigkeiten V. Mathematische Annalen. **21**:545-591.

Ciesielski K., H. Fejzic, C. Freiling. 2001. Measure Zero sets with Non-measurable sum. Real Anal. Exchange. **27(2)**:783-793.

Choudhury G., Arun M., Hemanta Kr. S. and Ranu P. 2019. Cantor Set as a Fractal and Its Application in Detecting Chaotic Nature of Piecewise Linear Maps. Proc.Natl. Acad. Sci.,India, Sect. A Phys,Sci.

Devaney R. L. 1992. A First Course in Chaotic Dynamical Systems. Addition Wesley Publishing Company INC, New York.

Dylan R. N. 2017. A Cantor Set-A Brief Introduction. http://wwwmpa.mpa-garching.mpg.de/dnelson/storage/dnelson.cantor-set.pdf.

Falconer K. 2003. Fractal geometry: mathematical foundation and applications. 2nd edn. Willey, Hoboken.

Goodson G. R. 2015. Chaotic dynamics: fractals, tailings and substitution. Towson University, Towson.

Hutchinsion J. E. 1981. Fractals and Self-similarity, Indiana University Mathematics Journal. **30**:713-747.

Lipschutz S. 1965. General topology. Schaum's outline series. Mc Grow Hill, New York.

Maendes P. 1999. Sum of Cantor sets: self-similarity and measure. Proc. Am. Math Soc. **127**:3305-3308.

Obeng-Denteh W., P. A. Yirenkyi, J. O. Asare. 2016. Cantor's Ternary Set Formula-Basic Approach. British Journal of Mathematics & Computer Science .**13(1)**: 1-6.

Robert W. V. The Elements of cantor Sets-With Applications. First Edition, Slippery Rock University.

Stettin R. 2017. Generalizations and Properties of the Ternary Cantor Set and Explorations in Similar Sets. Project paper, Ashland University.

Schoenfeld A. H., G. Gruenhage. 1975. An alternative characterization of the Cantor set. Proc Am Math Soc. **53(1)**:235-236.

Zhixing G. 2014. Cantor Set and its Properties. University of California, Santa Barbara.

Barishal University Journal Part 1, 6(2): 23-35 (2019) ISSN 2411-247X

NDVI BASED VEGETATION CHANGE DETECTION OF SUNDARBANS DUE TO THE EFFECT OF CYCLONE 'BULBUL'

Md. Hasnat Jaman*, Muhammad Risalat Rafiq, Nahin Rezwan, Md. Saiful Islam and Abu Jafor Mia

Department of Geology and Mining, University of Barishal, Barishal-8200

Abstract

Sundarbans is the world's largest mangrove forest with a variety of floral and faunal species which is contributing a positive environmental impact not only for Bangladesh but also for whole world. Almost every year, the Sundarbans acts as a bulwark to protect the people of Bangladesh from various natural calamities i.e., cyclones and tidal surges. The current study identified the change in the vegetation and quantified the damaged area in Sundarbans due to the effect of cyclone Bulbul. Total five (5) feature classes were defined using ArcMap 10.5 including water bodies, bare soil, sparse vegetation, intermediate vegetation and deep vegetation. This study found that the particular feature classes of vegetation were greatly affected by the cyclone Bulbul. From pre to post-Bulbul period, a total of about 10.0172 square kilometers of vegetated area were damaged. The results were calculated from Normalized Difference Vegetation Index (NDVI) values by using European Space Agency's Sentinel Application Platform (ESA SNAP) and represented as a classified map by doing maximum likelihood classification in ArcGIS environment. This study also infers that, cyclone Bulbul not only caused reduction of total vegetation area but also caused harm and death of many animals and animal species in Sundarbans. The final outcome showed that the cyclone Bulbul caused 0.177% of total forest loss in the Bangladesh part of Sundarbans.

Keywords: Sundarbans, Bulbul, Remote Sensing, NDVI, GIS, Vegetation.

Introduction:

The biodiversity and its preservation has been set up as the essential indicator of environmental sustainability (Kates et al., 2001). Many international organizations declared biomass and floristic diversity as first priority in the imposition of biomass and in tropical forests (Stork et al., 1997). Remote sensing technique has the advantage in

* *Corresponding Author's e-mail: mhjaman@bu.ac.bd*

monitoring environmental resources as well as in the investigation of environmental sustainability (Eastman and Fulk, 1993; Skidmore et al., 1997; Rogan and Chen, 2004; Fensholt et al., 2009; and Smiraglia et al., 2014). In the calculation of significant exogenous perturbation influences (Dahdouh-guebas, 2002), biomass and floristic diversity prognosis (Gibbs et al., 2007) and forest cover mapping (Chuvieco and Congalton, 1989) remote sensing has become very much efficient.

Bangladesh is a natural disaster prone region of South Asia for its' geographic location but the country is blessed with the largest mangrove forest in the world. The Sundarbans along the Bay of Bengal has evolved over the millennia through natural deposition of upstream sediments accompanied by intertidal segregation. This mangrove works as the shield for Bangladesh and West Bengal of India. However, it's very alarming that Sundarbans is being affected with both anthropogenic activities and natural calamities. Cyclone hits the southern coast of Bangladesh several times in a year. On November 7, 2019 a deep depression in Bay of Bengal moved towards central-east turned into cyclone 'Bulbul' (NAWGB, 2019). 'Bulbul' headed towards Bangladesh's coastal regions from the Bay of Bengal with a maximum sustained wind speed of 120 km/h which is rising up to 150 km/h in gusts. Thereafter it re-curved northeastwards and moved towards West Bengal - Bangladesh coasts on November 9, 2019 as a severe cyclonic storm with maximum sustained wind speed of 110-120 km/h gusting to 135 km/h. Southwestern Bangladesh has greatly affected due to this cyclone 'Bulbul'.

Normalized Difference Vegetation Index (NDVI) is one of the most widely used techniques to monitor the vegetation. In terms of chlorophyll reaction of electromagnetic spectrum, it (NDVI) permits investigation on areal setting as well as quality of vegetation (Chen et al., 2005 and Elmore et al., 2000). From the ratio difference between measured canopy reflectance in the red and near infrared bands NDVI can be estimated (Rao et al., 2005). In this study we detected the change in vegetation in Sundarbans of Bangladesh due to cyclone Bulbul by using remote sensing with particular tool called NDVI. The main purpose of this study was to observe the change in vegetation in terms of area after the cyclone Bulbul.

Study Area:

The Sundarbans, formerly **Sunderbunds**, is the largest tidal halophytic mangrove forest in the world. This mangrove forest lies on the tremendous delta on the Bay of Bengal which is shaped by the confluence of the Ganges, Brahmaputra and Meghna rivers across Bangladesh and West Bengal, India (Iftekhar and Islam, 2004a & 2004b). The study area lies between 21° 27' 30" to 22° 30' 00" N and 89° 02' 00" to 90° 00' 00" E. (Fig. 1).

Only two hundred years ago, the size of the Sundarbans was 16,700 sq. km. (Wahid, Alam & Rahman 2002) now, only two-thirds of it is in place.

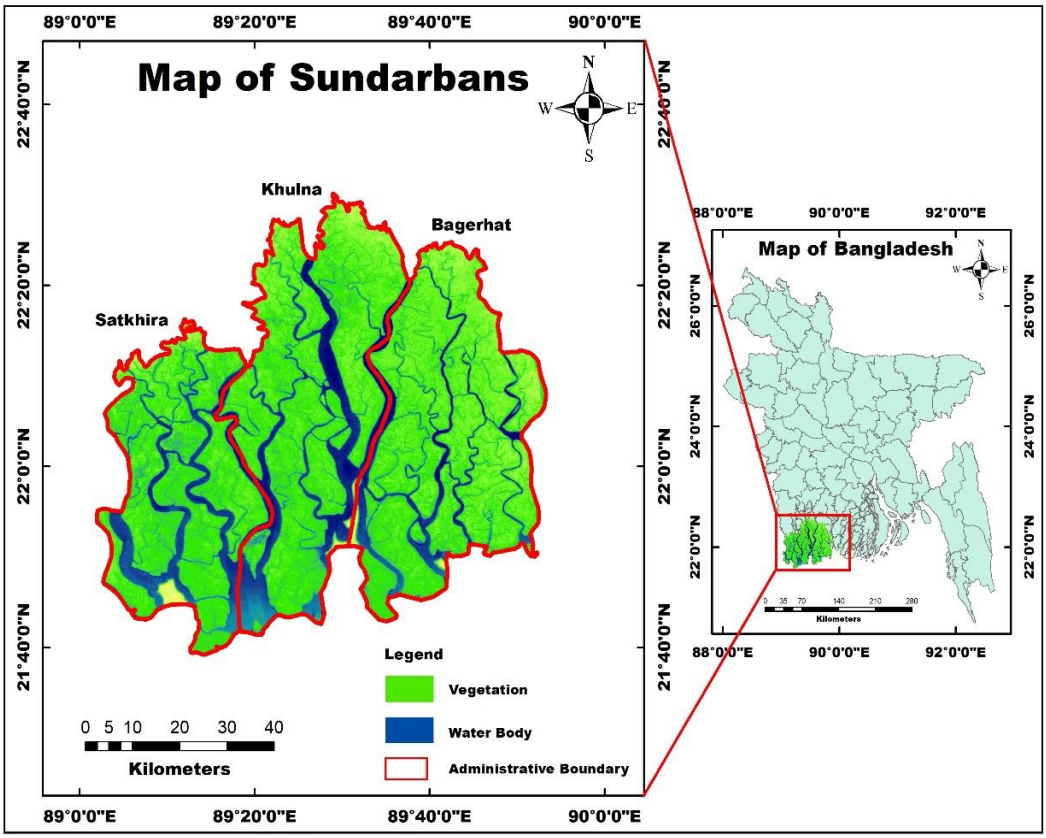

Fig. 1: Map of study area (Sundarbans) showing vegetation and water body

At present, the total area is approximately 10,000 sq. km. of which about 6,000 sq. km (60%) is in Bangladesh and the other 4,000 sq. km (40%) is in India. Practically, the total area of this forest has been decreased in recent days (Wahid, Alam & Rahman 2002). Our study focuses on the Bangladesh part of Sundarbans only. Elevation of this region is between 0.9-2.1 m above mean sea level (Iftekhar and Islam, 2004a). Here the monsoon season prolong from May to October and the climate is tropical (Ghosh et al., 2016).

Sundarbans is a low lying area with thick and sparse vegetation which is connected by numerous rivers, channels, islands and mudflats network. It is believed that the name of Sundarbans is derived from Sundari (*Heritiera fomes*), the name of the large mangrove trees that are most abundant in the area. Two more species of plants that

are dominant in this forest are Gewa (*Excoecaria agallocha*) which can tolerate moderate salinity and Goran (*Ceriops decandra)* which can tolerate high salinity (Anwar and Takewaka, 2014). Other floral taxon that made up the mangrove forest includes *Avicennia spp., Xylocarpus mekongensis, Xylocarpus granatum, Sonneratia apetala, Bruguiera gymnorrhiza, Aegiceras corniculatum, Rhizophora mucronata,* and *Nypa fruticans palms* (Komiyama et al., 2008).

Sundarban is blessed with floras including 87 monocotyledons, 17 pteridophytes, and the rest are dicotyledons which include 35 legumes, 29 kinds of grass, 19 sedges, and 18 euphorbias and 453 faunal wildlife, including 49 species of mammals, 290 species of birds, 120 species of fishes, 53 are reptiles, and 8 are amphibian species (Shimu et al., 2019). Sundarbans is famous for the Royal Bengal Tiger (*Panthera tigris*). UNESCO designated this mangrove as a world heritage site in 1987.

Background study of Bulbul:

In November 9, 2019 a strong tropical cyclone named 'Bulbul' struck the southern Bangladesh and West Bengal of India. According to its magnitude, cyclone "Bulbul" was categorized as a "Category 2" cyclone. It had an average wind speed of 130-148 km/h and average precipitation of 100-200 mm/h with maximum 400 mm/h which stayed for 36 hours and recorded as one of the longest duration since last 52 years (NAWGB, 2019).

According to the Bangladesh Meteorological Department (BMD) and the Indian Meteorological Department, a tropical Storm MATMO (28th October – 2ndNovember 2019) which occurred over west Pacific Ocean and later emerged into north Andaman Sea led the cyclone Bulbul. In the morning of 04th November it turned into a low pressure zone over north Andaman Sea. In 5th of November finding auspicious condition, it moved west- northwestwards and appeared as a depression (D) over east central and southeast Bay of Bengal. Next morning gaining energy it turned into a deep depression (DD) and moved west-northwards over east central and adjoining southeast area of the bay. Same night (6th November) Bulbul became a cyclonic storm and moved more north-northwest direction. The next day (7th of November), it kept on moving in north-northwest direction and turned into a severe cyclonic storm (SCS) over west central and adjoining east central Bay of Bengal. It was moving towards north constantly and in the morning of 8thNovember it turned into a very severe cyclonic storm (VSCS) over west central and adjoining east central Bay. Till afternoon (0900 UTC) of 9th of November, it continued to move nearly northwards before changing its path towards the northeastward in the evening of the same day.

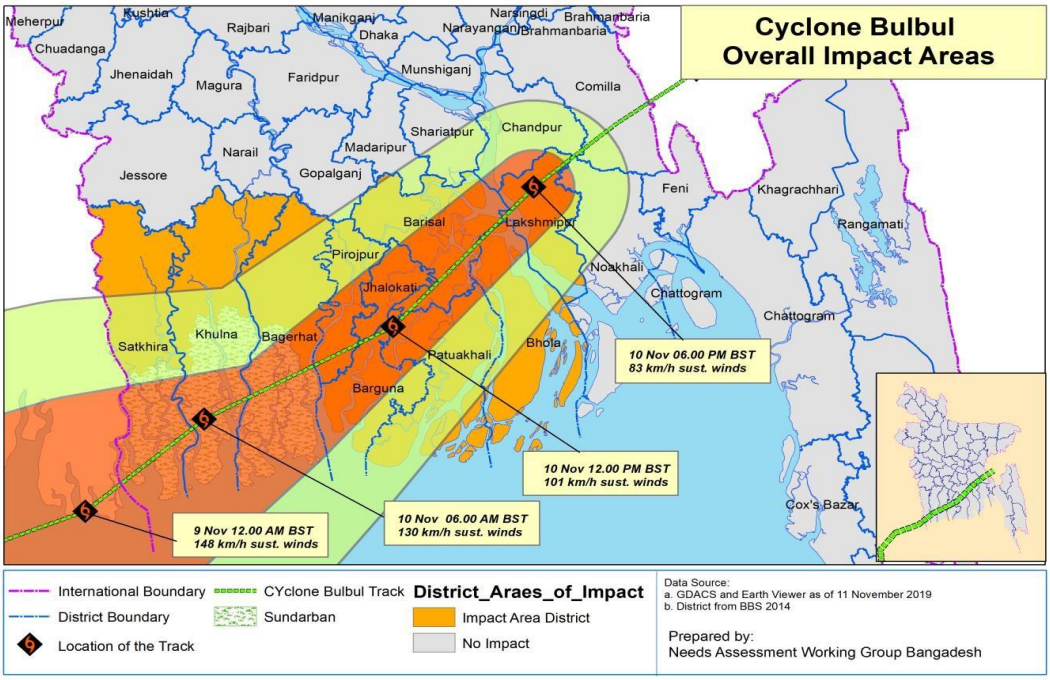

Fig. 2: Map shows the impact areas of cyclone Bulbul (NAWGB, 2019)

Afterward, it became weak and turned into a severe cyclonic storm (SCS). In the night (1500 to 1800 UTC) of 9th November as a severe cyclonic storm it crossed West Bengal coast, close to Sundarbans Dhanchi Forest near 21.55°N/88.5°E having a wind speed of 110-120 kmph gusting to 135 kmph (Hoque et al., 2020).

Cyclone 'Bulbul' entered Bangladesh region through Buri Goalini Range of the Sundarbans in the Shyamnagar upazila of Satkhira district (Fig. 2). It can be noted that Sundarbans had reduced the wind speed and weakened the storm that resulted in very low causalities in Bangladesh. According to Bangladesh Forest Department, about 4589 trees were damaged that clearly indicated a great loss of about 42 lakhs BDT (The Daily Star, October 7, 2020).

Methodology:

The main purpose of this study was to determine the change in vegetation due to cyclone Bulbul (November 09, 2019) by using satellite multispectral images data. Satellite data analysis is a convenient way for remote sensing. These data contain information in different bands and each band represents unique behavior. The acquired satellite data was divided into two parts. Image of October 14, 2019 was indicated as pre Bulbul data and

image of March 27, 2020 was indicated as post Bulbul data. Change in vegetation was determined by analyzing Normalized Difference Vegetation Index (NDVI).

1. Data Collection:

Data acquisition is the initial step. Many open sources provide free satellite imagery data for research purpose. Among those, Sentinel-2 imageries are chosen. Sentinel-2 is quite similar to Landsat imageries; however, Sentinel-2 has better resolution that helps to increase the accuracy of the result. Though historical images before 2014 is not available for Sentinel-2 and as this study was only limited to two images of 2019 and 2020, Sentinel-2 data was the best choice. Sentinel-2 data was downloaded from Copernicus open access hub (https://scihub.copernicus.eu/dhus/). To detect the change in vegetation precisely the images needed to be examined just before and after the cyclone (for instance, just before and after November 9, 2019). While downloading the images, cloud free images were considered. Because cloud free image gives the most accurate result and doesn't cause any other interference. Before final selection, clouds cover percentage of every Sentinel-2 data immediate before and after Bulbul was examined very carefully. No suitable Sentinel-2 data was found in between October 15, 2019 and March 26, 2020. Quality of other satellite images i.e., Landsat were also examined but found that, only Sentinel-2 provides cloud free data with better resolution which are closest to the occurrence of cyclone Bulbul.

Table 1: Detailed information of Satellite data

Sl. No	Satellite	Instrument	Image type	Processing Level	Date of acquisition	Spatial Resolution (meter)	Cloud Coverage (%)	Source
01	Sentinel-2	MSS	Multispectral	Level-2A	14.10.2019	10m	0.005551	Copernicus open access hub
02	Sentinel-2	MSS	Multispectral	Level-2A	27.03.2020	10m	0.063701	Copernicus open access hub

2. Image Processing:

ERDAS Imagine 2015, ArcMap 10.5 and European Space Agency's Sentinel Application Platform (ESA SNAP) tools were used for image preprocessing. Blue, Green, Red and Near Infrared bands were stacked together to produce a composite image. This was done for vegetation recognition, because chlorophyll in plants reflects more to near infrared

than the visible. Shape file of the study area was extracted from the administrative map of Bangladesh. Both composite image and shape file were converted into same projection system UTM ZONE 45N WGS 1984. Then a subset image of selective study area was created by using ERDAS Imagine 2015 software.

3. NDVI Calculation:

Normalized Difference Vegetation Index (NDVI) is formulated using near infrared (NIR) and visible red (R) light. Using the following formula NDVI of Sundarbans was calculated-

$$NDVI = \frac{(\mathrm{R800} - \mathrm{R680})}{(\mathrm{R800} + \mathrm{R680})}$$

Here, R_{800}= Near Infrared light; R_{680}= Visible Red light

NDVI was calculated by using ESA SNAP tool and classification was done with ArcMap 10.5

Table 2: Significance of NDVI values

Class	**NDVI value**
Vegetation	High – Very high
Waterbody / Cloud	Negative
Rock / Bare soil	Near zero

4. Data analysis and comparison:

This study involved two methods of data analysis. Such as:

- NDVI calculation.
- Maximum likelihood classification.

5. Image classification:

NDVI image classification was done with ArcGIS tool; different classes were defined according to their NDVI value (Table-3). Even vegetation was also classified depending on its concentration. Classified data has been represented in the map and histogram.

Table-3: Feature Class according to NDVI value

Features	NDVI Value
Water body	Negative value
Bare Soil	0.03
Sparse Vegetation	0.09
Intermediate Vegetation	0.14
Deep Vegetation	0.50

6. Area Calculation:

Reclassification was done by using the reclassify tool in ArcMap 10.5. As the cell size was 10 m, feature area was calculated by using the following formula:

Feature area = {10×10× (Count)} ÷ (1000×1000)} sq.km.

Result and Discussion:

In spite of becoming weaker in progressive time, cyclone "Bulbul" did a massive damage to south and southwestern region of Bangladesh. Fortunately, the Sundarbans stood as a shield saving thousands of human lives and properties. However, in return Sundarbans lost its vegetation. Classified NDVI map of pre Bulbul and post Bulbul event shown in Fig. 3.

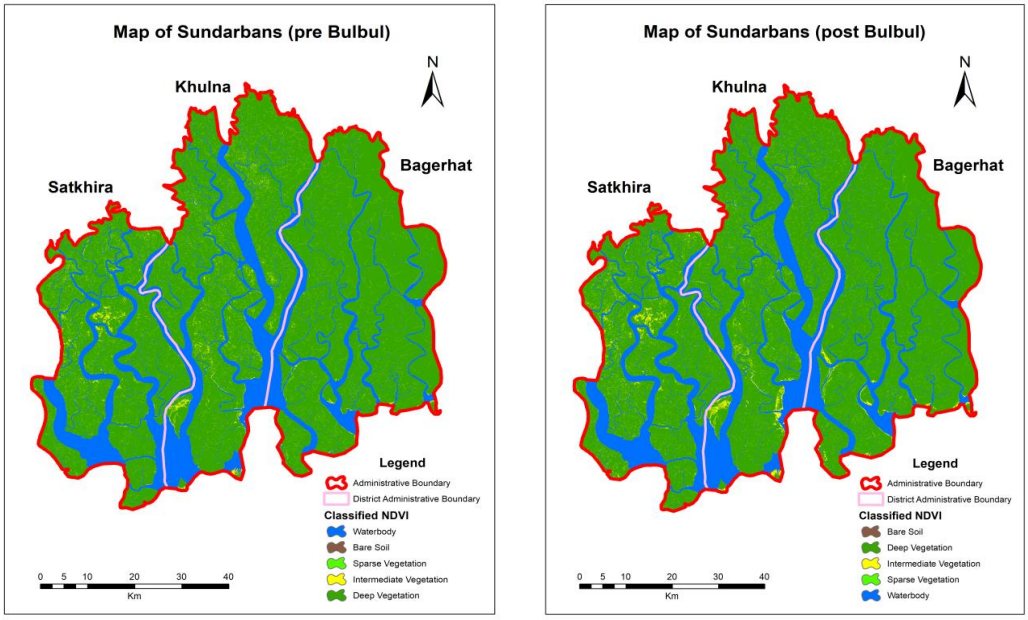

Fig. 3: Classified NDVI map of Sundarbans of pre and post Bulbul

Using NDVI result, the area of deep vegetation, sparse vegetation and intermediate vegetation as well as water bodies were calculated. Result shows that a total of 10.0172 sq. km of vegetation lost due the single event of cyclone Bulbul. Calculated area shows that before the cyclone the area of the sparse vegetation was 11.2122 sq. km which became 10.1918 sq. km losing about 1.0204 sq. km. Cyclone Bulbul affected the thick and deep vegetation the most as the deep vegetation stood firmly against the storm. Calculated area of features in Sundarbans for both pre Bulbul and post Bulbul is shown in Fig. 4 and Fig. 5 respectively.

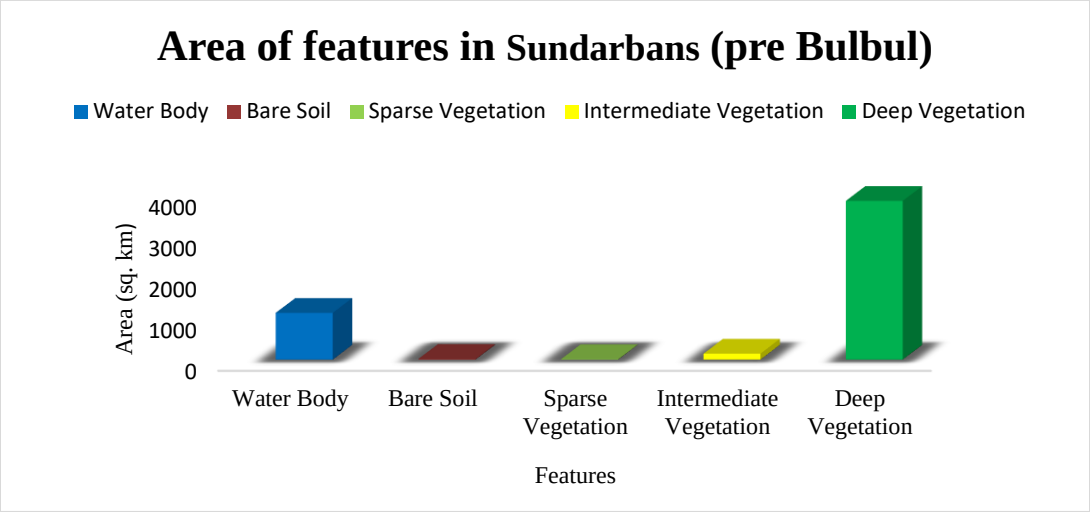

Fig. 4: Calculated area of features in Sundarbans (pre Bulbul)

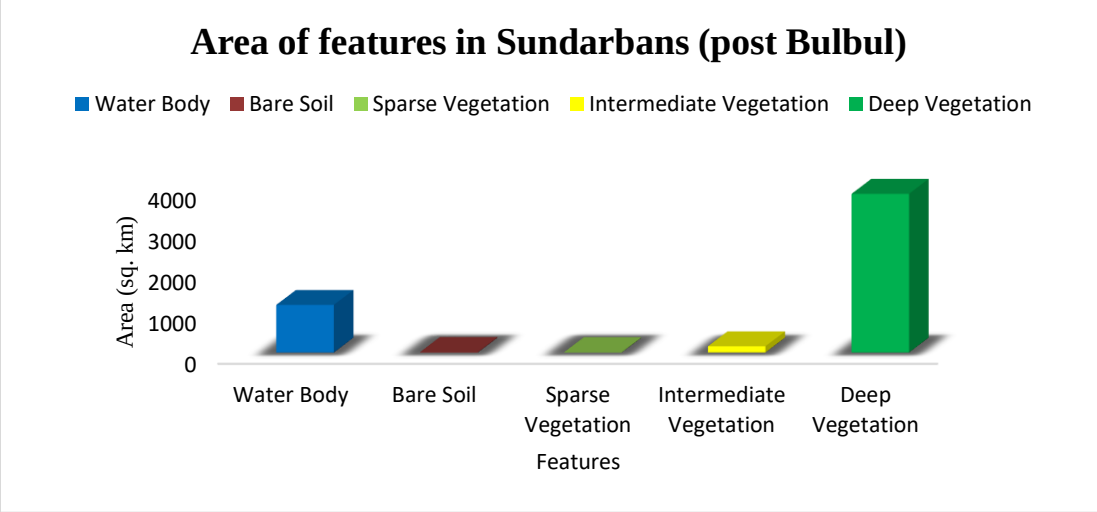

Fig. 5: Calculated area of features in Sundarbans (post Bulbul)

The area of deep vegetation decreased from 3869.3092 sq. km to 3853.9743 sq. km causing a net decrease of 15.3349 sq. km. As a single event Bulbul caused a huge destruction of vegetated area which is the heart of the forest.

This loss of vegetation perhaps took many lives of wild animals as well birds. Besides, it possibly made thousands of birds and animals homeless. During cyclone Bulbul 400 mm+ rainfall was recorded (NAWGB, 2019). Due to this heavy rainfall and high tide the water body inundated the adjacent bare lands. The area of water bodies including river, channels and other small canals was also calculated simultaneously with vegetation. The total water body area increased from 1140.3925 sq. km to 1156.7757 sq. km with a net increase of 16.3832 sq. km. The water body area calculation may not indicate the Bulbul effect but it is certain that Bulbul caused flooding. Due to this flooding bare soil decreased from 16.7157 sq. km to 13.3943 sq. km with a net decrease of 3.3214 square kilometers. Previously mentioned that immediate image after the cyclone occurrence was not suitable due to higher cloud coverage. Therefore, this estimation might be lower than the actual scenario of the impact of cyclone Bulbul in Sundarbans because in this gap of over four (4) months new plants have grown. For this reason, the area of intermediate vegetation was calculated. From pre and post Bulbul classified image it was found that intermediate vegetation increased to 152.1181 sq. km from 145.78 square kilometers. The net increase of intermediate vegetation found 6.3381 sq. km. Net change in vegetation in terms of area is represented in Fig. 6.

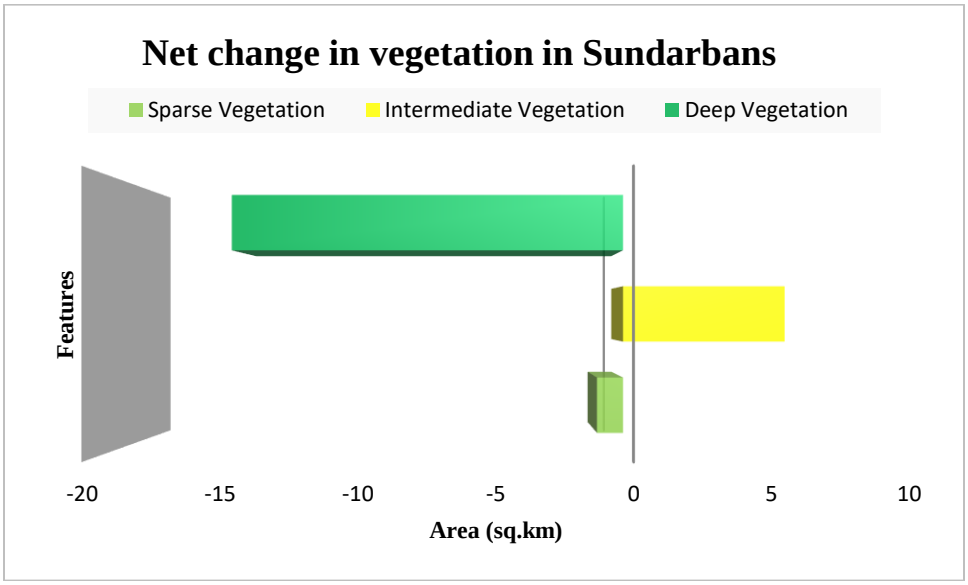

Fig. 6: Diagram showing Net change in vegetation at Sundarbans due to Bulbul

Besides, Bulbul tidal surge inundation in the agricultural land that caused reduction of fertility as well as production capability of crop land. Many people were homeless and starved for food and fresh water. This cyclone caused death of people, property damage and loss of plenty of trees in and around Sundarbans.

Sundarbans is losing its vegetation and wildlife due to anthropogenic activities. Moreover, this type of cyclones and storms hits Sundarbans almost every year causing great destruction. The combined effect of human activities and natural calamities is causing rapid loss of floral and faunal species in Sundarbans. If this continuous Bangladesh will be open to many natural disasters which will bear much suffering to us.

Conclusion:

The changes of vegetation in Sundarbans due to cyclone Bulbul are identified using remote sensing multispectral imagery. For detecting changes in Sundarbans mangrove forest, Sentinel-2 data was used. Two images, one before the occurrence of cyclone Bulbul and another about four months after, were used for Normalized Difference Vegetation Index (NDVI) and maximum likelihood classification to get the final output. The result shows the impact of Bulbul and resulting changes in vegetation in four months. We found that the net decrease of sparse vegetation is 1.0204 sq. km and deep vegetation is 15.3349 sq. km., alternatively the net increase of intermediate vegetation is 6.3381 sq. km. The net loss of vegetation is 10.0172 sq. km. which is about 0.177% of total area of Sundarbans in Bangladesh. This research work will support identifying the temporal changes due to cyclone Bulbul and according to that, the intended authority will be able to take appropriate steps for the safety and progress of Sundarbans as this type of natural calamity hits it frequently.

References:

Anwar, M. S. and S. Takewaka. 2014. Analyses on Phenological and Morphological Variations of Mangrove Forests along the Southwest Coast of Bangladesh. Journal of Coastal Conservation **18**: 339–57.

Chen, D., J. Huang and T. J. Jackson. 2005. Vegetation Water Content Estimation for Corn and Soybeans Using Spectral Indices Derived from MODIS Near- and Short-Wave Infrared Bands. Remote Sensing of Environment. **98**: 225–36.

Chuvieco, E. and R. G. Congalton. 1989. Application of Remote Sensing and Geographic Information Systems to Forest Fire Hazard Mapping. Remote Sensing of Environment. **29**: 147–59.

Dahdouh-guebas, F. 2002. The use of Remote Sensing and GIS in the sustainable management of tropical coastal ecosystems. Environment, Development and Sustainability. **4**: 93–112.

Eastman, J. R. and M. Fulk. 1993. Long Sequence Time SeriesEvaluation Using Standardized Principal Components. Photogrammetric Engineering and Remote Sensing. **59**: 1307–1312.

Elmore, A. J., J. F. Mustard, S. J.Manning and D. B. Lobell. 2000. Quantifying Vegetation Change in Semiarid Environments: Precision and Accuracy ofSpectral Mixture Analysis and the NormalizedDifferenceVegetation Index.Remote Sensing of Environment. **73**: 87–102.

Fensholt, R., K. Rasmussen, T. T. Nielsen and C. Mbow. 2009. Evaluation of Earth Observation Based Long Term Vegetation Trends - Intercomparing NDVI Time Series Trend Analysis Consistency of Sahel from AVHRR GIMMS, Terra MODIS and SPOT VGT Data. Remote Sensing of Environment. **113**: 1886–98.

Ghosh, M. K., L. Kumar and C. Roy. 2016.Mapping Long-Term Changes in Mangrove Species Composition and Distribution in the Sundarbans. Forests. **7**: 305

Gibbs, H. K., S. Brown, J. O. Niles and J. A. Foley. 2007. Monitoring and Estimating Tropical Forest Carbon Stocks: Making REDD a Reality. Environmental Research Letters. **2:** 045023.

Hoque, M. E, M. Y. Arafat, H. E. Alam, K. T. Ahmed and M. N. Uddin. 2020. Rapid Assessment of SST and Chlorophyll Concentration Variability Due to Cyclone Bulbul in the Bay of Bengal Using Remotely Sensed Satellite Image Data. Earth and Space Science Open Archive.

https://scihub.copernicus.eu/dhus/

https://www.thedailystar.net/country/cyclone-bulbul-damages-sundarbans-infrastructure-badly-1826563

Iftekhar, M. S. and M. R. Islam. 2004a. Degeneration of Bangladesh's Sundarbans Mangroves: A Management Issue. International Forestry Review. **6**: 123–35.

Iftekhar, M. S. and M. R. Islam. 2004b. Managing Mangroves in Bangladesh: A Strategy Analysis. Journal of Coastal Conservation. **10**: 139–46.

Kates, R. W., W. C. Clark, R. Corell, J. M. Hall, C. C. Jaeger, I. Lowe, J. McCarthy, H. J. Schellnhuber, B. Bolin, N. M. Dickson, S. Faucheux, G. C. Gallopin,A. Grübler, B. Huntley, J. Jäger, N. S. Jodha, R. E. Kasperson, A. Mabogunje, P. Matson, H. Mooney, B. Moore-III, T. O'Riordan and U. Svedlin. 2001. Sustainibility Science.Science. **292**: 641–42.

Komiyama, A., J. E. Ongand S. Poungparn. 2008. Allometry, Biomass, and Productivity of Mangrove Forests: A Review. Aquatic Botany. **89**: 128–37.

Needs Assessment Working Group Bangladesh (NAWGB) Assessment, Joint Rapid. 2019. Humantarian needs overview, Tropical cyclone matmo/ Bulbul- Oct 2019.

Rao, P. P. N., S. V. Shobha, K. S. Ramesh and R. K. Somashekhar. 2005. Satellite-Based Assessment of Agricultural Drought in Karnataka State. Journal of the Indian Society of Remote Sensing. **33**: 429–34.

Rogan, J. and D. Chen. 2004. Remote Sensing Technology for Mapping andMonitoring Land-Cover and Land-Use Change. Progress in Planning. **61**: 301–25.

Shimu, S. A., M. Aktar, M. I. Afjal, A. M. Nitu, M. P. Uddin and M. A. Mamun. 2019. NDVI Based Change Detection in Sundarban Mangrove Forest Using Remote Sensing Data. 2019 4th International Conference on Electrical Information and Communication Technology, EICT 2019, December: 1–5.

Skidmore, A. K., W. Bijker, K. Schmidt and L. Kumar. 1997. Use of Remote Sensing and GIS for Sustainable Land Management. ITC Journal. **3/4**:302–15.

Smiraglia, D., S. Rinaldo, T. Ceccarelli, S. Bajocco, L. Salvati, C. Ricotta and L. Perini. 2014. A Cost-Effective Approach for Improving the Quality of Soil Sealing Change Detection from Landsat Imagery. European Journal of Remote Sensing. **47**: 805–19.

Stork, N. E., T. J. B. Boyle, V. Dale, H. Eeley, B. Finegan, M. Lawes, N. Manokaran, R. Prabhu and J. Soberon. 1997. Criteria and Indicators for Assessing the Sustainability of Forest Management: Conservation of Biodiversity.Center for International Forestry Research. **62**: 01-25.

Wahid, S.M.; Alam, M.J. & Rahman, A. (2002). Mathematical river modelling to support ecological monitoring of the largest mangrove forest of the world – the Sundarbans. Proceedings of First Asia-Pacific DHI software conference, 17–18 June 2002.

Barishal University Journal Part 1, 6(2): 37-46 (2019) ISSN 2411-247X

APPLICATION OF $CaCl_2$ TO MITIGATE SALT STRESS ON LENTIL (*LENS CULINARIS* MEDIK.) VARITIES IN BANGLADESH

Anolisa, Dipalok Karmaker, Riyad Hossen, Subroto Kumar Das*

Department of Botany, University of Barishal, Barishal-8200, Bangladesh

Abstract

This study was conducted to investigate the mitigation of saline stress on lentil (*Lens culinaris* Medik.) by calcium chloride ($CaCl_2$) treatment in pot culture experiment. In the present investigation the effect of $CaCl_2$ on mitigation of salinity was determined by measuring different growth parameters such as plant height; number of leaves; flowers; pods and weight of seed. It was observed that individual use of sodium chloride (NaCl) causes a significant reduction in plant growth parameters compared to control where as 100 mg/L $CaCl_2$ in combination with NaCl, mitigates salinity and showed a significant increment in growth parameters. It was also observed that increasing amount of $CaCl_2$ (200 mg/L) in combination with NaCl causes a reduction in growth parameters.

Keywords: Salinity, lentil, calcium chloride ($CaCl_2$), mitigation, growth parameters.

Introduction

Salinity can be defined as the presence of soluble salts with excessive levels in soils or waters and it is one of the common abiotic factors which strongly limits crop yields. If these salts contain a high proportion of sodium ions, it is called sodicity. However, soil salinity could be regarded as the major problems in the world for agricultural production (Epstein et al., 1980). Over six percent of the world's land and approximately one-third of agricultural areas are affected by this increasing environmental problem (Laohavisit et al., 2013; Yadav et al., 2011). When any of the environmental factors exceeds the optimum tolerance of a plant, it stresses the plant and successively influences its development and structural, physiological and biochemical processes (Jaleel et al., 2007a). Several metabolic and physiological processes regulating plant growth can be damaged by salinity and sodicity through cellular ionic balance disruption. The most common ions associated with salinity are Na^+, Mg^{2+}, Cl^- and HCO_3^- of which Na^+ and Cl^-

* *Corresponding author: mrsubroto@yahoo.com*

showed dominant toxicity. Increased concentrations of cellular Na^+ and Cl^- inhibit most enzymes and interferes RNA binding (Serrano et al., 1999). Moreover, excessive uptake of Na^+ disrupts Na^+/K^+ homeostasis and may cause cellular injury and even cell death which leads to the plant growth inhibition (Lockhart, 2013;Romero et al., 2001). However, Calcium has been reported to play a significant role in the salinity tolerance as well as growth and development of plant (Cramer et al., 1987). Calcium ion is not only an essential structural element that strengthens plant cell walls and membranes but also, is a well-known secondary messenger in cell signaling processes (White and Broadley, 2003). It is implicated within the movement of cellular organelles like the spindle apparatus and secretary vesicles and plays a key role in integrating plant cell metabolism (Jaleel et al., 2007e).

Legumes have long been recognized to be either sensitive or moderately tolerant to salinity. Salt tolerance varies even among legumes, and most of them respond to saline conditions by salt exclusion, that is, exclusion of NaCl from the leaves (Manivannan et al., 2007). Lentil (*Lens culinaris* Medik.) is an important legume crop in many countries including Bangladesh since it provides protein-rich food for humans and animals and acts as soil quality improver by supplying increased nutrients to the soil (Katerji et al., 2001). In Bangladesh, lentil is placed the second position among the pulses according to cultivated area and production while first in terms of usage (Afzal et al., 1999). However, the cultivation of lentil has been challenged in Bangladesh due to the increasing trend of soil salinity in the coastal part of this of this country (Ashraf and Waheed, 1990). Irrigation management is an approach to improve salinity tolerance in crops (Paranychianakis and Chartzoulakis, 2005). Many authors stated that exogenous calcium alleviates stress in green gram, soybean and linseed (Manivannan et al., 2007; Arshi et al., 2010). The role of Ca^{2+} to minimize the effect of salt toxicity in the reduction of yield and quality of lentil is essential to investigate. Bangladesh is an overpopulated country and to fulfill the current need of lentil for added population, the yield of lentil needs to be increased and the saline prone areas (southern part of Bangladesh) must be undertaken in lentil cultivation through proper use of mitigating substance to migrate the toxicity of salt. However, according to the available literature and internet sources, no investigation has been initiated to determine the role of exogenous Ca^{2+} in Na stressed cultivated area for better yield production in lentil, but there are some reports on other legumes like *Vigna radiata* (Sharma and Dhanda, 2015). The objective of the present research is therefore based on to investigate the morphological and yield contributing characters of lentil under salt stress and to examine the role of Ca^{2+} on mitigation of salt stress in lentil in view of improvement of morphological, yield contributing characters and yield of lentil.

Materials and Methods

Six different varieties of lentil viz BARI masur-3 (BM-3), BARI masur-4 (BM-4), BARI masur-5 (BM-5), BARI masur-6 (BM-6), BARI masur-7 (BM-7), BARI masur-8 (BM-8) was collected from Bangladesh Agricultural Research Institute (BARI), Joydebpur, Gazipur and maintained in the Department of Botany, University of Barishal. These were cultivated in sterilized soil in 14cm plastic pots. Three replicates were taken for each variety. Twenty hand-selected seeds of each variety were used for each replicate. The experimental soil was taken from cultivated land near the University campus. All varieties were treated with different concentrations of different salts such as NaCl, $CaCl_2$ and combination of both NaCl & $CaCl_2$. Six different treatments i.e. T_1= 100 mg/L NaCl, T_2= 100 mg/L NaCl + 100 mg/L $CaCl_2$, T_3= 100 mg/L NaCl + 200 mg/L $CaCl_2$, T_4= 200 mg/L NaCl, T_5= 200 mg/L NaCl + 100 mg/L $CaCl_2$, T_6= 200 mg/L NaCl + 200 mg/L $CaCl_2$ were applied thrice in a week after 15 days of seed sowing. Control was treated with normal tap water only. After 30 and 60 DAS (days after sowing) data was collected for important morphological and yield-related traits. The study was conducted from September 2018 to February 2019 at Department of Botany, University of Barishal.

Statistical Analysis

The data was collected for determination of plant height, number of leaves, number of flowers, number of pods and seed yield per plant. The perpendicular distance from the ground level to the tip of the longest branch (plant height, cm) had measured on five randomly selected plants from each replicates and the average value was recorded.

Total number of leaves, flowers and seeds bearing pods from five randomly selected plants of each replicate was counted after 30 and 60 days interval after sowing and the average data has been recorded. The weight of twenty seeds of five randomly selected plants from each replicate was measured in gram with the help of a digital electrical balance and their mean weight was calculated. Analysis of variance was performed and significant differences among mean values were compared by LSD test at a 5% level of significance.

Results and Discussion

The results of the study on the effect of calcium on salinity levels and on morphological and yield contributing characters of lentil have been presented and possible interpretations have been made in the following heads.

Plant height

According to the present investigations, the interaction between salinity stress and calcium act as a mitigation agent on plant height. From table-1 it was observed that,

among all the treatments, 100 mg/L $CaCl_2$ showed the most positive response in respect of salinity mitigation as compared to control. The highest average plant height (15.40) next to control was found in treatment-2 where 100 mg/L $CaCl_2$ applied with 100 mg/L NaCl. Plant height showed a decreasing trend from treatment: 3-5 and the lowest average plant height (8.8) were found in treatment-4. These findings showed positive correlation with previous observation in mungbean (Qados, 2010) and pepper (Chartzoulakis and Klapaki, 2000) where plant height decreased with increase salinity level.

Table-1: Effect of $CaCl_2$ on plant height of BARI lentil varieties.

Lentil variety	Plant height (cm)						
	T0	T1	T2	T3	T4	T5	T6
BM-3	17.23	13.85	15.55	14.55	7.47	8.85	7.34
BM-4	15.98	13.89	14.68	14.85	7.19	12.25	7.98
BM-5	18.07	16.20	16.42	17.12	9.35	11.62	10.59
BM-6	16.25	15.35	15.75	15.14	9.72	11.25	10.41
BM-7	16.42	12.97	14.95	14.57	9.62	10.01	10.75
BM-8	16.24	14.95	14.96	16.12	9.42	11.37	10.37
Mean	16.7	14.54	15.40	15.39	8.8	10.89	9.57
CV (%)	4.77	8.11	4.27	6.67	13.03	11.37	15.69
SEM	0.33	0.48	0.27	0.42	0.46	0.51	0.61

Number of leaves per plant

The leaf number is a very important character for plant growth and development as the leaf is the main photosynthetic organ in plant. Salinity adversely affected in the production of leaf in lentil. The combined effect of sodium and calcium on the number of leaves per plant was significantly reflected among different level of the sodium and calcium concentration. Among all the treatments 100 mg/L $CaCl_2$ showed the most positive response in compared to 200 mg/L upon the entire lentil varieties used in the present investigation. The maximum number of leaves (49.92) was found in treatment-2 where 100 mg/L $CaCl_2$ applied with 100 mg/L NaCl (table-2). The lowest number of leaves (18.13) was found in treatment-4 where 200 mg/L NaCl was applied. Gradual

decrease in the leaf number with the increased salt concentration, compared with the control plant was observed and thus supported the observation of Qados (2011) in *Vicia faba* L., López-Aguilar et al., (2003) on three types of bean. Ahir et al., (2017) and Gama et al., (2017) also reported similar observation on Gladiolus and common bean (*Phaseolus vulgaris* L.) respectively; where number of leaves reduced with increasing level of salinity.

Table-2: Effect of $CaCl_2$ on the number of leaves of BARI lentil varieties.

Lentil variety	No. of leaves/plant						
	T_0	T_1	T_2	T_3	T_4	T_5	T_6
BM-3	74.35	37.15	52.2	44.35	11.5	20.0	11.9
BM-4	69.1	36.74	43.5	38.4	14.5	19.3	21.6
BM-5	77.75	48.25	51.95	44.35	21.05	22.06	19.75
BM-6	65.5	41.4	52.8	44.85	17.73	18.85	18.45
BM-7	60.65	42.53	57.25	51.3	23.35	32.3	26.45
BM-8	70.6	34.7	41.85	40.05	20.65	36.00	27.6
Mean	69.66	40.13	49.92	43.88	18.13	24.75	20.96
CV (%)	8.78	12.37	11.94	10.25	24.6	30.12	27.37
SEM	2.49	2.02	2.43	1.83	1.82	3.04	2.34

Number of flowers per plant

The number of flowers per plant of lentil showed significant differences with different levels of salinity that is presented in table-3. The highest number of flowers (16.1) per plant was observed in control. In the case of salinity treated experiments, the highest number of flowers (10.45) was found in treatment-2 and the lowest number of flowers per plant was 2.3 found in treatment-6 where 200 mg/L NaCl was applied with 200 mg/L $CaCl_2$. Present findings showed similarity with previous study of Veatch-Blohm et al., (2012) on three commonly planted *Narcissus* cultivars. The reduced number of flower with increase of salinity also found in *Matricaria chamomile* (Razmjoo et al., 2008) and Purslane (Alam et al., 2014).

Table-3: Effect of $CaCl_2$ on flower formation of of BARI lentil varieties.

Lentil variety	No. of flowers/plant						
	T0	T1	T2	T3	T4	T5	T6
BM-3	15.2	6.6	9.3	9.1	2.8	3.4	1.8
BM-4	16.8	7.0	11.1	9.3	3.9	2.9	2.3
BM-5	14.4	7.4	9.3	8.7	4.0	3.6	3.4
BM-6	15.5	7.9	10.9	8.4	2.2	2.4	2.3
BM-7	16.3	8.4	10.8	8.6	2.2	2.6	1.6
BM-8	18.4	8.4	11.3	8.8	2.6	3.2	2.4
Mean	16.1	7.62	10.45	8.82	2.95	3.02	2.32
CV (%)	8.73	9.77	8.68	3.76	27.43	15.47	27.22
SEM	0.57	0.30	0.37	0.14	0.33	0.19	0.26

Number of pods per plant

The number of pod is an important character of lentil as it is related to yields. It was observed that the number of pods per plant was significantly affected by the increasing salinity level that is shown in table-4. The highest number of pods per plant was recorded from T_0 (control treatment) as there was no salt applied. Among the salt treatments, the highest number of pods per plant (5.55) was found in treatment -2 and the lowest number of pods per plant (1.44) was found in treatment-4 (table- 4). Number of pods per plant varied significantly for the interactive effect of different salinity and calcium levels. It was also reported in several previous studies (Islam et al., 2008; Tesfaye et al., 2014; Alami-Milani and Aghaei-Gharachorlou, 2015) where the number of pods per plant significantly affected by salinity in lentil. They showed a significant reduction in pod number with increasing salinity as mentioned in this study.

Table-4: Effect of $CaCl_2$ on pod setting of BARI lentil varieties.

Lentil variety	No. of pods/plant						
	T0	T1	T2	T3	T4	T5	T6
BM-3	11.15	4.95	5.45	5.2	1.7	1.9	1.85
BM-4	11.25	4.7	5.4	4.8	1.4	1.55	1.25
BM-5	11.35	4.1	5.1	4.95	1.25	1.85	1.65
BM-6	11.75	3.9	5.0	4.55	1.05	1.5	1.35
BM-7	12.05	4.75	5.9	5.65	1.15	1.7	1.5
BM-8	13.3	5.8	6.45	5.6	2.1	2.95	2.45
Mean	11.81	4.7	5.55	5.12	1.44	1.99	1.68
CV (%)	6.82	14.35	9.77	8.61	27.35	28.0	26.01
SEM	0.33	0.28	0.22	0.18	0.16	0.22	0.18

Seed weight per plant

Twenty seed weight per plant in different levels of salinity was presented in table -5. It was observed that in treatment-2 the highest seed weight (twenty seed) was 0.3 gm the lowest seed weight was found to 0.24 in treatment-4.

Table-5: Effect of $CaCl_2$ on seed weight of BARI lentil varieties.

Lentil variety	Twenty Seed weight (gm)						
	T0	T1	T2	T3	T4	T5	T6
BM-3	0.35	0.25	0.28	0.28	0.24	0.27	0.23
BM-4	0.30	0.25	0.27	0.27	0.22	0.25	0.24
BM-5	0.32	0.26	0.28	0.26	0.20	0.22	0.21
BM-6	0.32	0.30	0.30	0.25	0.25	0.26	0.24
BM-7	0.30	0.25	0.28	0.26	0.21	0.25	0.25
BM-8	0.40	0.35	0.39	0.37	0.32	0.33	0.35
Mean	0.33	0.28	0.30	0.28	0.24	0.26	0.25
CV (%)	11.51	14.76	15.06	15.78	18.07	13.94	19.45
SEM	0.16	0.17	0.18	0.18	0.18	0.15	0.20

Conclusion

According to the present findings, the yield of lentil was gradually decreased due to increased salinity levels which could be reduced by the exogenous supply of calcium. Among the calcium levels, 100mg/L showed comparatively better response in growth parameters as compared to 200mg/L. The toxicity symptom was reduced by calcium through increasing K^+ and Ca^{2+} concentration by lowering Na+ concentration. This study could be strengthened by further work under field conditions and also at mature vegetative and reproductive stage of this crop.

Acknowledgements

The author thanks Ministry of Science & Technology, Bangladesh for providing financial support through R&D project (39.00.0000.012.002.04.18- 43, Date: 05-03-2019) and University of Barishal for institutional support to carry out this research.

References

Afzal MA, Bakr MA and Rahman ML 1999. Lentil cultivation in Bangladesh. Lentil, Blackgram and Mungbean Development pilot project, Pulses research station, BARI, Gazipur.

Ahir MP, Singh A and Patil SJ 2017. Response of different salinity levels on growth and yield of tuberose cv. Prajwal. Int. J.Chem.Stud. **5**(6): 2150-2152.

Alam MA, Juraimi AS, Rafii MY, Hamid AA and Aslani F.2014. Screening of purslane (*Portulaca oleracea* L.) accessions for high salt tolerance. Sci. Worl. J. **2014**:1–12.

Alami-Milani M and Aghaei-Gharachorlou P.2015. Effect of ascorbic acid application on yield and yield components of lentil (*Lens culinaris* Medik.) under salinity stress. Int. J.Bios. **6**: 43-49.

Arshi A, Ahmad A, Aref IM and Iqbal M.2010. Calcium interaction with salinity-induced effects on growth and metabolism of soybean (*Glycine max* L.) cultivars. J.Env. Biol. **31**: 795-801.

Ashraf M and Waheed A 1990. Screening of local/exotic accessions of lentil (*Lens culinaris* Medik.) for salt tolerance at two growth stages. Plant soil. **128**: 167-176.

Chartzoulakis K and Klapaki G. 2000. Response of two greenhouse pepper hybrids to NaCl salinity during different growth stages. Sci. Hort.**86**(3): 247-260.

Crame GR, Lynch J, Lauchli A and Epstein E 1987. Influx of Na+, K+, and Ca2+ in roots of salt-stressed cotton seedlings: Effects of supplemental Ca2+. Plant Physiology. **83**: 510-516.

Epstein E, Norlyn JD, Rush DW and Kingsbury RW 1980. Saline culture of crops: Genetic approach. Science. **210**: 399-404.

Gama PBS, Inanaga S, Tanaka K and Nakazawa R 2017. Physiological response of common bean (*Phaseolus vulgaris* L.) seedlings to salinity stress. African J.Biotech. **6** (2): 79–88.

Islam MR, Islam MZ, Islam MT, Rahman MM, and Chowdhury AKMMB 2008. Effects of salinity on growth parameters and yield attributes in *Lentil* genotypes. J. Env. Sci. Nat. Res. **1**(2): 79-86.

Jaleel CA, Gopi R, Manivannan P and Panneerselvam R 2007a. Antioxidative potentials as a protective mechanism in *Catharanthus roseus* (L.) G. Don. plants under salinity stress. Turkish J. Bot.**31**: 245–251.

Jaleel CA, Gopi R ,Manivannan P, Kishorekumar A, Gomatinayagam M and Panneerselvam R 2007e. Changes in biochemical constituents and induction of early sprouting by triadimefon treatment in white yam (*Dioscorea rotundata* Poir.) tubes during storage. J. Zhejiang Univ. Sci. **8**: 283-288.

Katerji N, Hoorn JWV, Hamdy A, Mastrorilli M, Oweis T and Erskine W 2001. Response of two varieties of lentil to soil salinity. Agri. Water Man. **47**: 179–190.

Laohavisit A, Siân LR, Shabala L, Chen C, RenatoColaço DDR, Swarbreck SM, Shaw E, Dark A, Shabala S, Shang Z and Davies JM. 2013. Salinity-induced calcium signaling and root adaptation in *Arabidopsis* require the calcium regulatory protein annexin1. Pl. Physiol. **163**: 253-262.

Lockhart J 2013. Salt of the earth: ethylene promotes salt tolerance by enhancing Na/K homeostasis. Pl. Cell. **25**:3150.

López-Aguilar R, Orduño-Cruz A, Lucero-Arce A, Murillo-Amador B and Troyo-Diéguez E 2003. Response to salinity of three grain legumes for potential cultivation in arid areas. Soil Sci Pl Nut. **49**(3): 329-336.

Manivannan P, Abdul Jaleel C, Kishorekumar A, Sankar B, Somasundaram R, Sridharan R and Panneerselvam R 2007. Changes in antioxidant metabolism of *Vigna unguiculata* (L.) Walp. by propiconazole under water deficit stress. Colloids and surfaces. Biointerfaces **57**(1):69-74.

Paranychianakis NV and Chartzoulakis KS. 2005. Irrigation of mediterranean crops with saline water: from physiology to management practices. Agr.Eco. Env. **106**: 171–187.

Qados AMSA 2010. Effect of arginine on growth, nutrient composition, yield and nutritional value of mung bean plants grown under salinity stress. Nature. **8**: 30-42.

Qados AMSA 2011. Effect of salt stress on plant growth and metabolism of bean plant

Vicia faba (L.). J.Saudi Soc.Agr.Sci.**10**(1): 7-15.

Razmjoo K, Heydarizadeh P and Sabzalian MR 2008. Effect of salinity and drought stresses on growth parameters and essential oil content of *Matricaria chamomile*. Int. J.Agr. Biol. **10**(4): 451-454.

Romero-Aranda R, Soria T and Cuartero J 2001. Tomato plant-water uptake and plant-water relationships under saline growth conditions. Pl. Sci.**160**: 265-272.

Serrano R, Mulet JM, Ríos JAG, Márquez de Larriona IF, Leube MP, Mendizabal I, Pascual-Ahuir A, Proft MRR, Montesinos C 1999. A glimpse of the mechanism of ion homeostasis during salt stress. J. Exp. Bot. **50**: 1023-1036.

Tesfaye A, Petros Y and Zeleke H 2014. Effect of salinity on yield and yield related traits of some accessions of Ethiopian Lentil (*Lens culinaris* Medik.) under greenhouse conditions. Int. J. T. E. E. E. **10**: 10-17.

Veatch-Blohm ME, Sawch D, Elia N and Pinciotti D 2012. Salinity tolerance of three commonly planted *Narcissus* cultivars. Hort. Sci. **49**(9): 1158-1164.

White PJ and Broadley MR. 2003. Calcium in plants. Ann. Bot. **92**:487-511.

Yadav S and Irfan M, Ahmad A, Hayat S 2011. Causes of salinity and plant manifestations to salt stress: a review. J. Env. Biol. **32**: 667-685.

Barishal University Journal Part 1, 6(2): 47-57 (2019) ISSN 2411-247X

APPLICATION OF SUGARCANE BAGASSE AS AN ADSORBENT FOR TREATMENT OF A TEXTILE DYE RHODAMINE B

Md. Nazmul Kayes*, Md. Mizanur Rahman Chowdhury, Md. Azanur Seikh, Mahmudul Hassan Suhag and Farzana Akter

Department of Chemistry, University of Barishal, Barishal-8200, Bangladesh

Abstract

Dyes are widely employed for colouring in textile industries and a significant loss of it is occurred during the manufacture and processing of dyes. These lost and untreated chemicals are discharged in the water resources, which damage the aquatic ecosystem. The study was carried out for the establishment of a standard wastewater treatment process using sugarcane bagasse (SB) as a bio-adsorbent to remove the reactive dyes. Various parameters such as contact time, amount of adsorbent, initial concentration of dye and temperature were considered to optimize the removal process. The adsorption behavior has been explained on the basis of pseudo-first-order, pseudo-second-order and intra-particle diffusion model. For sugarcane bagasse, the maximum removal efficiency of Rhodamine B (RB) was found at an adsorbent mass of 5.5 g/100 mL, at 19 ^{o}C temperature, at 1×10^{-4} M concentration and 45 minutes of contact time. The results of the experiment suggest that the SB could be a better adsorbent for the removal of reactive dyes from the wastewater.

Keywords: Adsorption, sugarcane bagasse, kinetic study, effect of temperature.

Introduction

The increase in industrialization and urban contamination causes the discharge of wastewater directly into water resources without proper treatment. Dyes are being an essential part of our civilized life. The widely uses of dye and their improper treatment in various industries such as textile, leather, paper, printing, food, solvent, rubber, plastic, cosmetics, petroleum, pesticides, wood preserving chemicals, paint, pigment and pharmaceuticals industry cause severe destruction of the aquatic environment (Berradi et al., 2019). Water pollution is a great threat toward both human health and the ecological environment. Organic dyes, one of the major water pollutants might be toxic, chemically

* *Corresponding author's E-mail: dmnkayes@bu.ac.bd*

stable and hard to degrade (Zhang et al., 2010, Adevemo et al., 2012). The water resource is polluted day by day due to the dumping of industrial wastes into rivers, eutrophication, spraying insecticides and by human activities, which causes harms not only the aquatic being but also contaminates the entire food chain (O'Mahony et al., 2002, Aksu and Çağatay, 2006, Miah et al., 2016). The untreated textile dye is not excluded from it. Several conventional methods, for instance, physical (adsorption, coagulation, and filtration), chemical (oxidation, reduction) and biological (aerobic and anaerobic microbial degradation) have been applied to dispose the hazardous dyes from industrial effluent (Czelej et al., 2016, Czelej et al., 2016). Among all these methods, the physical adsorption process at the solid-liquid interface is regarded as one of the economic, efficient and effective methods for the removal of dyes from the industrial effluent (Basnet and Zhao, 2014, Zhu et al., 2014). Dye degradation is a process in which large dye molecules are broken chemically into smaller molecules. The resulting products are water, carbon dioxide and mineral byproducts. All the dye molecules are not degraded and a large extent of it is found to the natural water resources. Many of these dye molecules are not reactive towards light, acids, bases and oxygen. The color of the material becomes permanent.

Since synthetic dyes have been widely used in many technological processes, the discharge of wastewater of these industries to the environment affect both human health and living organism of the aquatic ecosystem due to toxicity and carcinogenicity (Forgacs et al., 2004), So before their discharge, the treatment of dye contaminated water is essential with sanitization process. Adsorption is a method that involves the accumulation of a substance in molecular species in higher concentrations on the surface. Adsorption is affected by the temperature, pressure, nature of adsorbent, nature of adsorbate, concentration of adsorbate and adsorbent dose respectively. Activated carbon composites are the simplest and economical method for the removal of dye from aqueous solution by adsorption process (Hu et al. 2014, Yang et al. 2011, Madrakian et al. 2013).

Due to high cost of activated carbon, many researchers prefer to use natural adsorbents such as rice husk, banana peel, vine, soybean hull, coconut husk, sunflower seed hull, agricultural waste byproduct and teak wood bark for the purification of wastewater (Safa and Bhatti, 2011, Dabwan et al., 2015, Weng et al., 2013). In the present study, the adsorption of RB has been investigated by the sugarcane bagasse (SB). After crushing and extraction of juice from the sugarcane stalk there remain a fibrous residue which is called sugarcane bagasse. Sugarcane bagasse is also called the most abundant lignocelluloses agro-industrial residue (Siqueira et al., 2020). Since SB has numerous and variety of functional groups, so it shows a strong attractive force for the binding of pollutant ions (Okoro and Okoro, 2011). Therefore, it is expected that sugarcane bagasse

can efficiently remove its target adsorbent from an aqueous solution like toxic heavy metals, dyes, petroleum, phenolic compounds and organic nutrients.

Materials and Methods

SB was collected from the local area, washed with de-ionized water and dried in an oven till a constant weight was obtained. The sugarcane bagasse was ground in a blender (Miyako) and kept in desiccators for further use.

An aqueous solution of 1×10^{-3} M Rhodamine B (Alfa UK) was prepared in a 250 mL volumetric flask and kept as the stock solution. Diluted solutions of different concentrations were prepared by appropriate dilution.

A definite amount of SB was added to a solution of RB and allowed for agitation in an orbital shaker (Model No-JSOS-300). A small portion of the solution was collected after a definite time interval. The absorbance of each solution was measured with a double beam UV-Visible spectrophotometer (Lamda-365) and the removal efficiency was monitored. Deionized water was used as a reference for all the measurements. The procedure was repeated with the change of different parameters such as adsorbent dosage, concentration of the adsorbate, time and temperature. The percentage of adsorption was determined by -

$$\% \text{ of dye removal} = \frac{(A_0 - A_t)}{A_0} \times 100\%$$

where, A_0 and A_t are the initial absorbance of dye solution and absorbance of dye solution after adsorption at any time t respectively.

Results and Discussion

The wavelength at which aqueous solution of RB shows maximum absorption was determined spectroscopically and this value was 554 nm. The molar extinction coefficient was determined to be 7.85×10^4 $Lmol^{-1}cm^{-1}$. The concentrations of all solutions were monitored at this wavelength.

Effect of adsorbent dosage

The percentage of adsorption is found to be increased with increase of adsorbent dosage upto a maximum at 5.5 g and then decreases (Fig. 1). The removal efficacy of an adsorbent usually increases with the increase in its dose due to a large number of existing adsorption sites. On the contrary, the adsorption capacity decreases after a certain amount may be due to the unsaturation of adsorption sites. A decrease in adsorption density is also attributed to interactions of adsorbent particles for instance by aggregation. This is caused by high adsorbent concentration which decreases the entire surface area of the

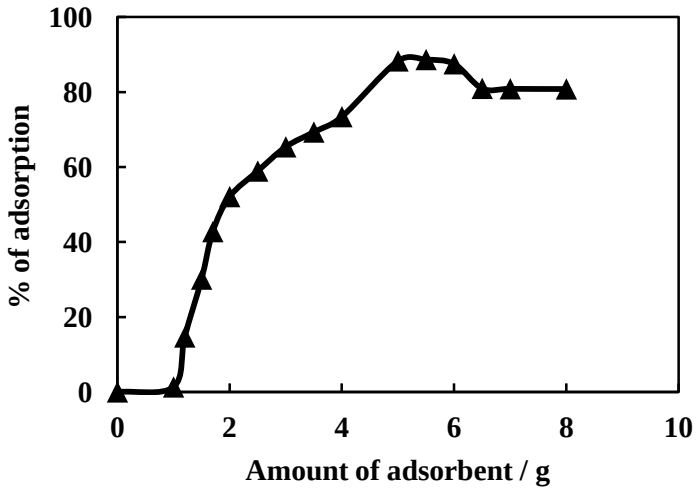

Fig. 1. % of adsorption vs. amount of adsorbent.

adsorbents and increases diffusion path length (Kayes et al., 2016). Adsorption sites may also overlap due to overcrowding of adsorbent particles and this also explains why the increase in adsorbent dosage could lead to a decline in adsorption.

Effect of dye concentration

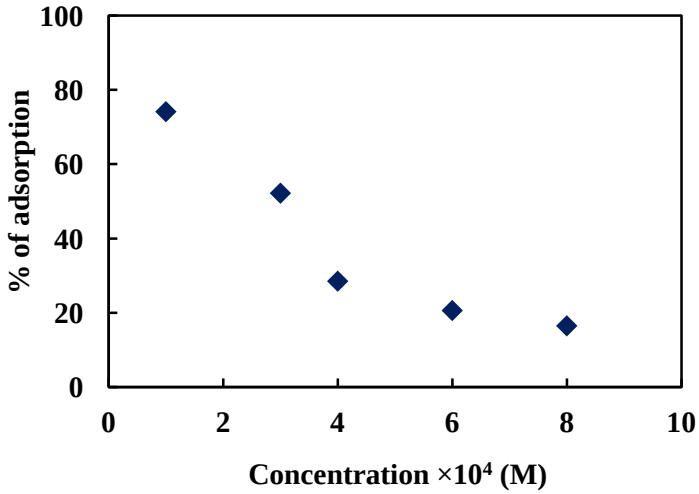

Fig. 2. % of adsorption vs. initial concentration of RB.

The initial dye concentration parameter provides a vital driving force to encounter all mass transfer resistance of the dye between the dye molecules and solid-phase adsorbent

(Ofomaja and Ho, 2007). Fig. 2 illustrated that the percentage of dye removal decreased from 74.17% to 16.50% for RB with the increase of dye concentration. The increase of dye concentration leads to a decrease in the adsorption process, suggesting the adsorption of this dye was highly dependent on dye concentration. This phenomenon was caused by unoccupied active sites on the bio-sorbent surface that were filled with dye molecules and saturation of bio-sorbent surface might be occurred when the dye concentration increased (Banerjee and Chattopadhyay, 2017).

Effect of temperature

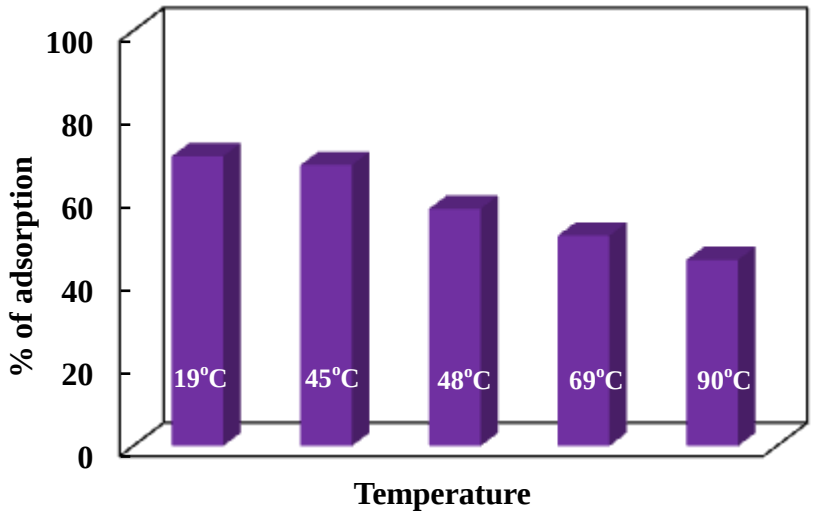

Fig. 3. % of adsorption at different temperature.

Temperature is an important parameter that influences the adsorption of dye. The adsorption of RB on sugarcane bagasse as a function of temperature is shown in Fig. 3. The percentage of adsorption has been found to be decreased with the increase of temperature which recommends that the adsorption is exothermic in nature. The maximum amount of dye adsorbed is 69.81% at 19^{o}C, while it is 44.84% at 90^{o}C. The percentage removal of RB explored that the increase in temperature leads to a reduction in the percentage of dye removal. This is due to the weakening of supportive forces between active sites on the adsorbent and dye to that between adjacent dye molecules during the adsorption process (Badii et al. 2010). A reduction after 19^{o}C was due to the decrease in surface activity at a higher temperature, which indicates that the adsorption process was exothermic and RB dye adsorption onto bagasse occurred mainly by physical adsorption (Ho et al., 2005, Aksu and Tezer, 2005). Therefore, the desorption of RB

molecules at higher temperatures may be due to the deterioration of adsorptive forces between the dye molecule and functional groups on the adsorbent surface.

Effect of contact time

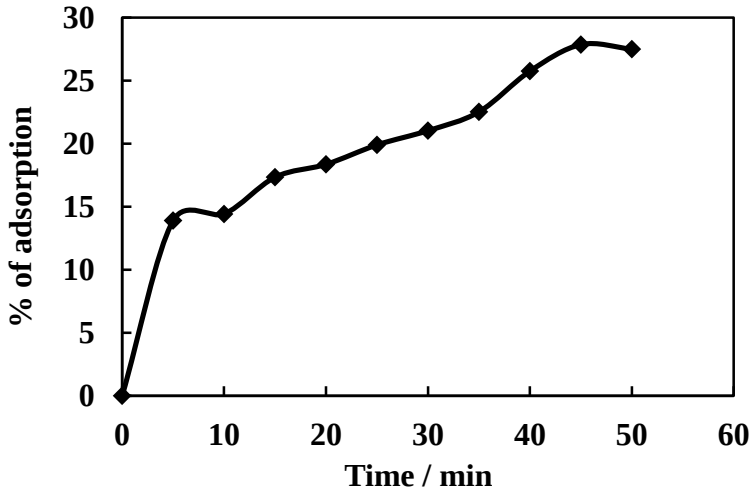

Fig. 4. % of adsorption vs. contact time.

The effect of contact time on the removal of RB on SB is investigated at different contact times (0, 5, 10, 15, 20, 25, 30, 35, 40, 45 and 50 minutes) using 100 mL solution with 1.0 g of the adsorbent (Fig. 4). Generally, the percent removal increases with increase of contact time, because a large number of free surface sites of bio-sorbent are available (Krishni et al., 2014). After 45 minutes of dye adsorption, the percentage of dye removal showed no significant difference in the amount of removing dye in this state. This could be considered as an equilibrium state since the active sites of bio-sorbent are considered to be fully occupied. There is a possibility of the adsorbate to desorb from the surface of the SB to the bulk solution and thus it is concluded that 45 minutes is the optimum time for RB removal using SB.

Kinetic studies

Several kinetic models (pseudo-first-order, pseudo-second-order, and intra-particle diffusion) have been applied to perceive the mechanism of dye adsorption from aqueous solution. The kinetic equations of pseudo-first and pseudo-second-order models are as follows (Tseng et al., 2010, Fytianos et al., 2000)

$$\log (q_e - q_t) = \log q_e - k_1 t \text{…….....} (1)$$

$$t/q_t = 1/(k_2 q_e^2) + t/q_e \text{……} (2)$$

Where q_e and q_t are the amount of adsorbate adsorbed on adsorbent (mg/g) at any time t. k_1 and k_2 are the rate constants for the pseudo-first and second-order respectively. The value of q_e and q_t are calculated by using the following equations (Vijayakumar et al., 2012),

$$q_t = \frac{(C_0 - C_t)\, V}{W} \quad \ldots\ldots\ldots\ldots\ldots\ldots(3)$$

$$q_e = \frac{(C_0 - C_e)\, V}{W} \quad \ldots\ldots\ldots\ldots\ldots\ldots(4)$$

Where, C_0 and C_t represents the initial and equilibrium concentration of dye in mg/L respectively. V is the volume of the solution (L) used for adsorption and W is the mass of dry adsorbent (g).

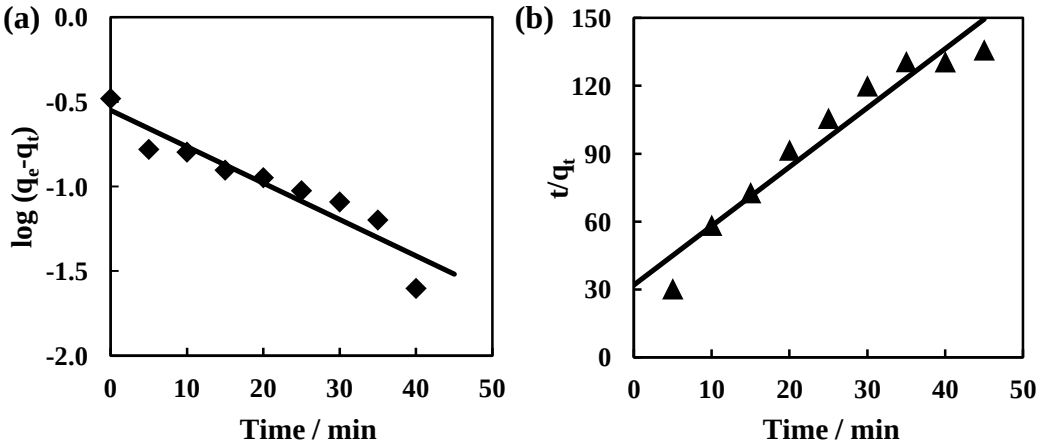

Fig. 5. (a) Pseudo-first order and (b) Pseudo-second order kinetic model for the adsorption of RB on sugarcane bagasse.

The values of kinetic parameters are obtained from the plot of log (q_e-q_t) vs log q_e and t/q_t vs t [Fig. 5]. All the determined values including correlation coefficient (R^2) are listed in table 1. The value of R^2 suggests that the adsorption process is followed by pseudo-second-order kinetics.

Table 1. Kinetic parameters for the pseudo-first and pseudo-second order models.

q_e	Pseudo-first order		Pseudo-second order	
(mg/g)	k_1	R^2	k_2	R^2
0.3313	0.021	0.890	0.285	0.935

The intra-particle diffusion (IPD) values can be obtained from the following equation,

$$q_t = k_p t^{1/2} \text{ .....(5)}$$

Where, k_p is acronym for the intra-particle rate constant (mg g^{-1} $min^{-1/2}$).

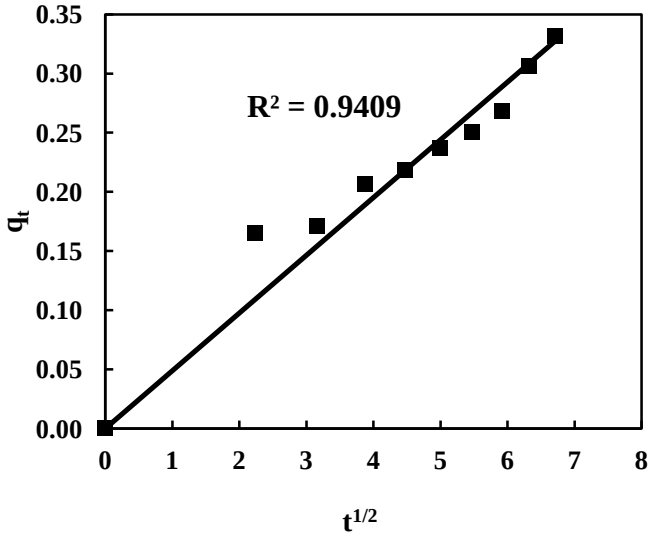

Fig. 6. A plot of IPD model for the adsorption of RB on sugarcane bagasse.

A plot of q_t vs $t^{1/2}$ is not a perfectly straight line which is an indication of occurring various steps such as transportation of RB molecules from bulk solution to the surface of SB through boundary layer diffusion, diffusion of the RB molecules from the external surface to the pores of SB and adsorption of the RB molecules to the active sites of the internal surface of the pores. The value of correlation coefficient (R^2) for IPD is 0.940 whereas it is 0.935 for the pseudo-second order kinetics. This suggests that the adsorption is followed by pseudo-second order kinetics but the plot not passing through the origin is an observation of some degree of boundary layer diffusion.

Conclusion

The extensive capability and the ease with which waste sugarcane bagasse can be combined with smart physiochemical characteristics makes it a potential replacement for commercially used adsorbents. The feasibility of RB removal from aqueous solution with sugarcane bagasse as a sorbent has been confirmed. Results revealed that the maximum removal of RB achieved at a bio-sorbent dosage of 5.5 g/100 mL (88.66%) with initial concentration of RB at 1×10^{-4} M, at temperature 19°C and at 45 minutes of contact time. The adsorption process is accompanied through pseudo-second-order kinetics with some

extent of boundary layer diffusion. All of the results are beneficial to the practical application of sugarcane bagasse for the treatment of dye. The sugarcane bagasse is an alternative substitute to activated carbon as bio-adsorbent, which is plentiful in the nature. Moreover, it has a high adsorption capacity for RB. Therefore, the use of sugarcane bagasse as an adsorbent for the removal of RB from aqueous dye solution is expected to be cost effective. Careless dumping of the above-mentioned adsorbents may cause serious environmental problems. Instead of careless dumping, their use as a bio-sorbent may save the environment from devastation.

References

Adevemo A. A., I. O. Adeoye and O. S. Bello. 2012. Metal organic frameworks as adsorbents for dye adsorption: overview, prospects and future challenges. Toxicological and Environmental Chemistry, 94: 1846-1863.

Aksu Z. and S. Tezer. 2005. Biosorption of Reactive Dyes on the Green Alga Chlorella vulgaris. Process Biochemistry, 40: 1347-1361.

Aksu Z. and Ş. Ş. Çağatay. 2006. Investigation of biosorption of Gemazol Turquise Blue-G reactive dye by dried *Rhizopus arrhizus* in batch and continuous systems. Separation and Purification Technology, 48 (1): 24-35.

Badii K., F. D. Ardejani, M. A. Saberi, N. Y. Limaee, and S. Z. Shafaei. 2010. Adsorption of acid blue 25 dye on diatomic in aqueous solutions. Indian Journal of Chemical Technology, 17: 7-16.

Banerjee S and M. C. Chattopadhyay. 2017. Adsorption characteristics for the removal of a toxic dye, tartrazine from aqueous solutions by a low cost agricultural by-product. Arabian Journal of Chemistry, 10: 16-29.

Basnet P. and Y. P. Zhao. 2014. Superior dye adsorption capacity of amorphous WO_3 sub-micrometer rods fabricated by glancing angle deposition. Journal of Materials Chemistry A, 2: 911-914.

Berradi M., R. Hsissou, M. Khudhair, M. Assouag, O.Cherkaoui, A. E. Bachiri and A. E. Harfi. 2019. Textile finishing dyes and their impact on aquatic environs. Heliyon, 5: e02711.

Czelej K., K. Cwieka and K. J. Kurzydlowski. 2016. CO_2 stability on the Ni low-index surfaces: Van der Waals corrected DFT analysis. Catalysis Communications, 80 (5): 33-38.

Czelej K.,K. Cwieka, J. C. Colmenares and and K. J. Kurzydlowski. 2016. Insight on the interaction of Methanol-Selective Oxidation intermediate with Au- or/and Pd-

containing Monometallic and Bimetallic Core@ Shell Catalysts. Langmuir, 32 (30): 7493-7502.

Dabwan A. H. A., N. Yuki, N. A. M. Asri, H. Katsumata, T. Suzuki and Satoshi Kaneco. 2015. Removal of Methylene Blue, Rhodamine B and Ammonium Ion from Aqueous Solution by Adsorption onto Sintering Porous Materials Prepared from Coconut Husk Waste. Open Journal of Inorganic Non-Metallic Materials, 5: 21-30.

Forgacs E. T. Cserháti, and G. Oros. 2004. Removal of synthetic dyes from wastewaters: a review. Environment International, 30: 953-971.

Fytianos K., E. Voudrias and E. Kokkalis. 2000. Sorption-Desorption Behaviour of 2,4-Dichlorophenol by Marine Sediments. Chemosphere, 40 (1): 3-6.

Ho Y., W. T. Chiu and C. C. Wang. 2005. Regression analysis for the sorption isotherms of basic dyes on sugarcane dust. Bioresource Technology, 96: 1285-1291.

Hu P., Y. Zhang and K. Tong. 2014. Removal of organic pollutants from red water by magnetic-activated coke. Desalination and Water Treatment, 54: 2710-2722.

Kayes M. N., M. J. Miah, M. Obaidullah, M. A. Hossain, M. M. Hossain, 2016. Immobilization of ZnO Suspension on Glass Substrate to Remove Filtration During the Removal of Remazol Red R from Aqueous Solution. Journal of Advances in Chemistry, 12 (6): 4127-4133.

Krishni R. R., K. Y Foo and B. H. Hameed. 2014. Adsorptive removal of methylene blue using the natural adsorbent-banana leaves. Desalination and Water Treatment, 52: 6104-6112.

Madrakian T., A. Afkhami, H. Mahmood-Kashani, and M. Ahmadi. 2013. Adsorption of some cationic and anionic dyes on magnetite nanoparticles-modified activated carbon from aqueous solutions: equilibrium and kinetics study. Journal of the Iranian Chemical Society, 10: 481-489.

Miah M. J., M. N. Kayes, M. Obaidullah, M. M. Hossain. 2016. Photodegradation Efficiency of Prepared and Commercial ZnO to Remove Textile Dye from Aqueous Solution. Journal of Advanced Chemical Sciences, 2 (3): 337-340.

Ofomaja A. E. and Ho Y. 2007. Equilibrium sorption of anionic dye from aqueous solution by palm kernel fibre as sorbent. Dyes and Pigments, 74: 60-66.

Okoro I. A. and S. O. Okoro.2011. Agricultural by products as green chemistry absorbents for the removal and recovery of metal ions from waste-water environments. Continental Journal of Water Air Soil Pollution, 2: 15-22.

O'Mahony T., E. Guibal, and J. M.Tobin.2002.Reactive dye biosorption by *Rhizopus arrhizus* biomass. Enzyme and Microbial Technology, 31(4): 456-463.

Safa Y. and H. N. Bhatti. 2011. Biosorption of Direct Red-31 and Direct Orange-26 dyes by rice husk: Application of factorial design analysis. Chemical engineering research and design, 89: 2566-2574.

Siqueira T. C. A., I. J. D. Silva, A. J. Rubio, R. Bergamasco, F. Gasparotto, E. A. D. S. Paccola and N. U. Yamaguchi. , 2020. Sugarcane Bagasse as an Efficient Biosorbent for Methylene Blue Removal: Kinetics, Isotherms and Thermodynamics. International Journal of Environmental Research and Public Health, 17 (2): 526.

Tseng R. L., F. C. Wu and R. S. Juang. 2010. Characteristics and Applications of the Lagergren's First-order Equation for Adsorption Kinetics. Journal of the Taiwan Institute of Chemical Engineers, 41: 661-669.

Vijayakumar G., R. Tamilarasan and M. Dharmendirakumar. 2012. Adsorption, Kinetic, Equilibrium and Thermodynamic studies on the removal of basic dye Rhodamine-B from aqueous solution by the use of natural adsorbent perlite. Journal of Materials and Environmental Science, 3 (1): 157-170.

Weng C., Y. Lin, Y. Chen, Y. C. Sharma. 2013. Spent green tea leaves for decolourisation of raw textile industry wastewater. Coloration Technology, 129 (4): 298-304.

Yang S. T., S. Chen, Y. Chang, A. Cao, Y. Liu, and H. Wang. 2011. Removal of methylene blue from aqueous solution by graphene oxide. Journal of Colloid and Interface Science. 359: 24-29.

Zhang H., X. Lv, Y. Li, Y. Wang and J. Li. 2010. P25-Graphene Composite as a High Performance Photocatalyst. ACS Nano, 4 (1): 380-386.

Zhu Z., Y. L. Bai, L. Zhang, D, Sun, J. Fang and S. Zhu. 2014. Two nanocage anionic metal-organic frameworks with rht topology and $\{[M(H_2O)_6]_6\}^{12+}$ charge aggregation for rapid and selective adsorption of cationic dyes. Chemical Communications, 50: 14674-14677.

Barishal University Journal Part 1, 6(2): 59-77 (2019) ISSN 2411-247X

PREPAREDNESS AND MANAGEMENT OF COASTAL STORM SURGE, KUAKATA, BANGLADESH

Alamgir Hosain[*1], Muhammad Risalat Rafiq[2], Md. Riaz Uddin[3]

[1]*Department of Coastal Studies and Disaster Management, University of Barishal, Barishal-8200*
[2]*Department of Geology and Mining, University of Barishal, Barishal-8200*
[3]*Department of Geology, University of Dhaka, Dhaka- 1000*

Abstract

Geographically, Bangladesh is vulnerable for natural disaster. The southern part of Bangladesh is a low-lying coastal area, where Kuakata is an important place of tourist destination for its sandy sea-beach. The shore of this region is struck by five strong cyclones from 1995 to 2010, caused severe flooding with massive damage of properties and loss of lives. Coastal inhabitants keep them protected from the impact of storm surge by polder, which is an earthen dike. Polder- 48 acts as a shield against coastal hazards in Kuakata. However, the polder was broken at several places during these cyclones. This analysis focused on community preparedness and management of coastal storm surge, cautioning system, and also the chances of polder breaching. The primary database is a questionnaire survey, and the secondary databases are all historical statistical data. As stated by individuals understanding, polder breaching probability is very high, and there is a shortage of suitable safety precautions. But, the people feel blameless about the warning system, and they get the most warning from radio and television media. Their insinuations are: a) increasingly establishing more cyclone shelter centers, b) fixing the polder breached area, and c) raising polder elevation. Policymakers and planners may use this research finding for an effective Integrated Coastal Zone Management (ICZM) approach.

Keywords: Storm Surge, Cyclone, Polder, Coast, Breaching.

I. Introduction

Bangladesh comprises a 710 km long coastal belt that ranges from the Raimongal River from the west to Teknaf to the southeast (Siddiqi, 2001). The entire land area of the country consists of 1,44,000 square km (Rahman et al., 2014) with a population of about 163 million (*Bangladesh | The World Bank Data*, 2020); of which about 49% live in the

[*]*Corresponding author's e-mail: ahosain@bu.ac.bd, alamgir_geo_du@yahoo.com*

coastal zones (Neumann et al., 2015). The massive population over the coastal belt is vulnerable to natural hazards, especially summertime flooding caused by coastal storm surge. The frequency of cyclones that cause coastal storm surge has increased rapidly in contrast to the previous occurrences because of climate change. From 1995 to 2010, the shore of Bangladesh experienced five severe cyclones continuously, which inducing flooding, damage to property, and lifestyles (Dasgupta et al., 2014). The intensity of flood, drought, and storm is also increasing day by day due to climate change (Khan et al., 2011). Moreover, more than 70% population of the southwestern part of this country identified diarrhea, dysentery, and skin diseases as the prime waterborne health risks. These issues are creating due to the scarcity of safe water as a consequence of climate change (Abedin et al., 2019), which have fallen the entire southern coastal folks in a miserable state.

Polder is an earthen dike in the coastal area and made to shield the inhabitants against flooding during high tide and storm surge (M. F. Islam et al., 2019). The entire southern shore belt of Bangladesh is encompassed by 123 polders. The crest level of present polders in coastal areas is adequate to safeguard the coastal storm surge using a 5 to 12 years return interval (S. Islam et al., 2013). However, in recent times, repeated cyclones, for example, SIDR (November 15, 2007), AILA (May 25, 2009), MOHASEN (May 16, 2013), ROANU (May 21, 2016), etc. causing damage to polders in different regions. The storm surge caused by the cyclone swept away the coastal structural protection steps. For example, polders are greatly affected by the storm surges, which weaken the polders in different places. As a consequence, the weaker part of the polder leads to breaching. Occasionally seawater intrudes throughout the breaching section of the polder and results in flooding. The intrusion of sea saline water reduces land fertility and agricultural soil growth. Also, the breaching portion of polders requires timely recovery to prevent future damage during cyclones. Recently, the crest level of polders has restructured and redesigned for an event of 25 years return period under the Coastal Embankment Improvement Project (CEIP) (BWDB, 2013). On the other hand, the frequency of cyclones has increased rapidly compared to the past due to climate change. As a consequence of global warming, the tropical cyclone intensity will increase by 2% to 11%, according to a projection by the year 2100 (Knutson et al., 2010). Damages caused by tropical cyclones will probably be raised by US$53 billion every year by the year 2100 because of climate change that is roughly twice without considering climate change (Mendelsohn et al., 2012). Subsequent sea-level rise may increase the substantial quantity

of flooding area. Cyclone of November 1970, which struck southern Bangladesh with a height of 9m storm surge, caused the departure of 300,000 individuals (Haider et al., 1991). After, in 1991's cyclone, the loss of lives was about 1, 45,000 (Haider et al., 1991). Again, the cyclone SIRD in 2007 impacted 8.9 million individuals, causing harm of US$1.67 billion (*Government of Bangladesh: Damage, Loss, and Needs Assessment for Recovery and Reconstruction after Cyclone Sidr*, 2008) and also US$70.3 million damage to the dike and structural management (Dasgupta et al., 2014). Besides, cyclone AILA in 2009 impacted 3.9 million individuals alongside the harm of US$270 million (Dasgupta et al., 2014).

Rivers, canals, beaches, mountains, waterfalls, green gardens, archaeological sites, and spiritual areas are the natural resources which are the tourist attraction in Bangladesh. These natural resources are leading to some substantial quantity of GDP each year in the tourism sector. The total contribution in GDP from Bangladesh travel & tourism industry is 3.0 percent, 2.9 percent for employment, and GDP growth in travel and tourism is +6.8 percent in 2019 (WTTC Annual Research: Key Highlights, Bangladesh, 2020). Though inside South-Asia, Bangladesh got the very smallest tourist arrivals and earnings gained by the tourism sector (Pennington & Thomsen, 2010), tourism is just one of the lucrative industries in Bangladesh (Elena et al., 2012). Hence, seashores would be the most revenue-earning industry in the tourism market, and shores should maintain security and tourist-friendly at any danger to enhance tourism businesses (Hossain & Islam, 2014).

Kuakata, as a tourist place, is a location of high financial value. Local shopkeepers, resort workers, employees, and transport workers acknowledge this place as a highly favorable destination for tour lovers. But, the 710-kilometer long coastal regions made Bangladesh more prone to coastal storm surge. The preparedness and protective steps against the adverse effect of storm surges are undeniable to keep a sustainable ecosystem. The multiple functions of the preparedness steps against the coastal storm surge are researched through a vigorous literature review to conduct a questionnaire for this study. To gather leading data from the individual relevant questions are prepared. Additional secondary data from various statistical investigations are used to get a better image. The gathered information is presented in a graphic way to represent the perceptions of neighborhood inhabitants to obtain a better mitigation solution from potential storm surge effects. Many men and women take personal protective measures to save their own lives and properties from coastal storm surge effects. Usually, they take shelter at the Cyclone

Shelter Centre (CSC) and keep dry food and garments with them during a storm surge. Their understanding of possible polder breaching is very high, which raises the concern for damaging consequences of future storm surge strikes. The findings from this community assessment can help policymakers to redesign both structural and non-structural development works. However, this analysis also arouses the pros and cons of present coastal security measures during a hazard. Authorities and policymakers can reduce the enormous quantity of loss regarding properties and lives due to future coastal storm surge by boosting both structural and non-structural safety measures in the coastal region.

II. Study Area

The study area Kuakata is located in south-western Bangladesh in the vicinity of Bay of Bengal at Kalapara Upazila, Patuakhali district, Barishal (division). This area situated between 20° 48' and 21° 52' N latitude and 90° 5' and 90° 14' E longitude. The area of study is surrounded by polder 48 which is 20 km in length (M. F. Islam et al., 2019). Polder 48 is surrounded by the Bay of Bengal from the west (titled 'West veribadh road'), south, and east (titled 'East veribadh road'); and by the Khapravanga River from the north (Fig 1). Several tidal inlets have spanned this polder at few distinct switch gate points. During a storm surge, tidal inlets possess a considerably destructive role by breaching the weaker zone of polder due to high wave attack; whereas, afforestation plays a constructive role to reduce the storm surge effects. A significant amount of beach berm deposit is covered by planted Jhau forest (Salt Cedar).I In the east and west part of the Kuakata shore, the Jhau forest makes the 18 km long shoreline a panoramic beauty (an attractive tourist spot). The neighborhood in and about this shore depends upon tourism. Other than tourism, their most common occupations are farming, fishing, and aquaculture.

The entire population of the area is 9177 that is 0.40 percent of the whole coastal inhabitants of the Patuakhali district. The number of total families is 2065 (that is 0.60 percent of the district number), and the amount of flying folks is 537 (that is 15.12 percent of the district number) (*Population & Housing Census 2011; Zila Report: Patuakhali*, 2011). As a cyclone-prone county with populated coastal regions, Bangladesh is highly vulnerable to coastal disaster.

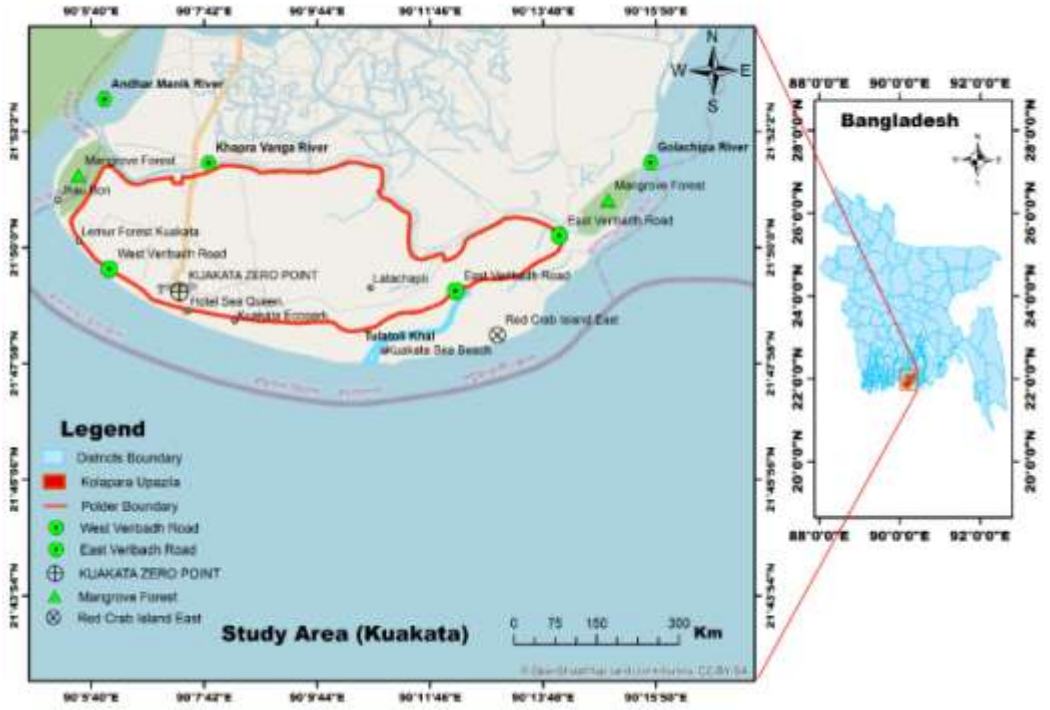

Fig. 1. Study area (Kuakata Pourosova, Kalapara Upazila, Patuakhali District).

III. Materials and Methods

As a tourist place, people in Kuakata are directly or indirectly involved in tourism-related occupations. Fishing is also among the most accessible jobs. In 2013, approximately 4.4 percent of the entire Gross Domestic Product (GDP) came from the tourism industry in Bangladesh (*WTTC Travel & Tourism Economic Impact 2014*, 2014). As a financially important tourist spot, Kuakata has faced the attack of several storm surges for the past couple of decades, which causes loss of lives and properties. Considering the economic importance of Kuakata, the preliminary grounding was to conduct a questionnaire survey at the beach area to detect peopleÕs practice, preparedness, and protective steps during storm the surge.

A questionnaire survey holding all the queries has conducted in Panjupara, Husain Para, Rakhine Palli, Rakhine Market, Kuakata beach, and Hazi Sarak area under Mahipur Union Parishad, Patuakhali Upazila (sub-district) (Fig. 1). The location map of the study

area has constructed using ArcGIS (version 10.3). Questions of this survey have prepared to get the innate understanding of local individuals (Appendix A) from the inspiration after Hofmann 2007 (an unpublished MS thesis). A random sampling method has been used for data collection to eliminate the effect of data clustering. The portion of the population of this study that has been worked with by sampling is 0.3 percent (Portion = Sample size (25) × 100 ÷ Total population (9177) = 0.3 percent).

Part of the questionnaire survey has conducted near polder 48. After collecting information in the poll near polder 48, all participant's responses and demography data have processed with Microsoft Excel 2010. Together with the principal survey information, comparative evaluation has shown in the plotted graph. Moreover, utilizing secondary data out of other accounts e.g. UN, WTTC, and BBS report, etc., few constructive recommendations are prepared.

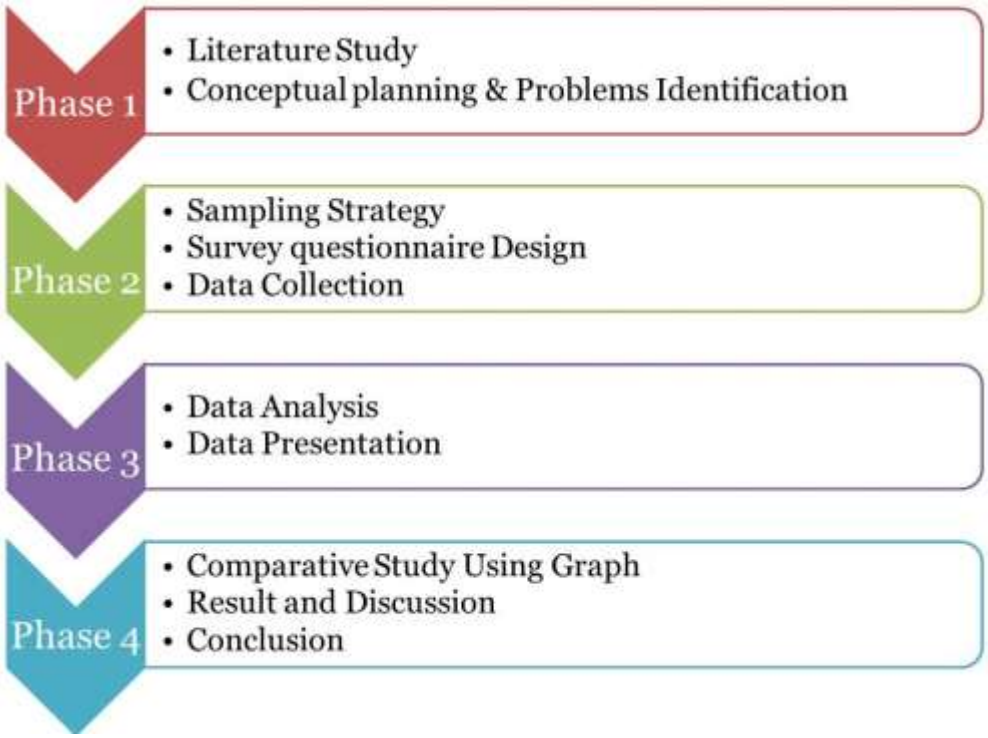

Fig. 2. Schematic shows steps in this study.

IV. Data Collection

Utilizing the qualitative questionnaire survey, an evaluation of the general understanding and preparedness to coastal storm surge has prepared. Initially, related questions have

been made to get a clear summary of different factors. Those factors includes individuals understanding towards storm surge, the preparedness practice followed by natives, the warning or broadcasting method practiced by local authorities, the social and infrastructural economic loss which was experienced by neighborhood level, the chance of polder breaching in the shore area, and the demography of the fellow poll participants. Except for five demographic queries, a total of 24 questions have been documented for the questionnaire. The primary data have been collected by one-to-one personal interview between an information collector and a resident and the survey has conducted in both home and small to medium business points in January 2018. No tourist has been regarded as survey participants to remove misleading information.

V. Results and Discussion

1. Demography: Most of the participants are neighborhood residents, and among the survey participants, 84 percent are masculine, and 16 percent of participants are feminine. A random sampling poll has conducted among various occupants. Among them, around 72 percent are self- employed, and the self-employed suggests as farmers, van (paddle three-wheeler run by foot) drivers, fisherman, and also small to moderate entrepreneurs. About 8% of those participants are under-employed and 8 percent are fully-employed in stores, resorts, or other business factors. Rests of those participants are retired senior citizens (8 percent) and students (4 percent) (Fig 3a).

Relating to earnings, most people (roughly 52 percent) have monthly income ranging from 5,000 Bangladeshi Taka (BDT) to BDT 15,000. About 16 percent of the people have a monthly earning of less than BDT 5,000, which is a minimum salary. There are considerable numbers of individuals (about 12 percent) that don't want to share, or perhaps they don't receive any predetermined quantity of money a month. Around 4 percent of the individuals have a high monthly earning, which is over BDT 50,000, and a similar percentage of individuals have a monthly income ranging from BDT 35,000 to BDT 50,000 (Fig 3b).

Most of the participant's age range is 35 years to 40 years (roughly 56 percent of total participants). The 2nd highest age range is 18 years to 34 years, which is 24 percent of the overall participants. The senior citizens who are greater than 67 years old are about 12 percent. There is 4 percent participant for each age group between 50 years to 67 years and who are less than 18 years old.

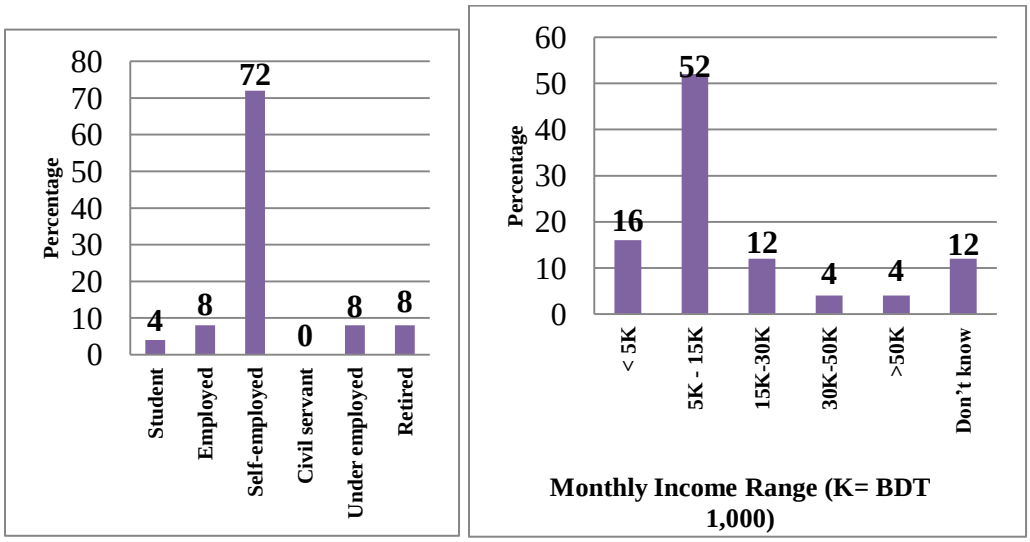

a) b)

Fig. 3. a) Participants professions and b) Participants income range.

In the duration of settlement, the maximum amount of individuals (about 28 percent) lives here in the two-year range one is for 30-39 years, and another is for 40-49 years (Fig. 4). Folks who live here for 50-59 years are roughly 24 percent; 20-29 years are 12 percent. Very few people (about 4 percent) live here for less than 20 years. The long duration settlement folks are also 4 percent who live here for greater than 60 years. In the broader picture, a few men and women are migrated here from other places, and possibly the tourism sector opportunity makes individuals attracted to migrate to Kuakata.

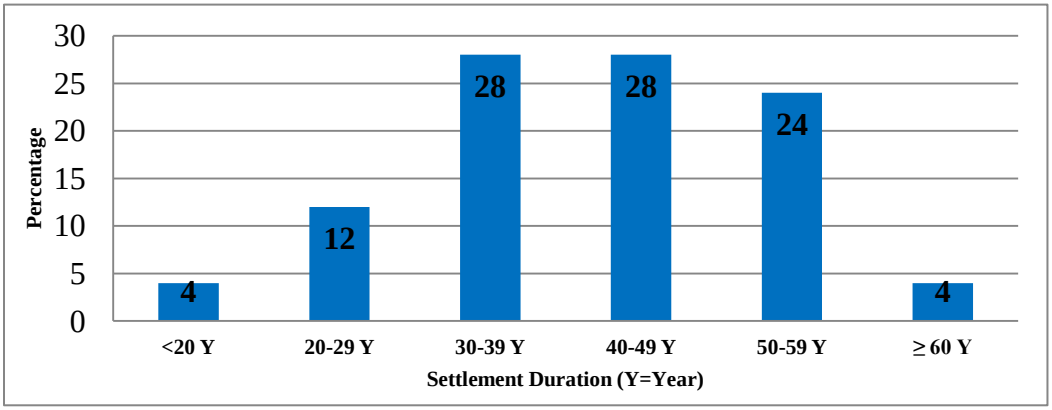

Fig. 4. Duration in year people settlement in Kuakata.

2. Participants Response in different indicators: Most of the individuals (around 96 percent) reported that they experienced a coastal storm surge. The vast majority of the local inhabitants (80 percent) also have experienced inundation of caused by coastal storm surge. Approximately one-third of inhabitants (64 percent) take personal protective measures to get rid of coastal storm surge effects. The rest of 36 percent of individuals do not take protective measures (Fig. 5).

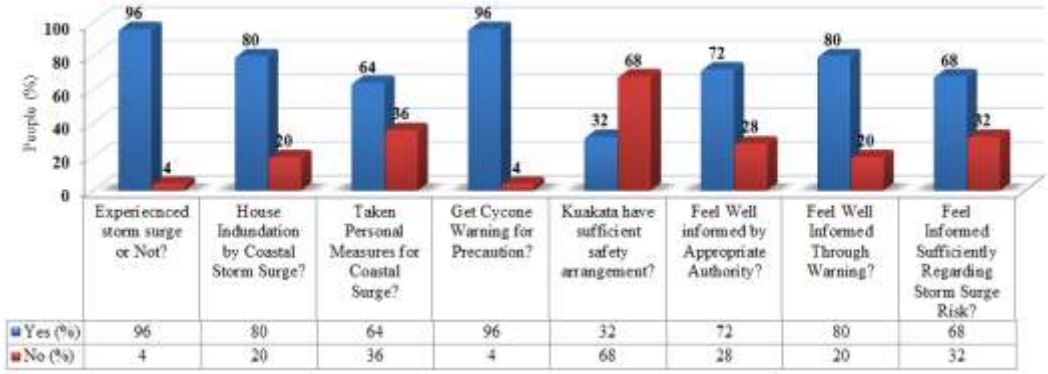

Fig. 5. Individuals response in different disaster risk and preparedness indicators.

Among the men and women who take personal protective measures, 24 percent take shelter in cyclone shelter centers with their self-motivation, and the same numbers of individuals keep dry food and clothes with them as private measures. Approximately 16 percent of people use a cellular phone as a tool for data sharing with friends, relatives as well as local disaster risk reduction authority. Roughly 12 percent of individuals of each four-team utilize the following personal protective steps as pre and syn-disaster approach to secure their properties form cyclone: 1) utilize rope to generate the home roof closely hooked with the floor, 2) increase home ground elevation to get rid of water inundation, 3) maintain crucial file including the registration of the land property and all precious academic and educational certificates, 4) use flashlight (Fig. 6).

At least, a single warning of the cyclone is by the maximum number of individuals, which is about 96 percent. Approximately 68 percent of individuals consider there are adequate safety arrangements to reduce the effects of storm surge. The majority of the individuals (around 72 percent) feel well informed about the approaching storm surge by proper authority. Approximately 80 percent of individuals are feeling well informed concerning warning systems just before the event about to happen by an integrated approach in disaster risk reduction strategy. About 32 percent are not feeling well informed about the storm surge hazard before or following the event, but they receive the cyclone warning. The lacking is to create people's perception of how devastating the

storm surge could be if it draws full power (Fig. 5). The cyclone attack in the year of 1970, 1977, 2008, and 2013 make a little scratch in individual memory but the disastrous cyclone Sidre attack in 2007 which was the most memorable cyclone to all individuals.

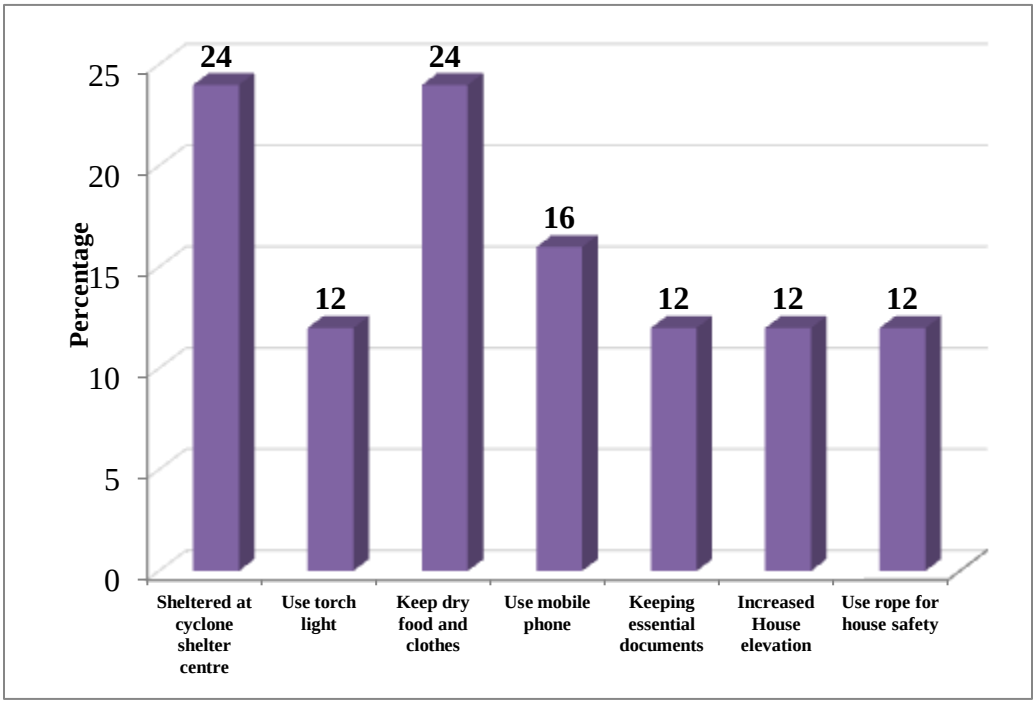

Fig. 6. Personal protective steps practiced by local individuals.

3. Storms Surge and Probability of Polder failure: All individuals are worried that shortly when cyclone will hit coast, they will suffer a lot as like past storm surge. Everyone is well informed about the construction of the polder which has been built to reduce the storm surge effect.

According to people's observation, the probability of polder failure is very high. There are at least four locations where the polder has been weakened due to several cyclonic attacks during the previous decade (M. F. Islam et al., 2019). Moreiver, around 52 percent peoples belief that there is a very high probability of polder failure in near future when any cyclone will attack (Fig. 7). The chance of moderate probability of polder breaking is stated by 12 percent of people. Only 12 percent of people consider the polder failure probability is very low, about 8 percent of peoples believe that the probability is less, and 4 percent of people think that the probability is high.

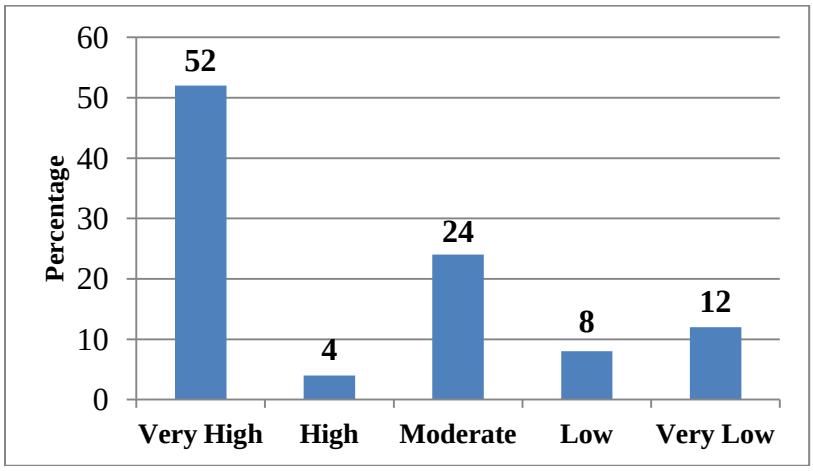

Fig. 7. Probability of polder bleaching according to people's perception.

4. Warning system of coastal storm surge: Individuals get the warning of cyclone and coastal storm surge through different media. Among them, the maximum number of individuals (27 percent) gets a warning through radio or television (Fig. 8). Approximately 25 percent of individuals get a warning from government authorities, and around 19 percent of people get warning from the neighborhood. The rest of the individuals get warning through the fire brigade and disaster management agency, which are private organizations (17 percent), internet (6 percent), friends (5 percent), and press (0 percent). The internet is not much popular in the village locality, but the use of the internet is increasing day by day. In the future, the capacity of getting cyclone information through the internet to village residents will increase.

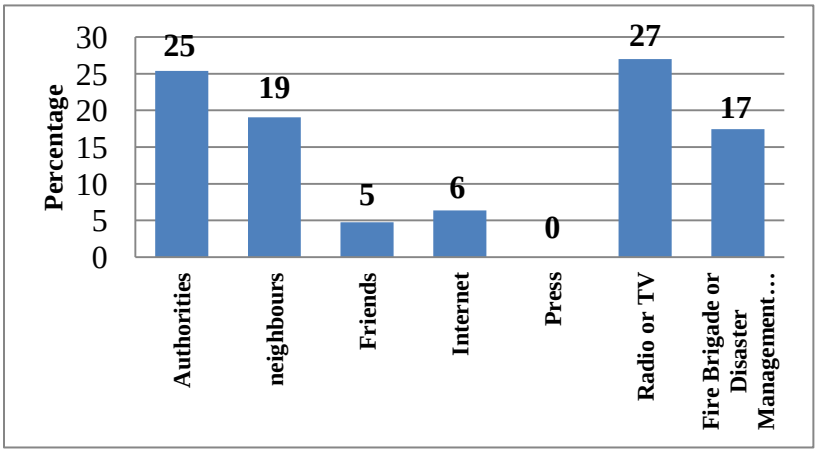

Fig. 8. Source of information about storm surge.

5. Measures for future storm surge: Individuals expect the care for protective measures, warning systems, and other infrastructural facilities from the proper authority. Maximum individuals (about 64 percent) consider government authority has the sole responsibility to set up the protective measures (Fig. 9a). Approximately 20 percent of people regard that the local authorities and the same amount of people consider NGOs should look after the measurement steps. Few people (12 percent) think the disaster management agencies should come up more enthusiastically to ensure protective steps. Only 4 percent of individuals consider the local residents also have the responsibility to take protective steps from cyclonic storm surge effects.

Appropriate action plan should be taken for future cyclone and storm surge to reduce the damage and loss of lives and properties. Local tenants suggested manifold approaches to reduce the damage from a future coastal surge. Maximum individuals (about 35 percent) consider that the authority should build more Cyclone Shelter Centers (CSC) as the existing number of shelter centers and their total capacity is not sufficient for the large population (Fig. 9b). According to 22 percent of folk's opinion, repairing polder could guard the vulnerable area against being flooded, and 13 percent of individuals suggested increasing polder height will be a better approach. Proper distribution of relief foods during and after storm surge could mitigate the unbearable pain of the hunger's mendicant condition is stated by roughly 13 percent of people. Among the rest of the individuals, 9 percent consider broadcasting of storm surge warnings should be a more appropriate way, and only 4 percent of people think that they should elevate their houses to mitigate the loss.

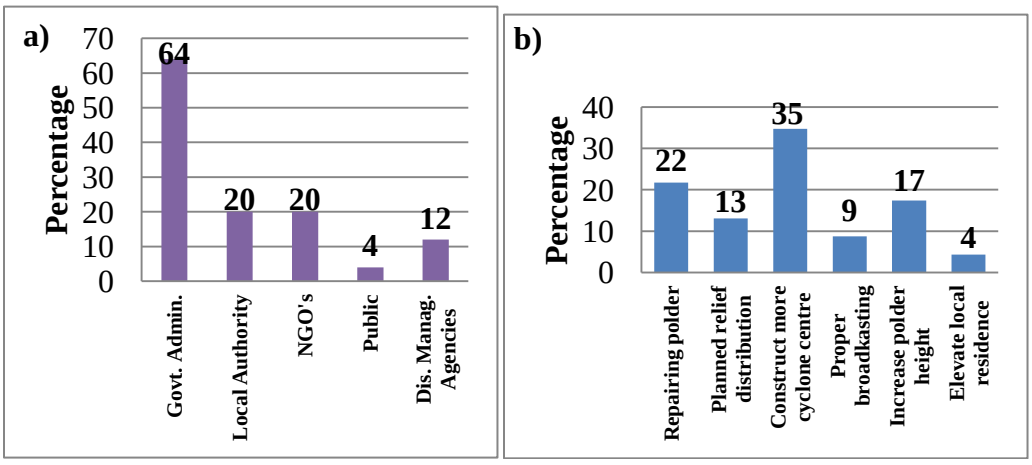

Fig. 9. a) Folk's expectations about who are the responsible group for protective measures; b) Which action could improve the safety steps and reduce loss in a future storm surge.

Individuals have a deep belief in their creator (God). They believe ALMIGHTY can save them or also can dismiss them. Though, many of them believe that polder height must increase immediately, and also the potential breaching place should fix and preserve occasionally. Individuals living permanently or temporarily close to the shore area are largely prone to this adverse impact of storm surge. They have suggested establishing more Cyclone Shelter Centers (CSC) in coastal areas. The present quantities of CSC aren't sufficient for an enormous population. They also recommended maintaining constant monitoring and management of all switch gates, which uphold the water exchange inside and outside of the polders. The government could utilize the local residents for this monitoring job which could also create employment opportunities. The majority of the people are self-employed and they've monthly average income involving US$175 into US$350 (BDT 15,000 into BDT 30,000) and in between 30-50 year age group.

Folk's perception of the probability of polder breaching is very high, and concerning this high probability, about two-thirds of individuals take protective measures. As personal protective measures, peoples mostly take shelter at Cyclone Shelter Center (CSC) and keep dry food and clothing with them. Over two-thirds of individuals do not believe Kuakata have enough security arrangement. However, they feel well informed throughout the storm surge via television and radio websites. Practically, everybody experienced a coastal storm surge, and they hope to get details information regarding cyclone storm surge from government authority and to take the responsibilities for executing appropriate actions to decrease the loss of lives and properties.

A suitable and efficient warning system may save lives and possessions. As the communication system in the distant area is inaccessible, engine bicycles might be an excellent choice of fast and timely broadcasting with the assistance of a volunteer. The majority of the people of the analysis area are Muslims, and they have mosques in every village. As folks are spiritual, they will perceive the significance of caution, which comes from the mosque's loudspeaker in contrast to some other broadcasting media. Every cyclone shelter center must have a warning system that guarantees the top excellent sound system. This sound system could save lives and properties during cyclone and storm surge. Though authorities send warning utilizing text messages to each cell phone user, individuals have suggested using a local language edition of warning messages could be more effective. Caution could differ from place to place since the urgency varies too. Utilizing a GPS tracking system or a cellular networking system may help to find the remote user location and send a brief message accordingly.

VI. Conclusion and Recommendation

Residents feel well informed, but they a feel a lack of safety measures in Kuakata during pre, syn, and post-disaster periods of coastal storm surge. Inhabitants are quite pleased with the warning system. However, they need appropriate safety measures from government jurisdiction. Radio and television is widely used by majority of the inhabitants as a warning telecasting media within this area. People also take protective steps as occurring at cyclone shelter centers and keeping dry food and clothes. Moreover, they believe constructing more cyclone shelter centers can lower the loss of life, and fixing as well as elevating polder can conserve their properties.

This analysis is a pilot project to evaluate the public understanding of coastal storm surge and also to locate polder breaching probability. A questionnaire survey and historic data are used for gathering individual perceptions. Detailed work can be done with an attitude survey in many polders in the entire coastal areas utilizing digital elevation model information with a questionnaire survey and Key Informant's Interview (KII). Thorough areal analysis in the southwestern beach region and collecting more data samples could be the better method of obtaining a broad areal picture. Planning a comprehensive and suitable response and mitigation system can lower the loss to a minimum.

VII. Acknowledgement

The authors significantly acknowledge the participation of the bachelor students of the department of coastal studies and disaster management, University of Barishal for their excellent efforts during data collection, and also to Swarnali Mahmood for her support and tips through the survey. The authors are also thankful to the University of Barishal for providing the working facility for this study group.

References

Abedin. M. A., A. E. Collins, U. Habiba, and R. Shaw. 2019. Climate Change, Water Scarcity, and Health Adaptation in Southwestern Coastal Bangladesh. International Journal of Disaster Risk Science. 10(1). 28–42. https://doi.org/10.1007/s13753-018-0211-8

Bangladesh | The World Bank Data. 2020. IBRD. IDA. https://data.worldbank.org/country/BD

BWDB. 2013. COASTAL EMBANKMENT IMPROVEMENT PROJECT, PHASE-I (CEIP-I). https://doi.org/https://www.bwdb.gov.bd/archive/pdf/364.pdf

Dasgupta. S., M. Huq, Z. H. Khan, M. M. Z. Ahmed, N. Mukherjee, M. F. Khan and K.

Pandey. 2014. Cyclones in a changing climate: the case of Bangladesh. Climate and Development. 6(2). 96–110. https://doi.org/10.1080/17565529.2013.868335

Elena. M., M. H. Lee, Suhartono, Hossein, N. Haizum and N. A. Bazilah. 2012. Fuzzy time series and sarima model for forecasting tourist arrivals to Bali. Jurnal Teknologi (Sciences and Engineering). https://doi.org/10.11113/jt.v57.1524

Government of Bangladesh: Damage, Loss, and Needs Assessment for Recovery and Reconstruction after Cyclone Sidr. 2008. https://reliefweb.int/report/bangladesh/cyclone-sidr-bangladesh-damage-loss-and-needs-assessment-disaster-recovery-and

Haider. R., A. A. Rahman and S. Huq. 1991. Cyclone '91 An Environmental and Perceptional Study. Bangladesh Centre for Advanced Studies (BCAS). http://www.bcas.net/book-details.php?book_id=31&title=Cyclone %9291 An Environmental and Perceptional Study

Hofmann. S. D. 2007. Awareness of and preparedness for storm-surges in a coastal community on the North Sea. Northumbria University. MS Thesis (Issue October). repository.tudelft.nl/islandora/object/uuid:8f7935ac-b019-49f0-b316-e891d0981d3a/datastream/OBJ

Hossain. S. and N. Islam. 2014. Estimating Recreational Benefits of the Kuakata Sea Beach: A Travel Cost Analysis. European Journal of Sustainable Development. 3(2). 119–132. https://doi.org/10.14207/ejsd.2014.v3n2p119

Islam. M. F., B. Bhattacharya and I. Popescu. 2019. Flood risk assessment due to cyclone-induced dike breaching in coastal areas of Bangladesh. Natural Hazards and Earth System Sciences. 19(2). 353–368. https://doi.org/10.5194/nhess-19-353-2019

Islam. S., R. Alam and I. Nur-A-Jahan. 2013. Adequacy Check of Existing Crest Level of Sea Facing Coastal Polders by the Extreme Value Analysis Method. IOSR Journal of Mechanical and Civil Engineering. 8(1). 89–96. https://doi.org/10.9790/1684-0818996

Khan. A. E., W. W. Xun, H. Ahsan and P. Vineis. 2011. Climate change, sea-level rise, & health impacts in. Environment. 53(5). 18–33. https://doi.org/10.1080/00139157.2011.604008

Knutson. T. R., J. L. McBride, J. Chan, K. Emanuel, G. Holland, C. Landsea, I. Held, J. P. Kossin, A. K. Srivastava and M. Sugi. 2010. Tropical cyclones and climate change. Nature Geoscience. 3(3). 157–163. https://doi.org/10.1038/ngeo779

Mendelsohn. R., K. Emanuel, S. Chonabayashi and L. Bakkensen. 2012. The impact of climate change on global tropical cyclone damage. Nature Climate Change. 2(3). 205–209. https://doi.org/10.1038/nclimate1357

B. Neumann, A. T. Vafeidis, J. Zimmermann and R. J. Nicholls. 2015. Future coastal population growth and exposure to sea-level rise and coastal flooding - A global assessment. PLoS ONE. 10(3). https://doi.org/10.1371/journal.pone.0118571

Pennington. J. W. and R. C. Thomsen. 2010. A Semiotic Model of Destination Representations Applied to Cultural and Heritage Tourism Marketing. Scandinavian Journal of Hospitality and Tourism. 10(1). 33–53. https://doi.org/10.1080/15022250903561895

Population & Housing Census 2011; Zila Report: Patuakhali. 2011.

Rahman. A., L. Hossain, A. Foysal and A. Akter. 2014. Impact of Climate Change on Food Security in South-West Coastal Region of Bangladesh. American Journal of Experimental Agriculture. 4(12). 1916–1934. https://doi.org/10.9734/ajea/2014/6165

Siddiqi. N. A. 2001. Mangrove forestry in Bangladesh. Institute of Forestry & Environmental Sciences, University of Chittagong.

WTTC Annual Research: Key Highlights, Bangladesh, 2020. https://wttc.org/Research/Economic-Impact.

Appendix A:

Interview

On

"Preparedness and Management of Coastal Surge at Kuakata, Bangladesh"

Date: Time: Place:

Please fill in this questionnaire and mark your chosen answers with one tick only where required.

1. How long have you lived at Kuakata?

   Answer:

2. Have you ever experienced a storm-surge (Sidr/Aila/any others)?

   Yes / no

3. Are you worried about the possibility of a storm-surge affecting Kuakata?

   Yes / no

4. Do you know in which year Kuakata had a storm-surge disaster?

   Answer:

5. Do you know about the polder construction in Kuakata as safety measures of storm-surge?

   Yes / no

6. How high would you rate the probability of a polder failure in Kuakata?

   Very High/ High/ Moderate/ Low/ Very Low

7. Is the house in which you live within reach of inundation in the case of a storm-surge?

   Yes / no

8. Did you take personal measures to be generally prepared for a storm-surge?

   Yes / no

9. If you have answered the previous question (7) with yes, which measures are these?

   Answer:

10. Do you know how to get information about precaution measures for your personal protection against storm-surges?

    Yes /no

11. If you have answered the previous question (9) with yes: Where do you get information from? (Please tick only three)

    Authorities/neighbors/friends/Internet/press/Radio or TV/fire brigade or disaster management agencies/other source of information

12. According to your opinion, does Kuakata have sufficient safety arrangements for storm-surges (e.g. disaster management arrangements, public warnings)?

    Yes/ no

13. If you have answered the previous question (11) with no, how could the safety in case of a storm-surge is enhanced according to your opinion?

    Answer:

14. Rate how well do you feel informed by the appropriate authorities on the risk of storm-surges in principle?

    Very High/ High/ Moderate/ Low/ Very Low

15. Do you remember if a storm-surge warning had been released at that time? Where did You hear about this?

    Authorities/neighbors/friends/Internet/press/Radio or TV/fire brigade or disaster management agencies/other source of information.

16. Do you have the feeling to be informed well through storm-surge warnings?

    Yes /no

17. Do you remember what the warning included? Did you understand the warning and its implications for you personally?

    Yes /no

18. Did you understand the warning and its implications for you personally?

    Yes /no

19. How much you feel personally threatened due to a sea level rise caused by climate change?

    Very High/ High/ Moderate/ Low/ Very Low

20. How high would you rate the influence of a rising sea level on the storm-surge risk in Kuakata?

    Very High/ High/ Moderate/ Low/ Very Low

21. Do you feel informed sufficiently regarding storm-surge risk in Kuakata?

    Yes /no

22. How would you like to be informed? Do you have any ideas how the topic could be implemented creatively in the community?

    Answer:

23. Who, in your opinion, should be paying for the protective measures?

    Answer:

24. Do you have any other comments on the risk of storm-surge in Kuakata?

    Answer:

GENERAL INFORMATIONS:

These questions are for statistical use only and will be kept with confidence.

Attendant name: ……..…, Contact No: ……..

a) Participant: Sex

    1. F 2. M

b) To which of the following age groups do you belong?

    1. Under 18 2. 18-34 3. 35-49 4. 49-67 5. Greater than 67

c) How many people are there in your household in each of the following groups?

    1. Less than 10 2. 11-17 3. 17-5 4. Greater than 50 5. Other adults

d) Would you tell me to which of the following groups you belong?

    1. Student 2. Employed 3. Self-employed 4. Civil servant 5. Part-time employed 6. Retired.

e) Which of the letters on this card represents the gross monthly income, from all sources, of your household?

    1. Below 5,000 2. 5,000-15,000 3. 15,000-30,000 4. 30,000-50,000

    5. 50,000 and more 6. Don’t know

Reporter name: ……

Barishal University Journal Part 1

ISSN:2411-247X

University of Barishal, Barishal 8200, Bangladesh

INSTRUCTIONS TO THE CONTRIBUTORS

Preparation of manuscripts

The following guidelines should be followed strictly in submitting the manuscript of the journal.

All manuscripts must be written in English and typed on a good quality (A4) bond paper with double space and sufficient margins (left and top 3.80 cm. right and bottom 2.55 cm) and be submitted in duplicate to the Associate Editor at the University address stated below. **The Editorial Board will arrange review of the article**. Decision of the Editorial Board on any article is final.

The manuscript of a full paper or review papers within fifteen typed pages including tables, figures, graphs, etc. while that of a short communication should not exceed six pages.

The manuscript should contain the following subtitles in sequence; Title, Abstract, Keywords, Introduction, Materials and Methods, Results and Discussion, Acknowledgements, if any, and References. These sub-titles however may not be applicable in case of **short communication or review paper.**

Title: Title of the paper should be brief and specific. The author should prepare the manuscript in such a way that there should be a title page with only the title of the paper, the names and address of the authors, and running head on it. The second page should carry the title of the paper with Abstract to be followed by Introduction, etc. without author's name.

Abstract: It should not exceed 200 words. It should include only the gist of the paper, i.e. just the results. Abstract is not the summary and in any case, it should not contain the subject of the materials and methods and /or any descriptive part of the paper.

Keywords: Should not exceed 6 words.

Introduction: It should be concise and include relevant literature and define clearly the objective of the study.

Materials and Methods: Special / standard methods should be cited only as references and should not be described except for the modification which should be stated. No sub-heads should be used.

Results and Discussion: The section should include precise statement of results obtained, figures, tables, and discussion.

Table, Graphs and Figures: The paper should contain minimum number of tables, graphs, and figures. However, these should be typed separately. Table title should be on the top of the table and written as **Table 1.** Caption for the figures graphs and graphs should be on the bottom of the figure and be written as **Fig 1. The same data should not be used in both the tables and figures or graphs.** The figures and graphs should be properly labeled with bold, solid lines so that these can stand reduction up to half or less

of the original. The photographs should be submitted on glossy paper. Legend of the graphs and figures should be typed and given separately at the end of text.

The references and specific names are extremely important. The authors must be sure about the corrections of citations and spellings.

Citation style: In the text, references should be cited within brackets quoting author's surname and the year of the publication in the appropriate place. Two or more references when put within the same bracket should be separated by a comma. For example, (Khan, 2005), (Parvin and Zakia, 2009) and (Rahman, 2010), salinity is widely (Khan et al., 2002); (Parvez and Rahim, 2004; and Rafi, 2005), results are partially agree well with the findings of (Harun, 2010 and Akter, 2011). Units of measurements to be used as SI units.

References: References should be arranged alphabetically according to author's surname at the end of the paper. Names of journals and books should be in italics giving edition, year of publication and name of the publishers. Examples:

Islam. M. S., M. R. Islam and M. M. Rahman. 2015. Incompatibility relationship in wild housefly *Musca domestica* L. collected from different parts of Bangladesh. Journal of Asiatic Society of Bangladesh (Science). **29**: 23-30.

Islam. A. K. M and K. Moniruzzaman. 2015. Euglenophyta of Bangladesh. L. Genus Trachelomonas Her. Inc. Revue ges Hydrobioligy. **66:** 109-125.

Khan, M. S. 2013. Angiosperms. In: Two Centuries of plant Sciences in Bangladesh and Adjacent Regions (ed. A. K. M Nurul Islam). pp. 175-194. Asiatic Society of Bangladesh. Dhaka.

Bhuiyan. A. L. 2010. Fishes of Dhaka. Asiatic Society of Bangladesh, Dhaka. 148pp.

The author (s) must submit one printed copy of the revised paper and soft copy in the CD as MS Word format.

Final galley proof will be sent author (s) and is expected to be returned within five days as notice. No major alternations in the text are desirable at this stage.

Papers should be submitted in **duplicate** to:

Hena Rani Biswas. Associate Editor, Barishal University Journal Part 1, Department of Mathematics, University of Barishal, Barishal 8200, Bangladesh.

Off-Prints

Author(s) of each paper is/are entitled to get off-prints upon request.

Declaration

While submitting a paper the authors are to sign a declaration to the effect that (i) the work reported has been carried out by them and they jointly prepared the manuscript; (ii) they take public responsibility for the contents of the paper; (iii) the paper has not been published before in any referred scientific journal or has not been submitted to such journal for publication; and (iv) the accord consent to the Barishal University Journal to publish the paper.

Faculty of Science & Engineering and Bio-Sciences
University of Barisal
Barisal 8200